Master Thesis

Fluidized Bed Mixing Investigation: Development of a New Digital Image Analysis Method

ausgeführt zum Zwecke der Erlangung des akademischen Grades eines Diplom-Ingenieurs

unter der Leitung von

Univ.Prof. Dipl.-Ing. Dr.techn. Hermann Hofbauer

Institut für Verfahrenstechnik, Umwelttechnik und technische Biowissenschaften

E 166

eingereicht an der Technischen Universität Wien

Fakultät für Maschinenwesen und Betriebswissenschaften

von

Werner Liemberger

Matr. Nr.: 0726546

Lindengasse 44a/9

1070 Wien

Wien, am 26.9.2013

Werner Liemberger

TECHNISCHE UNIVERSITÄT WIEN
Vienna University of Technology

Prof. Dr. Hermann Hofbauer

CHALMERS
UNIVERSITY OF TECHNOLOGY

Prof. Dr. Henrik Thunman

Ass. Prof. Dr. David Pallarès

M.Sc. Erik Sette

Universität für Bodenkultur Wien
University of Natural Resources
and Applied Life Sciences, Vienna

Prof. Dr. Christoph Pfeifer

Eidesstattliche Erklärung

Ich erkläre an Eides statt, dass ich die vorliegende Arbeit selbstständig verfasst, andere als die angegebenen Quellen/Hilfsmittel nicht benutzt, und die den benutzten Quellen wörtlich und inhaltlich entnommenen Stellen als solche kenntlich gemacht habe.

Wien, am 26.9.2013

Werner Liemberger

Kurzfassung

Vermischung spielt bei der Auslegung, Optimierung und Betriebsweise großer Wirbelschichten eine Schlüsselrolle um deren Effizienz zu steigern.

Diese Arbeit untersucht das seitliche Mischverhalten in einem Kaltmodell einer Blasenbildenden Wirbelschicht bei unterschiedlichen, zum Vergasungs- und Verbrennungsprozess passenden, Betriebsbedingungen.

Die Analysen wurden mittels digitaler Bildanalyse durchgeführt. Dafür wurde ein Objektdetektierungsalgorithmus entwickelt und validiert. Anschließend wurden zwei theoretisch unterschiedliche Modelle implementiert (Einzelpartikelverfolgung, multiple Partikelstreuung).

Alle für die Auswertung notwendigen Parameter wurden untersucht. Dabei wurde der Einfluss der Mischzellenbreite bei der Einzelpartikelverfolgungsmethode gefunden. Ohne diesen Parameter, welcher weitere Untersuchungen benötigt, können nur Größenbereiche der Dispersionskoeffizienten angegeben werden.

Die Verläufe von beiden Methoden sind miteinander vergleichbar. Dennoch sind jene Werte der Einzelpartikelverfolgung höher.

Hinaufskalierte Dispersionskoeffizienten der Einzelpartikelverfolgung liegen in einem Bereich zwischen 0.0064 und $0.112\,\mathrm{m^2\,s^{-1}}$ was sie vergleichbar mit Literaturwerten[1] (0.0001 bis $0.1\,\mathrm{m^2\,s^{-1}}$) macht.

[1] siehe (Niklasson et al.; 2002, Seite 3)

Abstract

Mixing is an important key issue in large fluidized beds to design, optimize and control the reactors efficiency.

This thesis investigates lateral fuel mixing in a cold flow model at several operation conditions, relevant to gasification and combustion processes.

The analysis was done with digital image analysis. A new object detection algorithm was developed and validated. Furthermore two different analysis models were developed (single particle tracking and multiple particle spreading).

Further on several algorithm settings are investigated. Thereby the influence of the mixing cell length on single particle tracking was found out. Without this parameter, which needs further investigation, only a range of dispersion coefficients can be given.

The trends of both methods are comparable. Nevertheless the values are higher for the single particle tracking method.

Scaled up single particle tracking dispersion coefficient results are in the range of 0.0064 to $0.112\,\mathrm{m^2\,s^{-1}}$ which makes them comparable to those found in literature[2] (0.0001 to $0.1\,\mathrm{m^2\,s^{-1}}$).

[2]see (Niklasson et al.; 2002, page 3)

Acknowledgments

I would like to express my sincere thanks to everyone who has contributed to this work. I thank Professor Hermann Hofbauer for introducing the fluidized bed topic in an inspiring way during his lecture and for giving me the opportunity and support to realize this work.

Moreover I thank Professor Henrik Thunman for giving me the chance of writing my thesis at the division of Energy Technology, department of Energy and Environment at Chalmers University of Technology, Gothenburg, Sweden. Further on I would like to thank him for giving me a great overview of biomass gasification, problems and their research approaches.

I own special thank to David Pallarès for all the great discussions, his ability to express complex things in easy meaningful graphs and his excellent scientific support.

Erik Sette deserves thank for his support and the time he spent in all out countless discussions. I thank Nicolas Berguerand for helping me organizing everything.

I own another special thank to Professor Christoph Pfeifer. He gave me the contact and support to write my thesis at Chalmers. Furthermore he greatly supported me during my time in Sweden and afterwards, when and wherever possible. I would like to thank everyone in the office for the great and inspiring atmosphere.

Finally I would like to thank my parents for their encouragement over the past years.

Contents

List of Figures

List of Tables

List of Symbols

symbol	unit	name
Ar	–	Archimedes number
L	–	characteristic length
C	mol m^{-3}	concentration
ρ_f	kg m^{-3}	fluid density
ρ_s	kg m^{-3}	particle density
d_{sv}	m	particle diameter
D	m^{2}s^{-1}	dispersion coefficient
μ	Pa s	dynamic viscosity
φ	–	form factor
g	m s^{-2}	gravity
Re	–	Reynolds number
G_s	kg s^{-1}	solids flux
U^*	–	dimensionless fluidization velocity
u_{mf}	m s^{-1}	minimum fluidization velocity
u_0	m s^{-1}	superficial velocity

List of Indices

L large

M model

Chapter 1

Introduction

1.1 Motivation

The world's energy consumption is increasing. Furthermore, fossil fuels (coal, oil, gas) and uranium will run out someday. Therefore it is essential to develop new technologies based on renewable energy sources. Efficient use of renewable energy, especially biomass, reduces the emission of climate active gases (keyword CO_2 footprint). Further on transport distances and energy import dependency are reduced. This independence decreases the political influence of exporting countries.

A major problem with most renewable energy sources is that availability and demand is not always simultaneous. However this is needed to ensure electrical power grid stability (Leitner; 2010, page 2). Therefore energy storage is needed. Storing a huge amount of energy over a long time is one of the biggest problems and the importance is increasing by extending the use of renewable energy sources.

Biomass is chemically bounded energy. It can be used whenever it is needed and therefore it acts as energy storage. The bounded energy can be converted into electricity by burning biomass. The hot exhaust gases are converted into mechanical (engine or turbine) and afterwards into electrical (generator) energy. In case of combustion, biomass is burned directly. A different approach is gasification. Under special conditions (e.g. limited amount of oxygen), biomass can be converted into gas. After some additional conditioning steps high-grade synthesis gas is produced. This gas can be burned directly in gas engines or gas turbines to produce heat and power. Alternatively Synthetic Natural Gas (SNG), Hydrogen, or high quality liquid fuels (Fischer-Tropsch) diesel can be produced.

At Vienna University of Technology a dual fluidized bed gasification process has been developed. This process is successfully demonstrated in industrial scale in Güssing (8 MW) and Oberwart (10 MW). Currently a large application (GoBiGas project, Gothenburg, Sweden) based on this knowledge is under construction. The aim of this project is to produce in a first step 20 MW SNG and in the end 100 MW.

Compared to Austria there are no allowances for biomass power plants in Sweden. Therefore this technology can only be used, if it is price-competitive by its own. This can only be achieved, if it has an accurate size. Most of Austrians large biomass power plants are sized around 10 $MW_{\text{fuel, input}}$ (upper limit to get allowances). Compared to this, the GoBiGas project is planned with a fuel input of 32 $MW_{\text{fuel, input}}$ for its first step (REPOTEC; 2013).

The sizes of these power plants are different and therefore requirements change. To build such large applications it is important to make them as efficient as possible, especially if they have to be price-competitive without any financial support. This can be achieved if the whole process is split up, analysed and optimised part by part and as a whole.

1.2 Aim of the Work

One of these previous mentioned process parts is the fuel distribution.

In case of combustion the fuel should be well distributed to avoid strong over- or understochiometric regions, which would lead to unbalance. This can be done by multiple fuel feeding points (Highley and Merrick; 1971), which leads to high investment costs. In contrast it can be reached if the fuel particles spread on their own in a controlled way.

In case of gasification it is important that almost no fuel reaches the outlet side to ensure a high conversion rate/efficiency.

In both cases it is important to know the influence of different parameters (e.g. operation conditions, installed internals) on the mixing to design the reactor in an appropriate way.

To test multiple different combinations a lab scale model is needed. A common way to study fluidized beds is to use a cold flow model[1].

There are multiple ways to measure spreading, or mixing. Mostly it is done by measuring time-resolved concentrations on single or multiple positions.

In this work the investigation is done by digital image analysis. Two new algorithms are developed to follow a single particle (single particle tracking), or a batch of particles (multiple particle spreading). After applying the expression proposed by Einstein in (Einstein; 1906) the dispersion coefficient[2] is estimated under different conditions[3]. Furthermore the work investigates the influence of chosen parameters.

[1] described in Sect. 2.1 (page 4)
[2] see Sect. 2.3.1 (page 11)
[3] see Sect. 4.2 (page 67)

Chapter 2

Theory

This chapter gives a short summary on the underlying theory. Among others the term "fluidized bed" is explained and which problems are commonly encountered when applying laboratory results on industrial applications. Furthermore a short introduction to digital image analysis is given.

2.1 Fluidized Beds

"Fluidization is an operation which puts solid particles in a fluid like state through suspension[1] in a gas or liquid." (Kunii and Levenspiel; 1991, page 1). As shown in Fig. 2.1 (page 5) a fluid is passed through an amount of particles, called bed.

2.1.1 Characterisation of Fluidized Beds

Depending on the superficial velocity, a ratio between fluid flow and cross section of the empty bed, fluidized beds behave in different ways, as illustrated in Fig. 2.1 (page 5).

In Fig. 2.1 (page 5) c) and d) behave differently. In c) the fluidization medium is liquid and in d) it is gas. Compared to a liquid-solid system the bed height of a bubbling fluidized bed is, due to instabilities of bubbles and channelling, not much higher than the one with minimum fluidization. In literature they are sometimes called aggregative or heterogeneous fluidized bed as well. By further increasing the superficial velocity a bed

[1] A suspension is a dispersion where unsolvable solid particles are thinly dispersed in a fluid phase.

reaches a turbulent fluidization state and afterwards pneumatic transport. In the last case the bed material is transported with the fluid.

Describing all the phenomena for the different systems is beside the purpose of this work. Therefore it is referenced to (Kunii and Levenspiel; 1991).

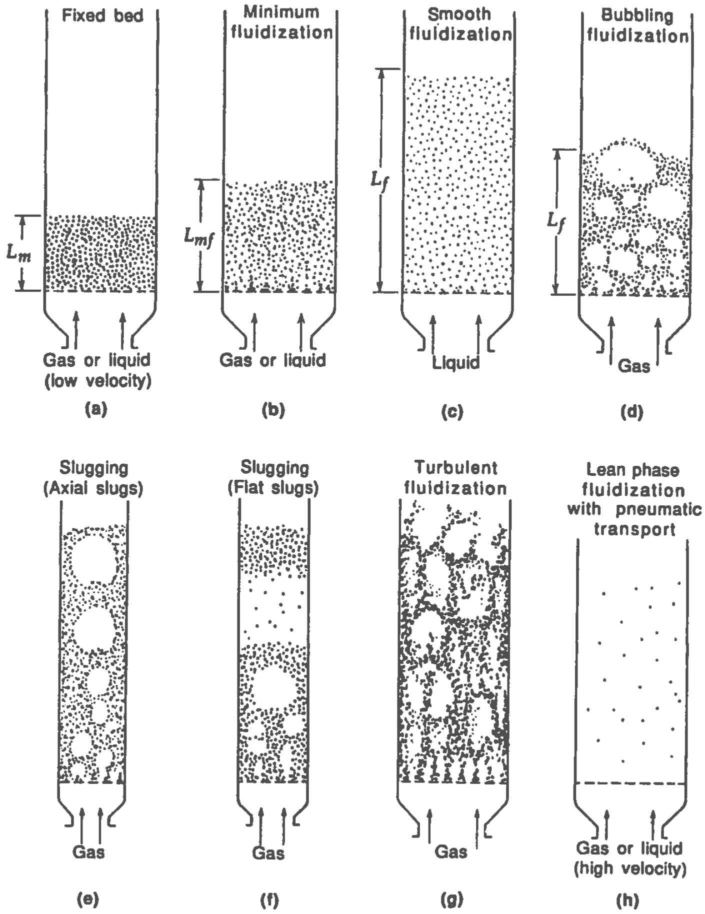

Figure 2.1: Characterisation of fluidized beds (Kunii and Levenspiel; 1991, Fig. 1, page 2)

This work investigates bubbling fluidized beds, because they are common in industrial combustion and gasification.

Grace et al. describe in (Grace et al.; 1997, page 12) a way to categorise fluidized beds with a diagram displayed in Fig. 2.2 (page 6).

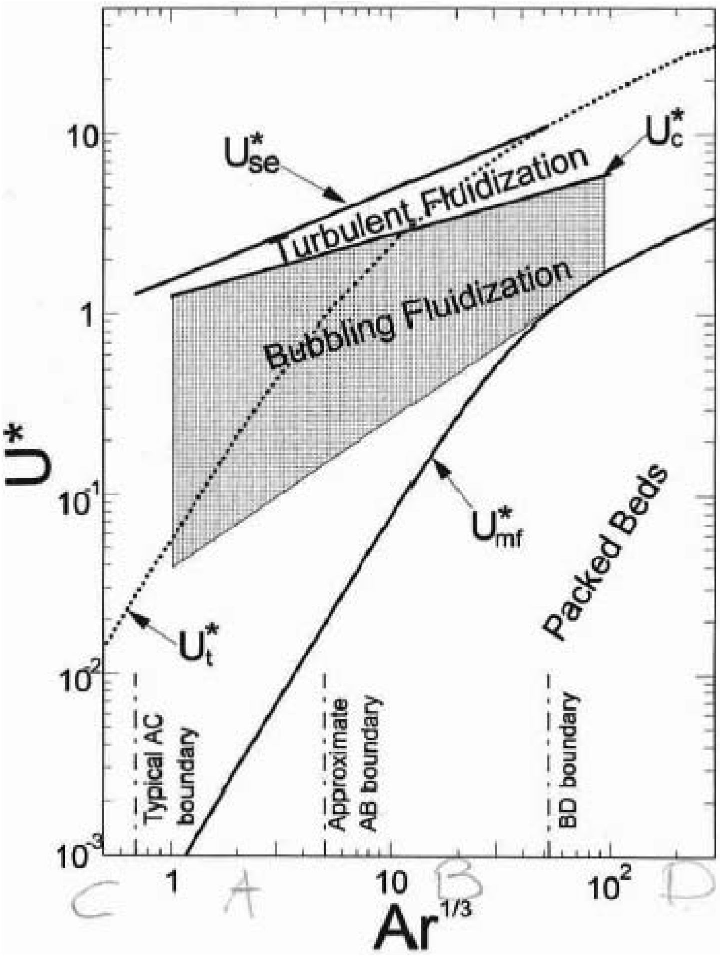

Figure 2.2: Flow regime map for gas-solid fluidization. Heavy lines indicate transition velocities, while the shaded region is the typical operation range of bubbling fluidized beds (Bi and Grace, 1995b) (Grace et al.; 1997, Fig. 1.4 on page 12)

2.1.2 Bed Material

Physical properties of the solid particles used as bed material influence the fluid dynamics of the whole system. According to literature the most common way to categorise particles with similar fluid dynamics was found by Geldart in (Geldart; 1973) and is displayed in Fig. 2.3 (page 7). The particles are classified by their diameter and difference in densities (solid-gas). Typical bed materials for gasification and combustion are in group B, sand-like.

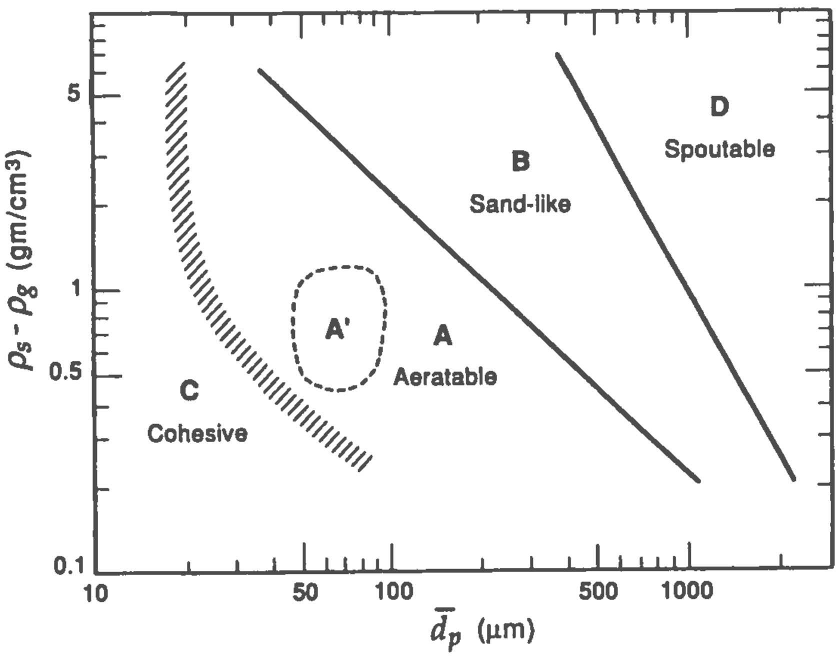

Figure 2.3: Classification of particles by Geldart (Kunii and Levenspiel; 1991, Fig. 9, page 78)

2.2 Scaling

To investigate a fluidized bed small units are usually used, mainly due to cost reasons. Fluidized beds are often used for combustion or other chemical applications with high temperatures. To simplify experiments, investigating fluid dynamics of fluidized beds, these models operate under cold conditions. Therefore they are called "cold flow models".

To draw inferences from experiments under cold conditions the model needs an appropriate design and the results have to be scaled up afterwards.

2.2.1 Cold Flow Model

A cold flow model is compared to a pilot plant or an industrial application a much smaller model of a reactor. It is called cold flow model, because it usually operates under ambient conditions. This means for instance that it works with ambient temperature instead of e.g. 900 °C.

Several physical properties are depending on the temperature, especially those from gases. For instance the viscosity (values are from (Kothandaraman and Subramanyan; 2004, page 24)) of air changes from $16.03 \times 10^{-5}\,\mathrm{m^2\,s^{-1}}$ at 900 °C to $1.56 \times 10^{-5}\,\mathrm{m^2\,s^{-1}}$ at 20 °C. The difference is about a factor of 10.

Scaling needs to be done following a theoretically-derived set of scaling laws which respect the conservation equations of mass and momentum.

The most common scaling laws are those formulated by (Glicksman et al.; 1994) (see Sect. 2.2.2 (page 9)).

There are several factors that have an important influence on the results, but describing all of them is beside the purpose of this work. An example is, that the reactors volume to surface ratio is different between cold flow model and industrial application. Therefore the surface (compared to the volume) of a cold flow model is much higher, and wall effects are maybe dominating. To reduce this effect a large model is needed.

The cold flow model used in this work and the way to scale up the results is described in Sect. 3.5 (page 55).

2.2.2 Scaling Laws

The following equations represent the dimensionless parameters formulated by (Glicksman et al.; 1994, eq. 35 on page 343), also known as scaling laws:

$$\frac{{u_0}^2}{g \cdot L} \tag{2.2.1}$$

$$\frac{\rho_s}{\rho_f} \tag{2.2.2}$$

$$\frac{\rho_s \cdot u_0}{\mu} \tag{2.2.3}$$

$$\frac{\rho_f \cdot u_0 \cdot L}{\mu} \tag{2.2.4}$$

$$\frac{G_s}{\rho_s \cdot u_0} \tag{2.2.5}$$

$$\text{bed geometry} \tag{2.2.6}$$

$$\varphi \tag{2.2.7}$$

$$\text{particle size distribution} \tag{2.2.8}$$

To ensure similarity between two systems they need an identical geometry, scaled by a factor. This means that all lengths are scaled by the same factor. Due to manufacturing limitations (tolerances, cost reasons) it is not always possible to fully ensure this.

After choosing one property, all the others are fixed. A common way is to chose air at ambient temperature as fluid. Therefore the other parameters (e.g. bed material density) are given.

A major problem is typically to find an appropriate bed material with the needed density. Additionally it should be cheap, not reactive with air and not hazardous. Furthermore, to ensure fluid dynamically similarity, it has to be in the same Geldart group.

2.3 Mixing

Mixing is a very important phenomenon for the performance of industrial applications. In case of combustion, fast mixing is intended for good fuel burn out (Pallarès et al.; 2007). In gasification a lower mixing level is needed, because the gasification reactions are slower compared to combustion (Gómez-Barea and Leckner; 2010).

To increase the performance of reactors it is important to control mixing within the reactor design. Therefore the influence of different parameters needs to be known.

In fluidized beds fluid dynamics are complex, because of particle gas interactions. This makes Computational Fluid Dynamics (CFD) time consuming and therefore expensive. Thus it is common to use empirical methods to investigate fluid dynamics and mixing.

Mixing (in fluidized beds) is often split up into two parts, the vertical and horizontal (lateral). If the bed height is much lower than the bed width (typical for commercial gasifiers and boilers (Knoebig et al.; 1999; Sette; 2013)), vertical mixing is much faster (Ito et al.; 1999).

To simplify the complex fluid dynamics, lateral solids mixing is often described as random walk process[2]. According to the random walk theory an overall macroscopic movement can be calculated from many microscopic movements.

The order of magnitude defining a macroscopic length depends on the phenomena studied. In molecular diffusion it is given by the mean free path. Molecular velocities between one collision and the next one are not relevant, but global movements at a scale larger than that in-between collisions (i.e. larger than the mean free path) is the correct one for analysis.

Lateral solids mixing is "expressed as an averaged dispersion coefficient, although the mixing process is highly convective" (Pallarès et al.; 2007, page 930).

The term dispersion has several meanings. In matters of transport (and fluid dynamics) it is the expansion from one substance into another medium. It is the combination of convection and diffusion. The overall mixing is described by an diffusion like equation. The two dimensional form is expressed in Eq. (2.3.1) (page 10).

$$\frac{\partial C}{\partial t} = D_x \cdot \frac{\partial^2 C}{\partial x^2} + D_y \cdot \frac{\partial^2 C}{\partial y^2} \tag{2.3.1}$$

[2](Pearson; 1905)

The equation is quite easy to solve, if reactor dimensions and dispersion coefficients are known. Finding the dispersion coefficient is the overall purpose of this work.

2.3.1 Dispersion Coefficient

The solids dispersion coefficient has the same unit as the diffusion coefficient ($\mathrm{m^2\,s^{-1}}$). Typical values for molecular diffusion coefficients for gases are around 10^{-5} to $10^{-4}\,\mathrm{m^2\,s^{-1}}$, for liquids around $10^{-9}\,\mathrm{m^2\,s^{-1}}$ (common organic solvents, mercury and molten iron) and 10^{-30} to $10^{-12}\,\mathrm{m^2\,s^{-1}}$ for solids (Cussler; 1997). A lateral solid dispersion coefficient for fuel particles found for a fluidised bed under hot conditions has the order of $0.1\,\mathrm{m^2\,s^{-1}}$ (Niklasson et al.; 2002).

According to Einstein the dispersion coefficient can be evaluated from experimental data by using Eq. (2.3.2) (page 11) which was proposed in (Einstein; 1906).

$$D_x = \frac{\Delta x^2}{2 \cdot \Delta t} \tag{2.3.2}$$

The dispersion coefficient can be defined for different directions. In case of a symmetrical bed and an even gas nozzles distribution it can be assumed that the dispersion coefficients are equal in both horizontal directions.

$$D_x = D_y = D \tag{2.3.3}$$

2.3.2 Solid Mixing in Bubbling Fluidized Beds

Mixing is caused by bubbles rising through the bed material and erupting at the surface (Shi and Fan; 1985).

Bubbles rising through the bed material are effected by coalescence (see Fig. 2.4 (page 12)). This means that with increasing distance from the distribution plate bubbles grow together. This, simplified, results in an increase of the bubble rising speed. The higher speed and bubble volume results in more energetic eruptions.

In previous 2D experiments the mixing behaviour was investigated. It was found that mixing patterns establish, which are structured in horizontally aligned vortexes generated by the bubble flow (Pallarès and Johnsson; 2006; Pallarès et al.; 2007; Soria-Verdugo et al.; 2011). Regions with upwards moving direction are established in the main bubble paths,

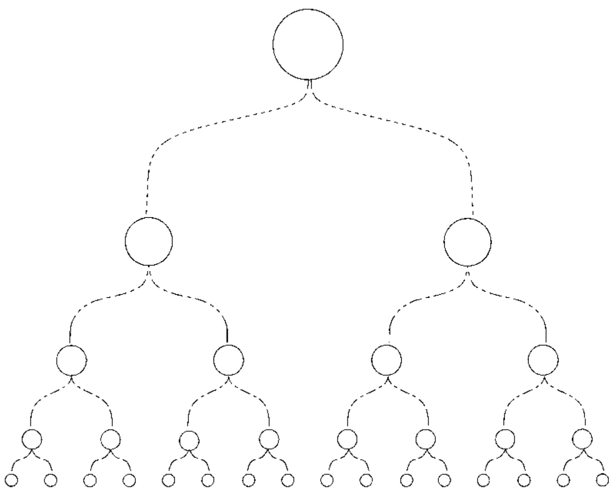

Figure 2.4: Dalton's bubble coalescence model (Yang; 2003, figure 13, page 73)

while downwards moving flows are in the nearby emulsion phase induced by the emulsion drift (displayed in Fig. 2.5 (page 12)).

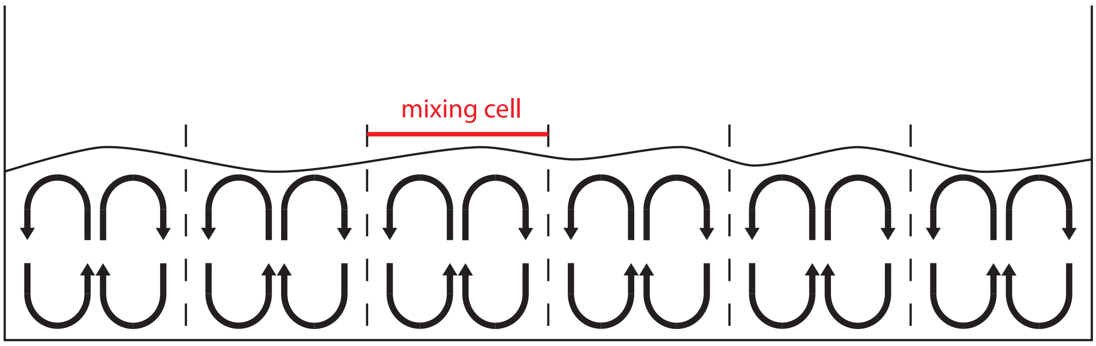

Figure 2.5: Mixing patterns without coalescence forming a mixing cell

The width of mixing cells increase with the influence of bubble coalescence, therefore they grow with bed height. If the bubble coalescence can be avoided e.g. with internals, this effect is reduced or non-existing.

2.4 Digital Image Analysis

Visual observations have always been very important. In former times it was only possible to describe them. With the development of cameras it is possible to record and "save" them. A couple of years ago the development of computers and cameras has reached a stage where they are quite cheap and powerful.

Moore proposed in (Moore; 1965) that the number of transistors on a chip roughly doubles every two years (Moore's law). Figure 2.6 (page 13) shows that his prediction was correct. As a result of this rapid development, nowadays a personal computer is strong

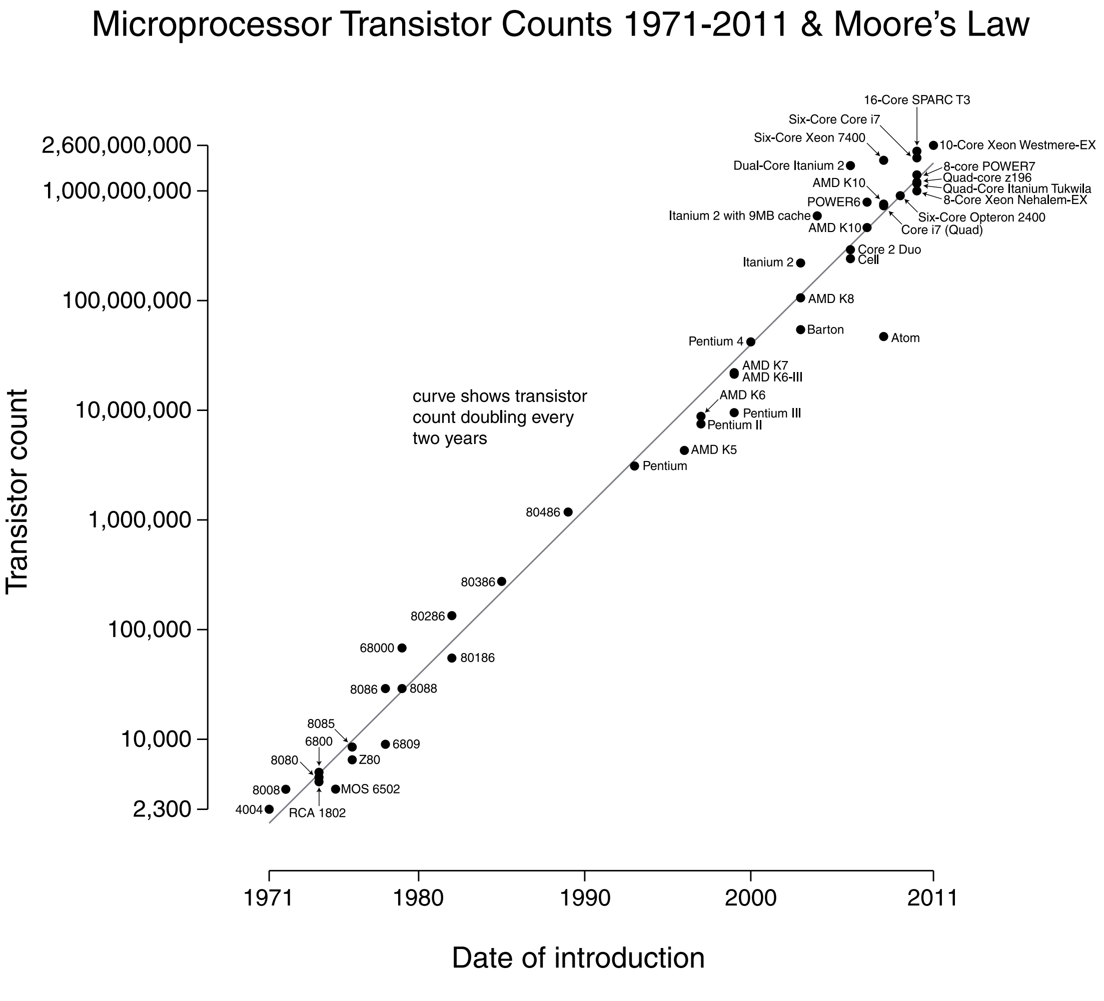

Figure 2.6: Moore's Law

enough to process a lot of data. Further on it is possible for every scientist and engineer to use their own computers to process image analysis. Hence this is a reason why digital image processing is rapidly expanding (Jähne; 2005, page 3).

By looking at today's pocket camera resolution (around 10 mega pixels) it can be seen that we are talking from about 10 (in case of a greyscale image) to 30 (in case of a colour image) million data cells per image. In case the interest lies on video analysis it should be mentioned that a standard video has about 24 frames (images) per second, but mostly a smaller resolution. All in all it is a lot of data.

2.4.1 Image

On the technical point of view an image is a huge array of digital numbers, or in other words, a multidimensional matrix. Two dimensions are needed to define the x and y coordinates of each element, called pixel. Pixel is an abbreviations of the word picture element (Jähne; 2005, page 31). Each pixel could have either one, in a greyscale (intensity) image, or three values, in a colour image. Fig. 2.7 (page 14) visualises this.

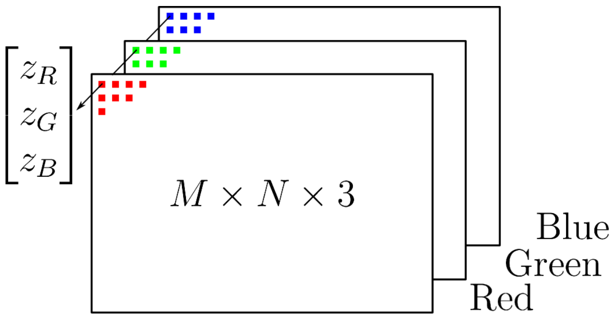

Figure 2.7: RGB image (Cattin; 2008, Fig. 2.22 on slide 30)

2.4.2 Colourspaces

The following section introduces two different colour spaces. The first one, RGB, is used by most cameras to store the sensor information. The second one, HSV, is needed for the colour classification (see Sect. 3.2 (page 29)).

2.4.2.1 RGB - Red Green Blue

The Red, Green and Blue (RGB) colour space is based on the idea that every colour is a combination of red, green and blue. With these three parameters a three dimensional matrix, or cube as displayed in Fig. 2.8 (page 15) and Fig. 2.9 (page 15), is defined, where every parameter goes from 0 to 100 percent.

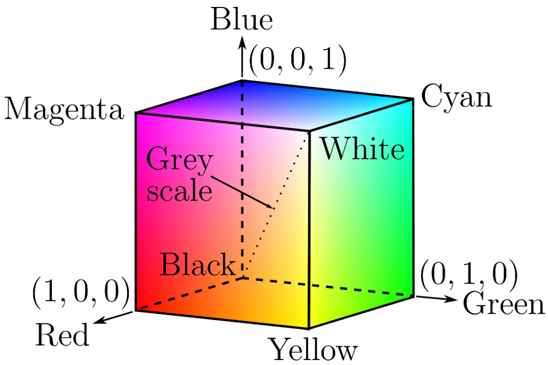

Figure 2.8: RGB colour cube (Cattin; 2008, Fig. 2.23 on slide 30)

There are 2 extreme cases. Case one is, that all three parameters are at 100%. This is the point where the resulting colour is white. The other is, that everything is zero. Here the resulting colour is black. Based on different combinations different colours are possible (displayed in Fig. 2.9 (page 15)).

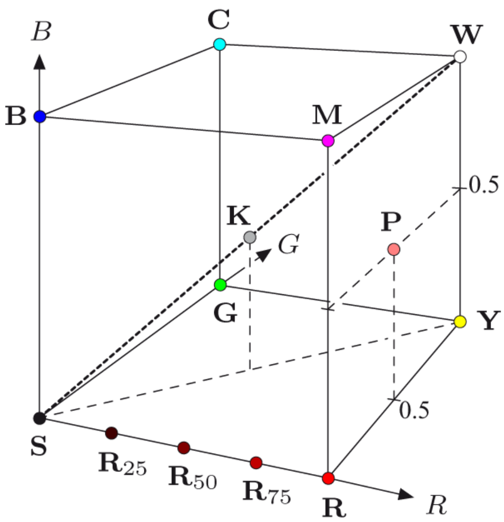

		RGB Value		
Point	Color	R	G	B
S	Black	0.00	0.00	0.00
R	Red	1.00	0.00	0.00
Y	Yellow	1.00	1.00	0.00
G	Green	0.00	1.00	0.00
C	Cyan	0.00	1.00	1.00
B	Blue	0.00	0.00	1.00
M	Magenta	1.00	0.00	1.00
W	White	1.00	1.00	1.00
K	50% Gray	0.50	0.50	0.50
$\mathbf{R}_{75}$	75% Red	0.75	0.00	0.00
$\mathbf{R}_{50}$	50% Red	0.50	0.00	0.00
$\mathbf{R}_{25}$	25% Red	0.25	0.00	0.00
P	Pink	1.00	0.50	0.50

Figure 2.9: RGB colour cube with colour combinations (Burger and Burge; 2009, Fig. 8.1 on page 186)

2.4.2.2 HSV - Hue, Saturation and Value

This colour space describes colours by their hue, saturation and value. Sometimes it is also called HSB (hue, saturation and brightness).

According to its mathematical definition it is a cylinder. As it can be seen in Fig. 2.10 (page 16), hue is the angle, saturation the radius and value the height of the cylinder. As described in (Burger and Burge; 2009, page 205) it is traditionally shown as upside-down, six-sided pyramid. A coloured visualisation is displayed in Fig. 2.11 (page 16).

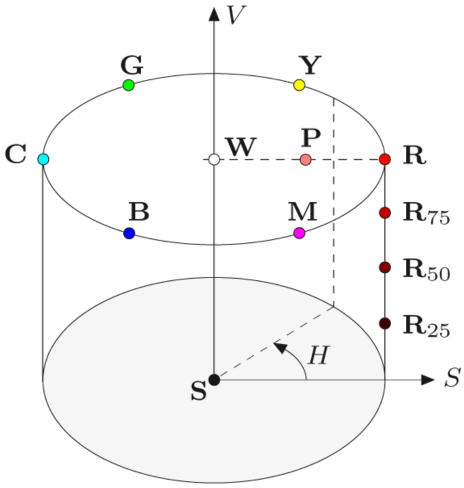

RGB/HSV Values

Pt.	Color	R	G	B	H	S	V
S	Black	0.00	0.00	0.00	—	0.00	0.00
R	Red	1.00	0.00	0.00	0	1.00	1.00
Y	Yellow	1.00	1.00	0.00	1/6	1.00	1.00
G	Green	0.00	1.00	0.00	2/6	1.00	1.00
C	Cyan	0.00	1.00	1.00	3/6	1.00	1.00
B	Blue	0.00	0.00	1.00	4/6	1.00	1.00
M	Magenta	1.00	0.00	1.00	5/6	1.00	1.00
W	White	1.00	1.00	1.00	—	0.00	1.00
$\mathbf{R}_{75}$	75% Red	0.75	0.00	0.00	0	1.00	0.75
$\mathbf{R}_{50}$	50% Red	0.50	0.00	0.00	0	1.00	0.50
$\mathbf{R}_{25}$	25% Red	0.25	0.00	0.00	0	1.00	0.25
P	Pink	1.00	0.50	0.50	0	0.5	1.00

Figure 2.10: HSV cylinder with colour combinations (Burger and Burge; 2009, Fig. 8.13 on page 209)

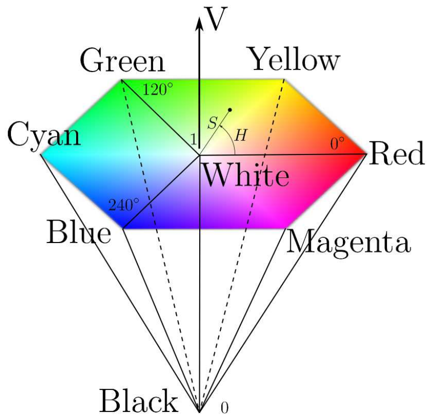

Figure 2.11: HSV hexagonal cone (Cattin; 2008, Fig 2.25 on slide 33)

2.4.3 Conversion to Greyscale

Converting a colour image to greyscale means, that an equivalent grey or luminance value Y for every pixel is computed. Burger and Burge describe in (Burger and Burge; 2009, page 201) that there are several ways to do this. If the colour space is RGB, the simplest one is to use an average value based on the red, green and blue values.

The perception is that red and green are brighter than blue. Therefore the result appears to be too dark in the red and green areas and too bright in the blue one. That is the reason why a weighted sum is used instead.

2.5 Image Noise

Image noise, or often just called noise, is a measuring error from the image sensor. The signals are affected by electronic noise. As a result wrong colour values are returned. Wrong means that they have no connection to the original image content. There are several approaches to reduce this effect and many of them are used camera intern. Going deeper into this complex topic is beside the purpose of this work.

2.6 Perspective View

The whole work is based on the analysis of horizontal movements of a particle from one point to another. The surface of the fluidized bed is not always completely flat and parallel to the camera sensor, therefore three dimensional movements are recorded. Without the information of the distance between camera and particle an exact measurement is not possible. If assumed that the information of interest is just the horizontal movement than this would not be a problem as long as the camera sensor has the same size as the observed area. For the cold flow model area of 900 cm^2 this would be really expensive.

A cheaper approach is to use a lens which projects the large area on a much smaller sensor. There are some physical limitations which should not be ignored.

The most important one is the perspective. If an object is closer to the camera it appears bigger than one that is more far away. In case the same object, but with a different distance, is projected onto the same sensor then the angle of view is different.

This means if an object is close to the camera a lens with a greater angle, often called as wide-angle, is needed. In contrast, if the distance of the object to the lens increases a lens with a smaller angle, telephoto-lens, is required. The angle of view, according to the focal distance, can be seen in Fig. 2.12 (page 18).

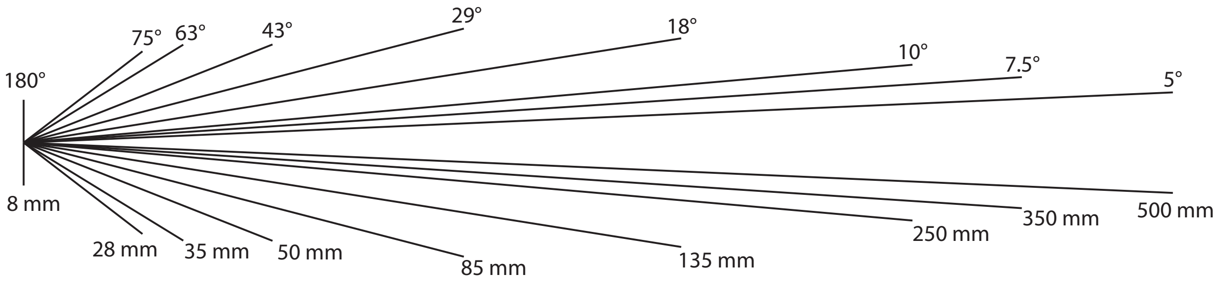

Figure 2.12: Angle of view for various focal distances

Based on the geometric information (correlation of distance and angle of view) the following can be seen. A particle, located close to the side of the cold flow model, changing its distance to the camera produce a horizontal movement. The amount of this is depending on the angle of view and the difference in distance. The difference of a 10 cm increase, according to the chosen angle of view, can be seen in Fig. 2.13 (page 18). Further on it is

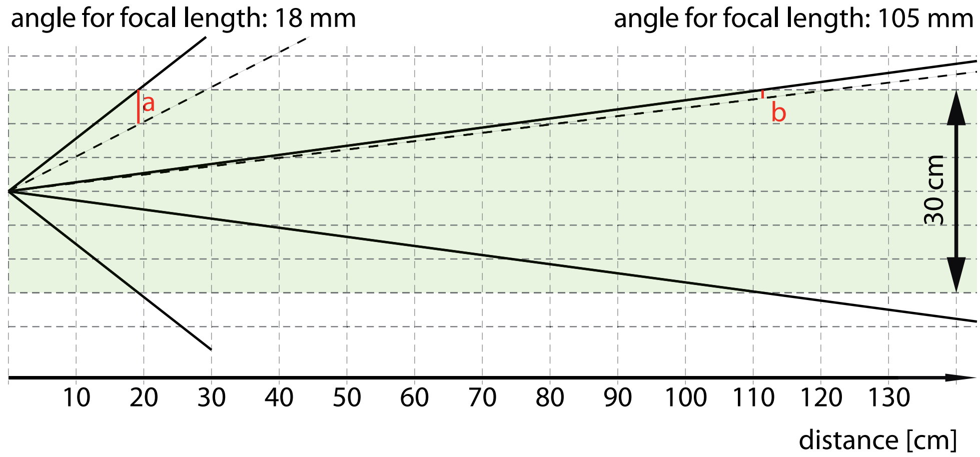

Figure 2.13: Diagonal angle of view of used lens. Used focal distance was about 50 mm. Dashed lines show the angle of view for a point 10 cm more far away.

shown additionally, that if a particle reduces the distance to the camera, for example if a bubble ejects a particle, it might be out of range and not detected any more.

The definition of the angle of view is based on the longest length, the diagonal (see Fig. 2.14 (page 19)).

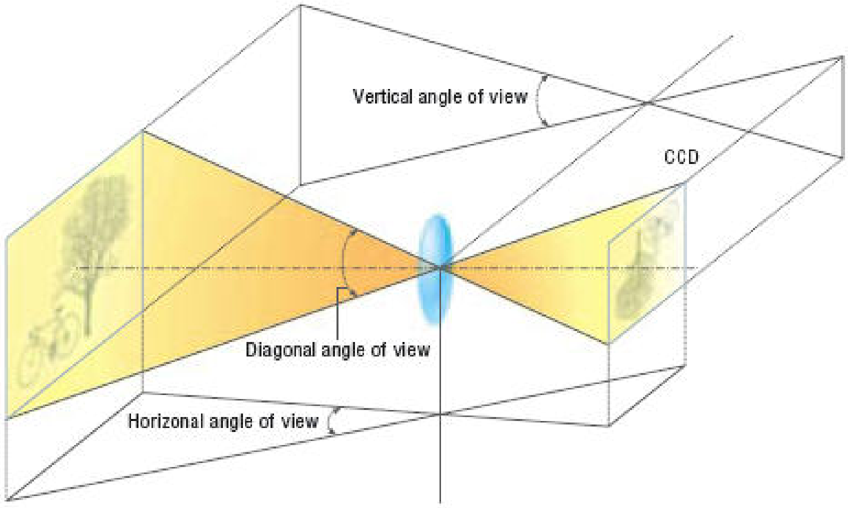

Figure 2.14: Angles of view for different lengths

Chapter 3

Method

There are several steps needed to extract desired data from video files. The wanted data (particle centroid coordinates and size) must be detected and classified. Figure 3.1 (page 21) shows two possible ways to do it. The left part shows the old and the right the new algorithm developed within this thesis. As it can be seen, the main parts are the same.

In both algorithms a mask, which is used to detect the objects, is created. In case of the old algorithm three (one for each colour) different masks are defined. Therefore the object detection is called for all different colours separately and the results are already categorised.

In contrast, the new algorithm is more complex. First some filters are applied before the mask is generated. This mask is valid for all colours and extracts the particles. Consequently the particles have to be classified, based on their colours, afterwards.

The following sections describe the different steps of the new algorithm.

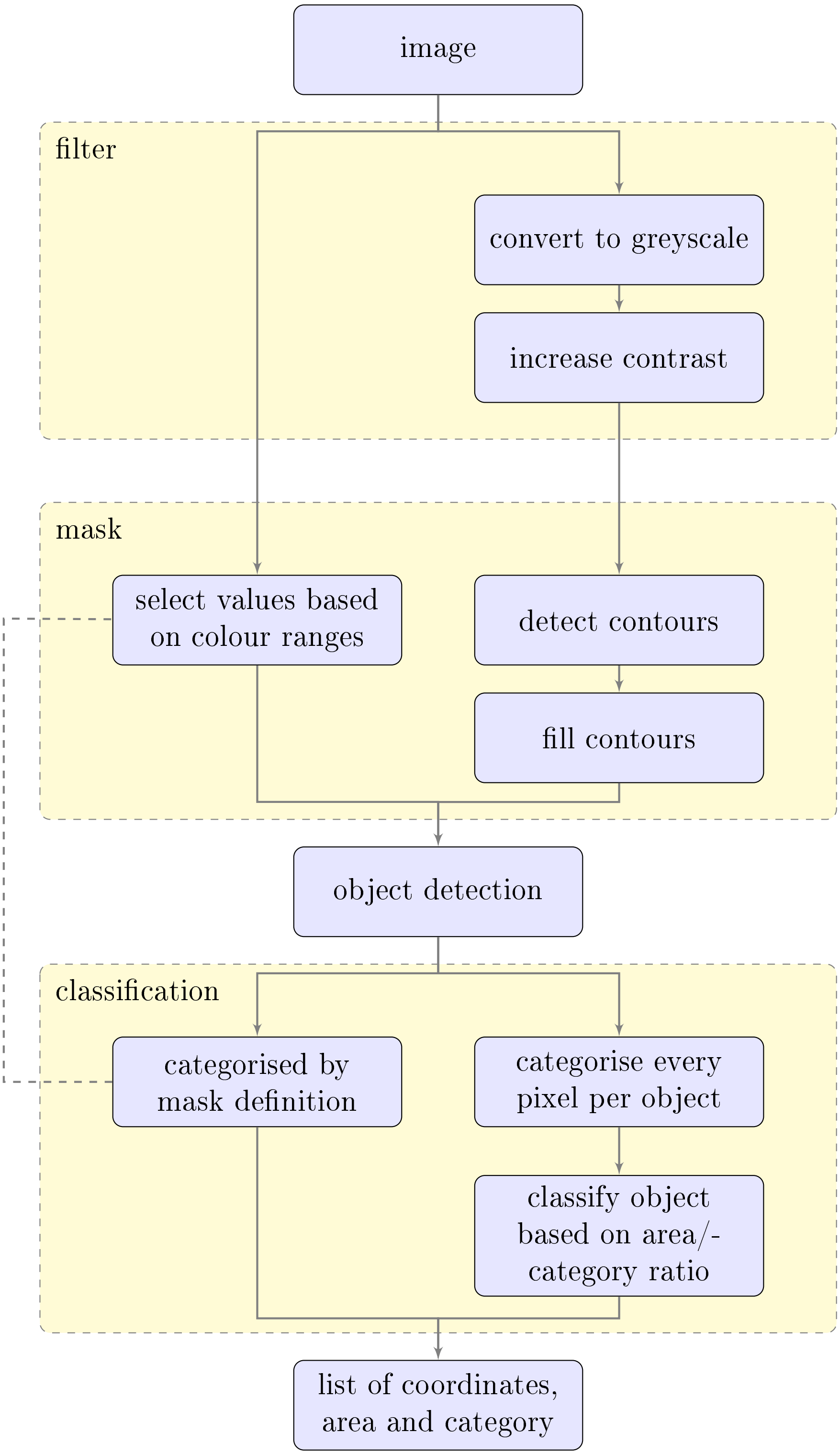

Figure 3.1: Basic detection algorithm steps with two implementations. Left part describes the old, right the new algorithm.

3.1 Particle Detection

There are many ways to extract particles from an image, but most of them have similar steps. As already described a mask is needed. This mask is used to filter some parts from the rest of the image.

Afterwards these extracted parts have to be identified as objects. This means that connected areas have to be found. There are several ways how this can be done. In this work the focus lies on the detection of connected coloured regions to extract them and compute their centroid coordinates. These objects, now seen as particles, are classified afterwards before they are used for further calculations.

Previous Algorithm In the previous algorithm the mask creation and categorisation was done in a single step. It was done by filtering the image with a specific filter for one colour (e.g. red). As described in Sect. 3.2.1 (page 29) some kind of colour borders are needed. Therefore an upper or lower limit for red and green together with two different limits for blue (has two different areas) are used.

It is very important to mention that it was just an upper or lower limit. By looking at the RGB cube (Fig. 2.8 (page 15)) defining a region with just one limit means that it always has to go until the maximum or minimum values (to the outer sides of the cube). It is not possible to define some regions in the middle with just one limit. Therefore it is more complicated, if possible, to use different colours in parallel.

The created mask (for a specific colour) is used to detect the objects afterwards. Because it was just defined for one colour the found objects are already categorised. The biggest advantage of this code is, that it is really fast. As most important disadvantage the greater colour definition sensitivity is pointed out. More on this and the problems with it are described in Sect. 3.1.1 (page 24).

Idea of New Algorithm The idea of the new detection algorithm is, that it extracts those areas detected as particles first and categorises them afterwards. To find those regions, several steps are needed.

First is computed by detecting the edges of all particles and filling those contours afterwards.

The mask is analysed to find connected regions (true values of the binary image), the particles. Further on the colour of each selected pixel is categorised based on the definitions, chosen in Sect. 3.2.1 (page 29). The results of these main steps are shown in Fig. 3.2 (page 23).

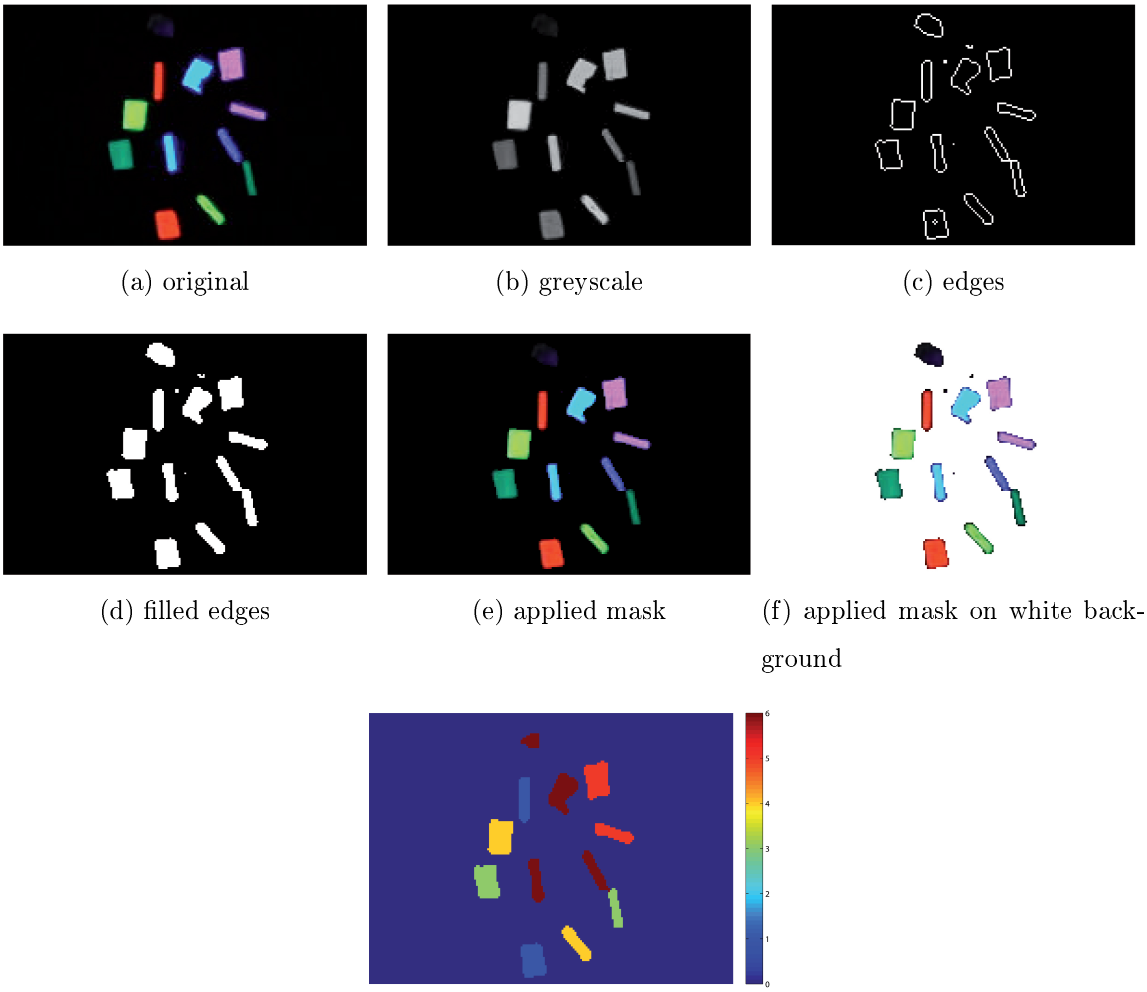

(a) original

(b) greyscale

(c) edges

(d) filled edges

(e) applied mask

(f) applied mask on white background

(g) categorised particles

Figure 3.2: Main steps of the new algorithm displayed as images. Applied mask is printed on white background for presentation purpose, therefore (f) is an optional plot.

As result a list of all particles with category, frame number (time), area and coordinates of their centre is returned.

3.1.1 Creating a Mask

A mask is a kind of selector, a binary image (values of each pixel is either true (1) or false (0)). It describes with its Boolean values if a pixel should be chosen or not. Compared to the original image this is a data reduction of more than two thirds (extremely depending on the storage implementation).

It is needed to separate the particles pixels from those of the bed material. In other words, the particles are extracted. There are several different ways the mask can be computed.

One is to find those regions with similar colours by checking its colours with a lookup table and use the result of this step as mask (old algorithm). This method is really fast, because it just checks every pixel with RGB colour borders.

In this work a more complex way with edge detection and filling was chosen. The reason for this was, that the old algorithm is very sensitive to a good colour definition list. This means if a colour is not in the colour list, the pixel was not selected by the mask. In other words this means, that the area of a particle is wrong or multiple particle (with wrong and smaller areas) are detected.

Figure 3.3a (page 24) shows the shape of a particle. In case some parts are covered, or the colour intensity is different a particle might look like the one displayed in Fig. 3.3b (page 24). If the middle section is not defined in the colour range, these pixels are not selected. As result Fig. 3.3c (page 24) will run through the object detection process and instead of one large particle two smaller ones are extracted (with different centroid coordinates).

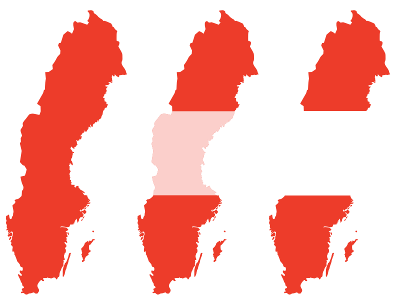

(a) particle (b) covered (c) split

Figure 3.3: Colour sensitivity demonstration

Contrary the new algorithm detects the particle shape and classifies it based on the mean category. Therefore the whole particle is detected.

In case the colour borders (of the old algorithm) are extended, it is likely that some parts are detected which are not correct. For instance it has been observed that the old algorithm often detects parts of the bed material as particles, because it looks bluish if the ultraviolet (UV) lamp is too close.

Summarised this means that the old algorithm could separate particles, if specific colours are not defined and the new always detects the whole particle before it is categorised afterwards.

3.1.1.1 Edge Detection

Figure 3.4a (page 25) shows the values of red, green and blue from a part (dotted line in Fig. 3.4b (page 25)) of the image. This plot, called histogram, shows that there are

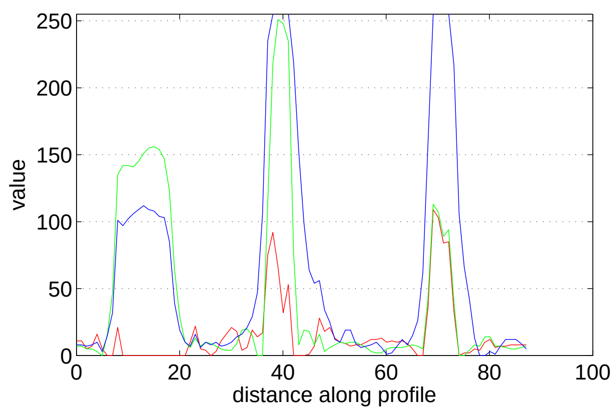

(a) histogram

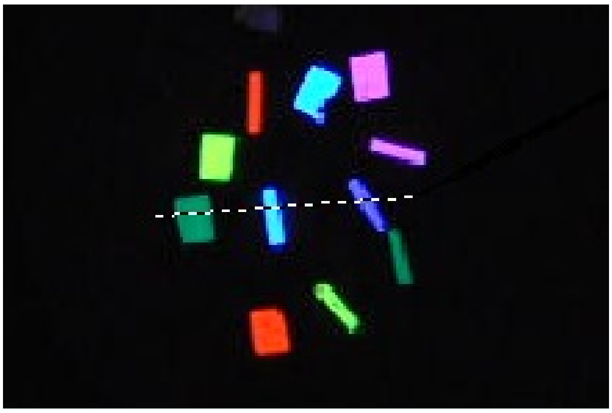

(b) dotted line shows the histogram origin

Figure 3.4: Colour histogram and its location

huge gradients for each colour. To see the intensity difference the image is converted into greyscale (see Fig. 3.5a (page 26)). The used data type is unit8, defined from 0 to 255. Therefore the ordinate goes from 0 to 255.

According to literature, there are several ways to compute the location on the actual edge. In this work a method based on the second derivative is used. The second derivative measures the local curvature of a function. Figure 3.6 (page 26) illustrates the idea behind this.

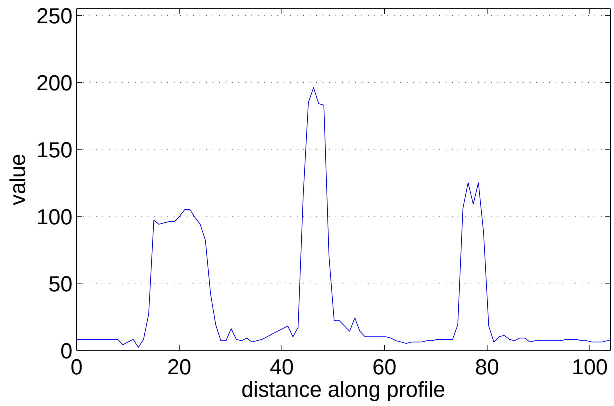

(a) histogram of greyscale image

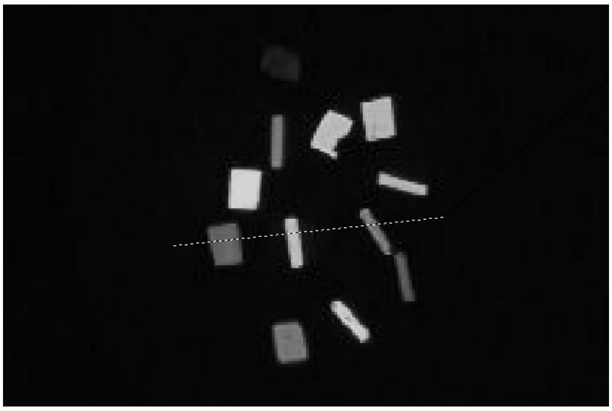

(b) dotted line shows the histogram origin

Figure 3.5: Greyscale histogram and its location

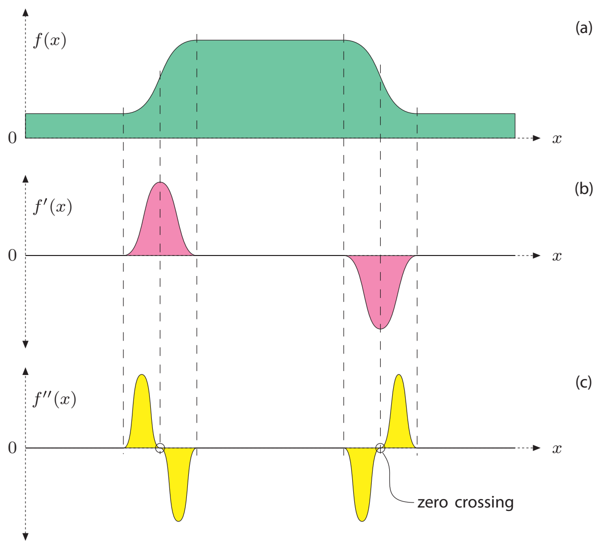

Figure 3.6: Principle of edge detection with the second derivative: original function (a), first derivative (b) and second derivative (c). Edge points are located where the second derivative crosses through zero (Burger and Burge; 2009, Fig. 6.9 on page 143)

3.1.1.2 Filling

Soille wrote in his book, that "holes of a binary image correspond to the set of its regional minima which are not connected to the image border" (Soille; 1999, page 173-174). The author provided an algorithm to close those holes which was used in this work. The result of the filled contours can be seen in Fig. 3.2d (page 23).

3.1.2 Region Detection

This is a very important step in the detection algorithm. Now the connected regions (often called connected components) are detected.

In literature this step is categorised as a segmentation step. Jähne describes in his book (Jähne; 2005, page 454-458) that this is quite a complex algorithm. According to him it is theoretically not possible to solve it in a direct way, which makes it time consuming. Going deeper into this algorithm is beyond the purpose of this work. As a result, a list of objects with centroid coordinate and area is returned.

3.1.3 Particle Classification

In a first approach the mean colour was used to classify particles. It was found that this is not working for two reasons. First, if multiple particle stick together the calculated mean colour leads to wrong classifications. Second, dark particle edges changes the mean colour. Furthermore this effect increases for smaller particles, because the particles circumference compared to its area is larger.

On the right bottom side of Fig. 3.7 (page 28) two connected particles can be seen. By comparing these images with Fig. 3.2a (page 23) it can be seen that their colours are different. In conclusion, this approach was discarded and a new one was developed, where every pixel is categorised.

Based on the classification borders (see Sect. 3.2 (page 29)) every pixel of each particle is classified. Each category is checked if the colour is inside the colour borders.

Afterwards the particle is categorised based on the main category. Sometime it happens that particles stick together. By just categorising the particle to the main category an information loss is produced. Therefore the particle is sorted into several categories,

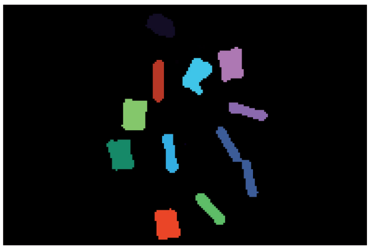

(a) Particle with mean colour

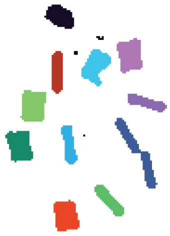

(b) Particles with mean colour on white background

Figure 3.7: Particle mean colour

if the amount of categorised pixels reaches a certain level. This level is very important. Imagine if just one pixel is detected in a second category. Without this level the particle would be sorted into a second category.

As described before, it is sorted into several categories. This means that the same detected particle is in multiple categories, with the same size and coordinate.

This simplification does of course have an influence on the results. Wrong centroid coordinates leads to different dispersion coefficients (see Sect. 3.4.2 (page 49)).

Shorter distances are more affected than long ones. For single particle tracking the problem with connected particles was observed very rarely, probably because the surface times are quite low. Therefore a filter to split connected particles was not developed.

In contrast, in multiple particle spreading experiments only one colour was used. Therefore it would be interesting to separate connected particles of the same colour as well. Especially the results in the beginning are affected, because there are many particles located close to each other.

Such a filter should split particles. Further on it should be avoided that the area of these particles is changed. Developing and validating such a filter is difficult and therefore time consuming, which is the main reason why it was not developed during this work and hence not used.

3.2 Colour Classification

During the experiments videos are recorded. These videos contain information (size, location) of coloured particles. To increase the contrast between bed material and particles the experiments are carried out under UV light conditions with special coloured particles (see Sect. 4.1.2 (page 63)). These particles have to be categorised, based on their colours. The problem is that the colour of each detected pixel per particle is not exactly the same.

Reasons for this are various. For example the particles could be covered by a thin layer of bed material decreasing the intensity of the colour. If the coat thickens is different, the colour can be influenced by the particle material, because it is not fully covered. Furthermore the intensity of a particles colour is depending on the strength of the UV radiation. There are some small bed material particles above the bed. This decrease the recorded particle colour intensity. Additionally it is depending on the distance particle-lamp and particle-camera.

To classify a particle, some kind of colour ranges are needed. These limits should be as narrow as possible to exclude all other colours and as wide as necessary to include all colours of a single category. Additionally it would be preferable that the borders are described by the same parameters for each category and with as less parameters as possible. Furthermore a way should be chosen which is not CPU-intensive to use afterwards, because, as described in Sect. 3.1.3 (page 27), this classification is called very often during the extraction algorithm. Finding these borders is described in the next section.

3.2.1 Find Classification Borders

The classification borders were found by recording several videos with many same coloured particles. To find possible errors in the detection algorithm a video without any particles was recorded additionally.

Sometimes it has been seen that there are some unpainted areas on the particles, because the UV active paint adhere not really good on the aluminium[1] surfaces. To find the influence of this, a video with unpainted particles was recorded.

[1] more on particles see Sect. 4.1 (page 60)

All these video files were analysed to find all different, unique, colours. Therefore all "particles" have been extracted by using the extraction algorithm described in Sect. 3.1 (page 22).

From these regions (detected as particles) a list of all colour values of each pixel was extracted. Figure 3.8 (page 31) shows the extraction result. The amount of the different colours (per video file) is represented in the diameter of each data point. This plot also visualises, that there are overlapping regions between the colours.

Choosing classification borders is nothing else, than setting limits for different areas, or in this case volumes. For the colours extracted in the video with red particles (see Fig. 3.9 (page 32)), this could be described by a rectangular prism.

In contrast, it is not possible to define a narrow border prism for the white particle video (see Fig. 3.10 (page 32)).

This problem was solved by converting the colours into the HSV colour space. As written in Sect. 2.4.2.2 (page 16) here the colours are defined by their hue, saturation and value. Especially the first parameter is very important. All the converted colours can be seen in Fig. 3.11 (page 33). Figure 3.12a (page 33) only includes the red data and Fig. 3.12b (page 33) red and white.

Now the limits can be defined by six values, a lower and upper limit for each parameter (hue, saturation and value). After removing overlapping regions with other colours the borders were set. The limits for the red class can be seen in Fig. 3.13 (page 34). All limits with colours are represented in Fig. 3.14 (page 35) and Fig. 3.15 (page 36). Figure 3.16 (page 36) shows them without the colours.

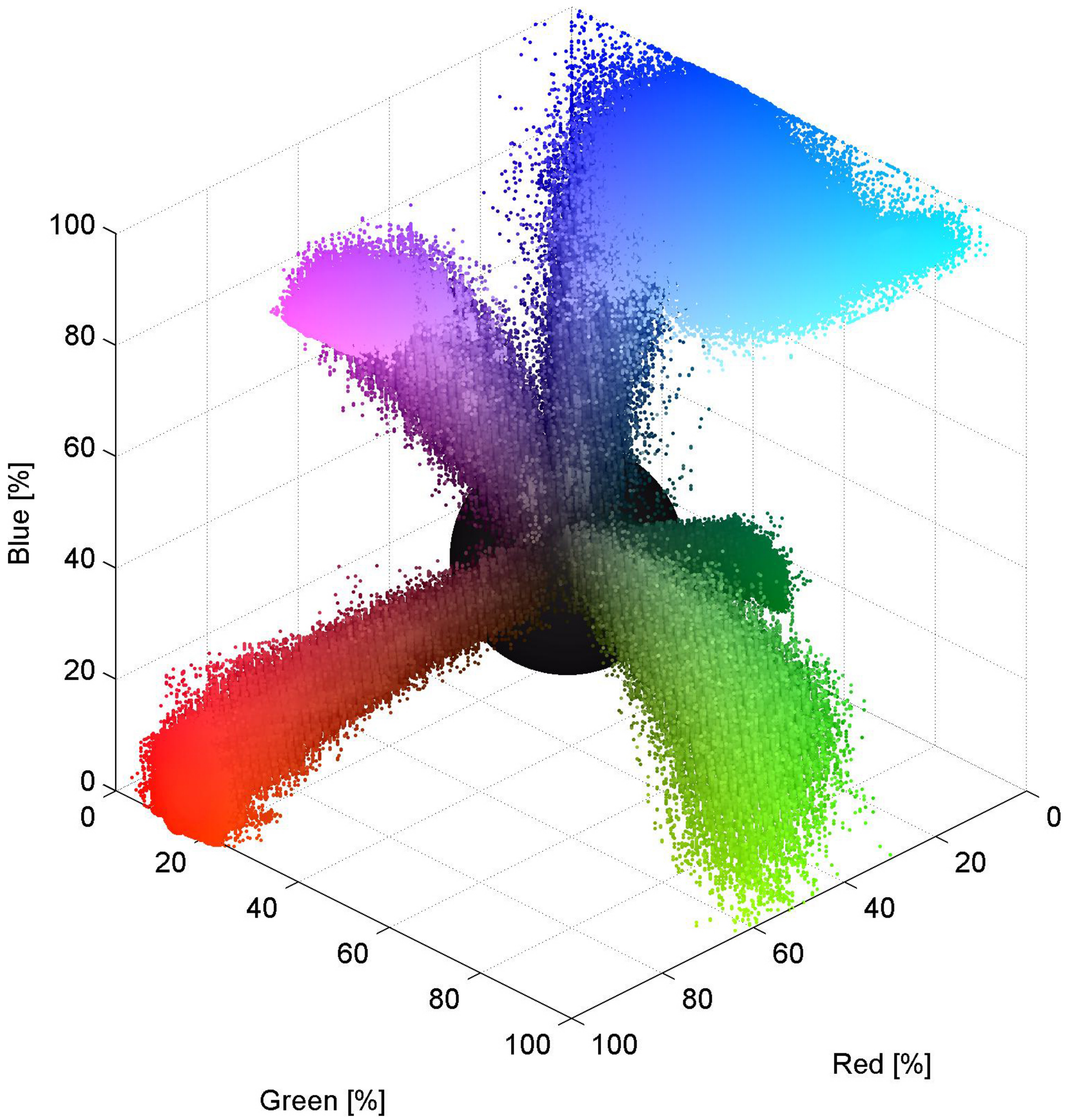

Figure 3.8: Detected colours. The amount of a specific colour, detected in a video, is used as circle diameter. Larger circles are colours (per video file) more often detected.

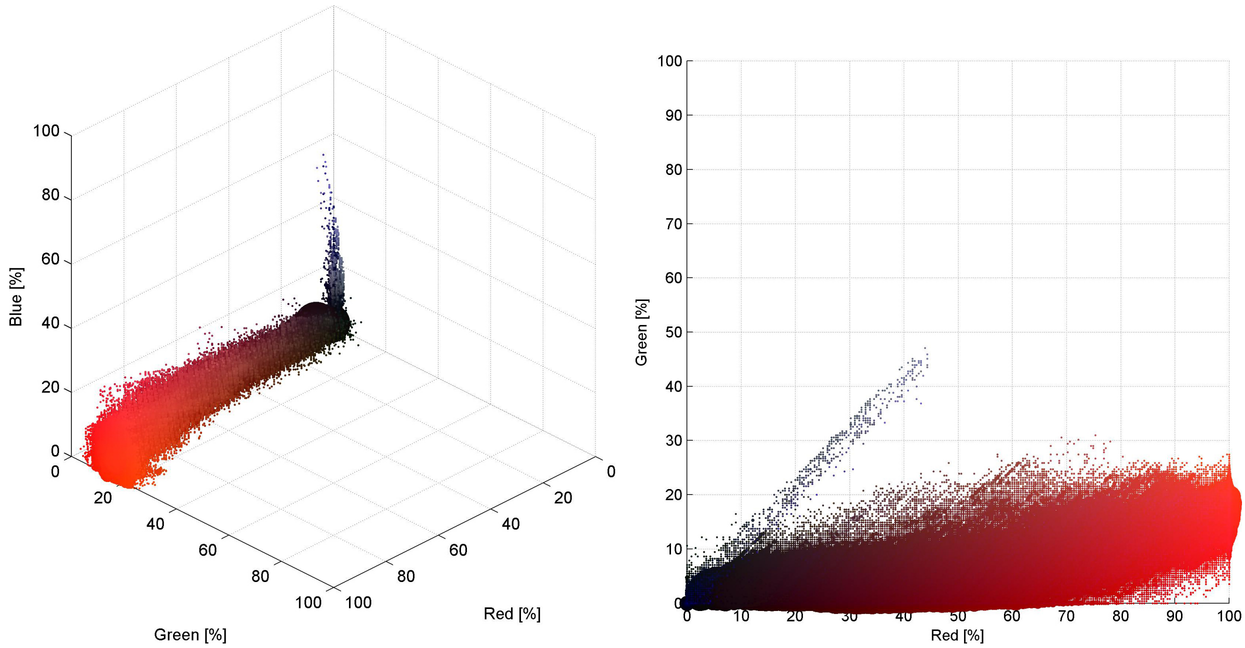

(a) three dimensional (b) two dimensional

Figure 3.9: Colours found in video with red particles. The amount of a specific colour, detected in a video, is used as circle diameter. Larger circles are more often detected colours.

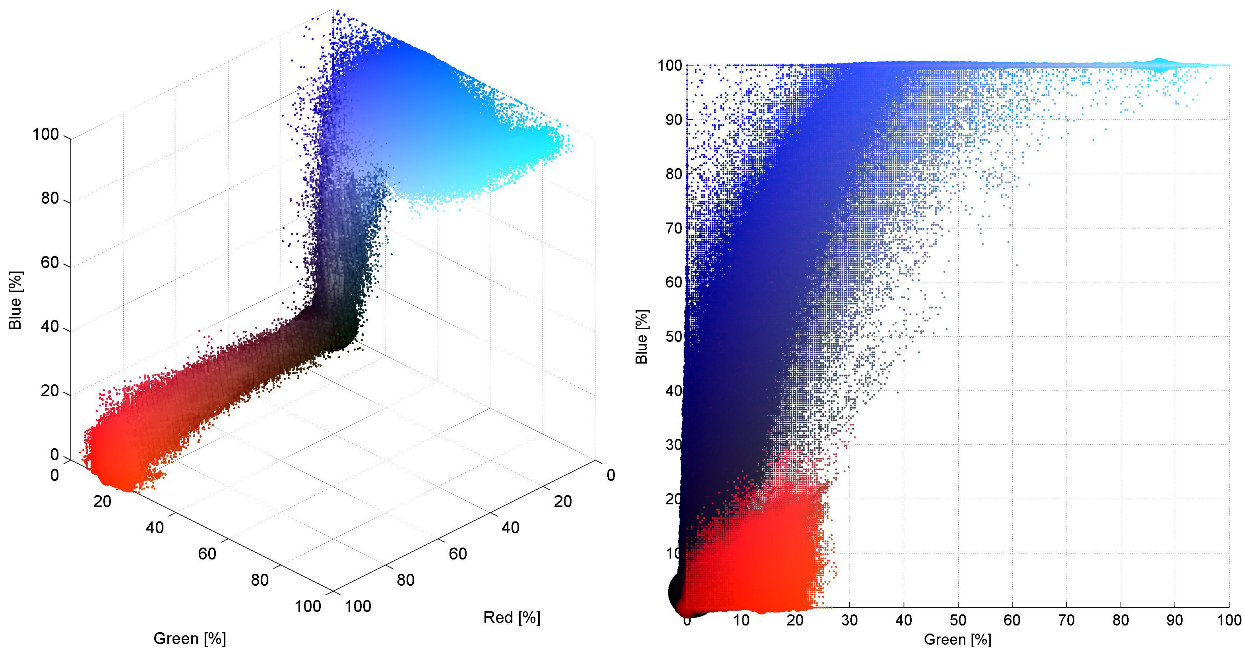

(a) three dimensional (b) two dimensional

Figure 3.10: Colours detected in videos with red and white particles

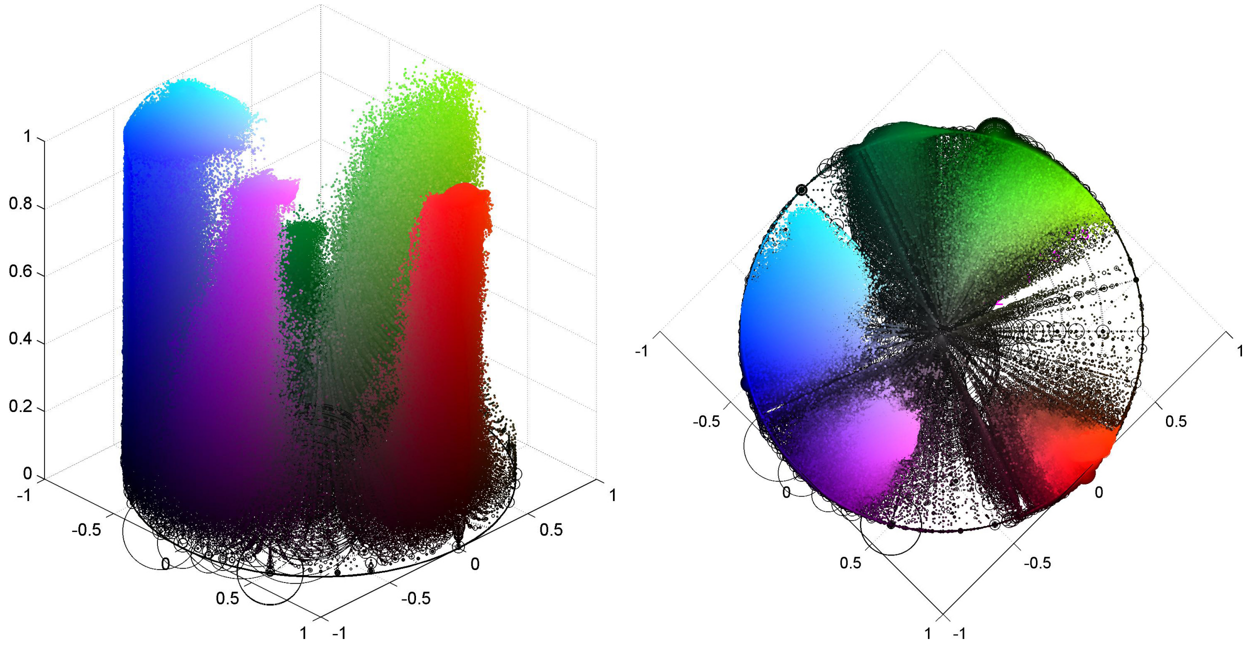

(a) three dimensional (b) from above

Figure 3.11: Converted colours in HSV colour space

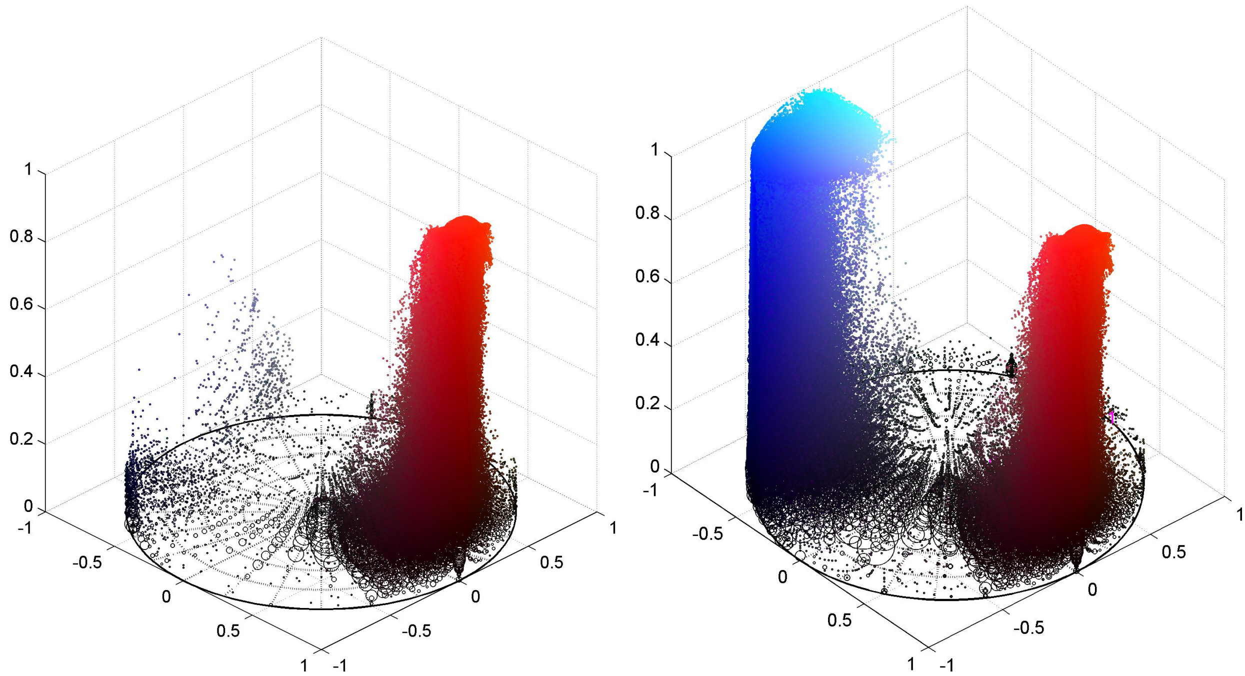

(a) HSV colours of red particle video (b) HSV colours of red or white particle video

Figure 3.12: HSV colours of a single video file and in combination with a second one

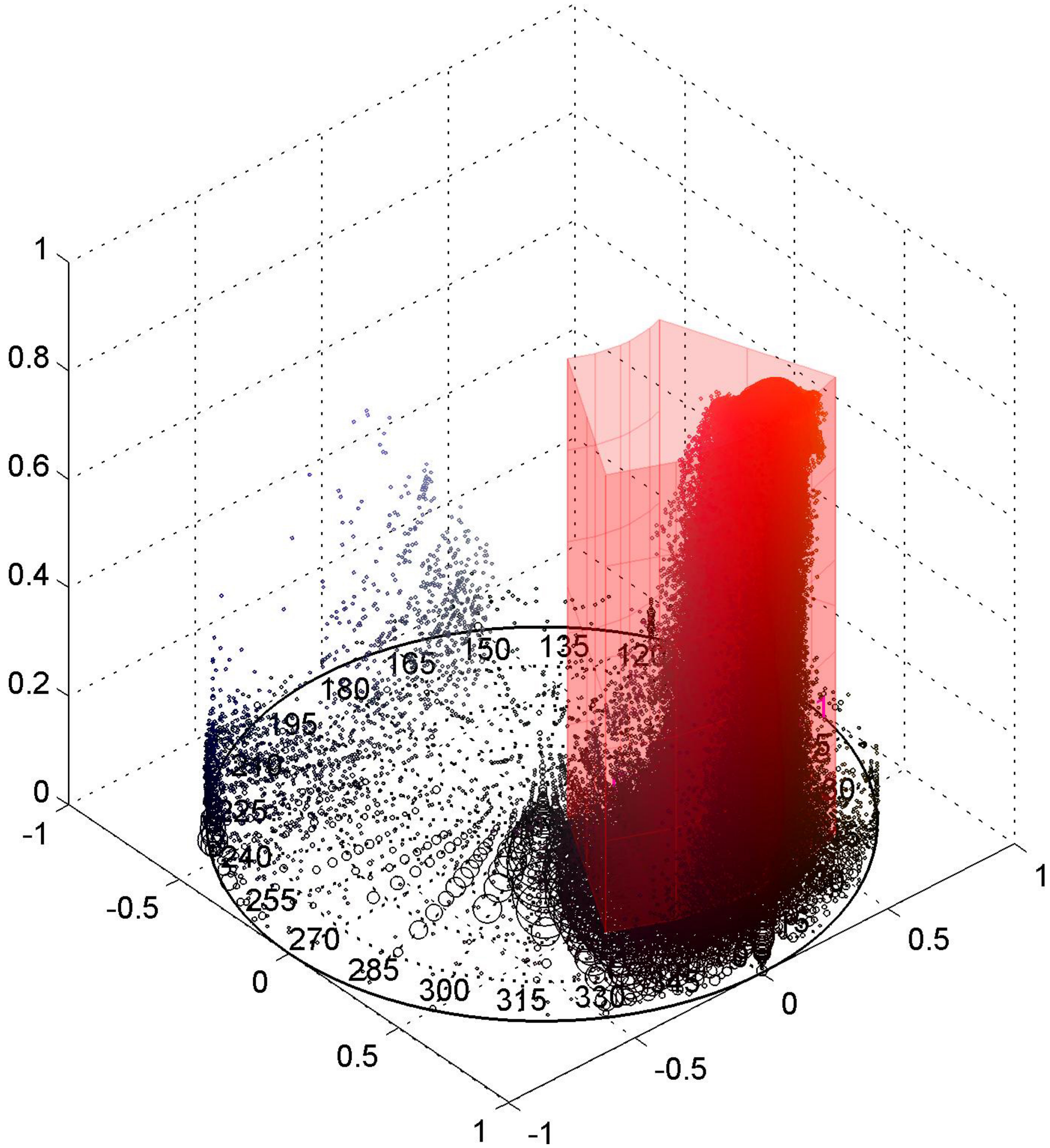

Figure 3.13: HSV colours of red video and classification limits

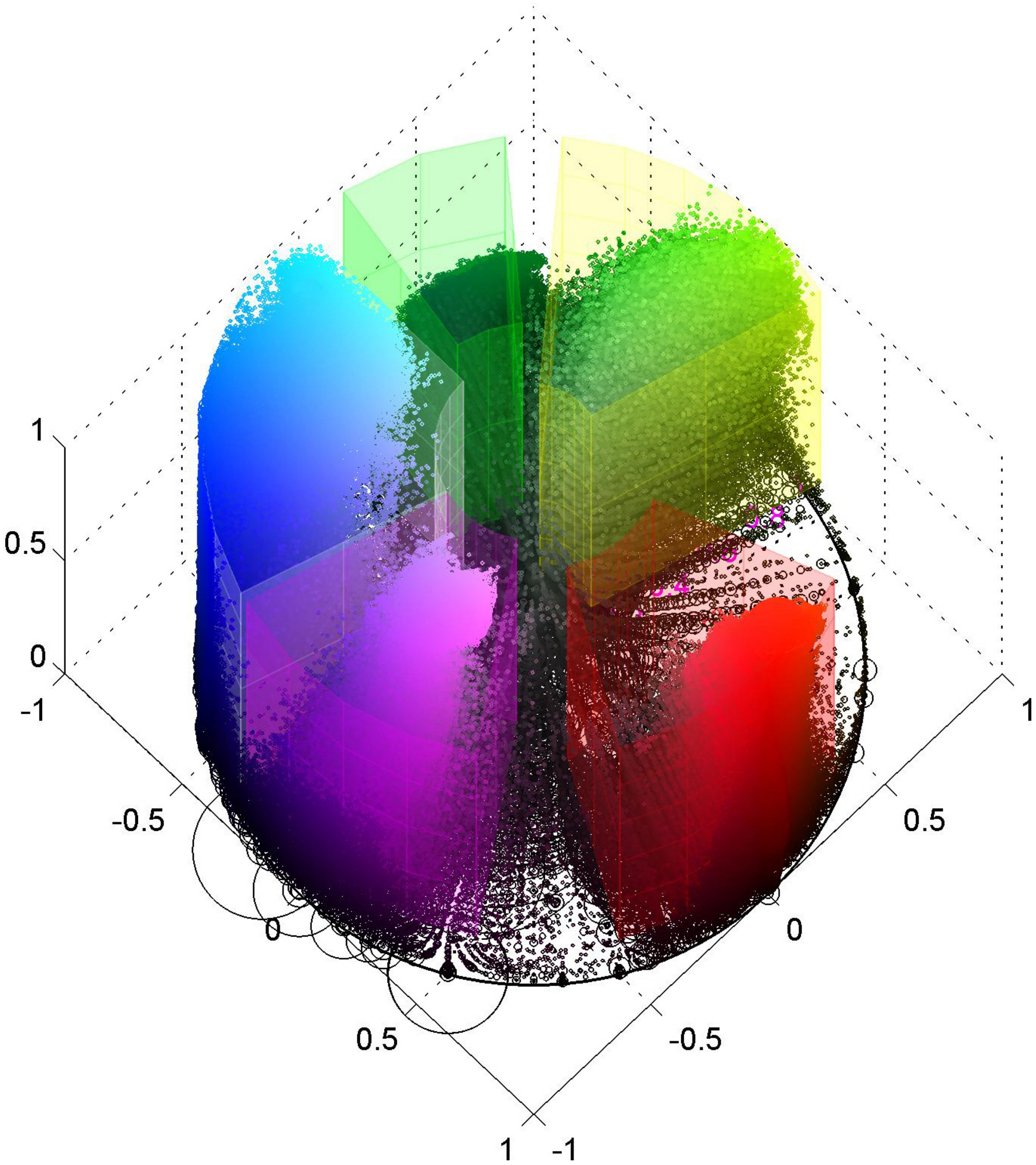

Figure 3.14: Converted colours of all particles and their borders in a large graph seen from aerial perspective

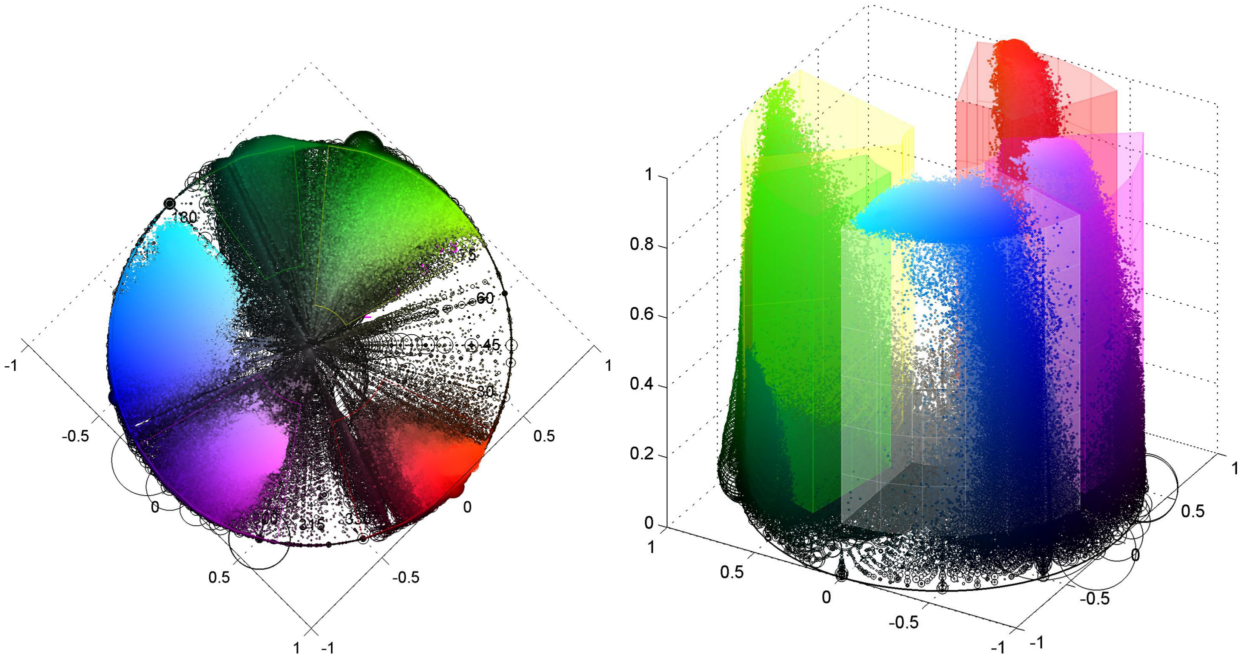

(a) above (b) rotated

Figure 3.15: Converted colours of all particles and their borders

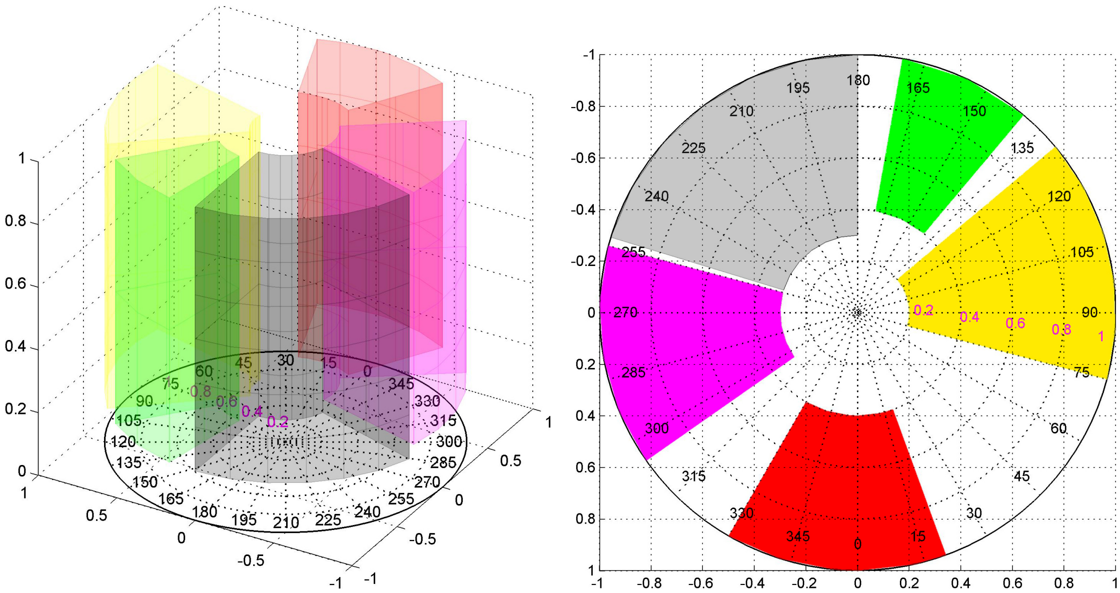

(a) three dimensional (b) above

Figure 3.16: Classification borders in HSV space. White border is displayed in black.

3.2.2 Verification

To verify the chosen borders the video files were analysed again to see if some of the particles are sorted into wrong categories.

The results of this can be seen in Table 3.1 (page 38). This table shows that the percentage of particles detected in the wanted category varies between 49.19 and 91.42 %. Additional it is shown, that the quality of the categorised particles is good (98.44 to 99.30%). This means that if something is categorised, then it is in the correct category. The small percentages of detected particles per category for green and yellow occur from the very tight border definitions for these two regions. This was necessary, because the detected colours are quite similar. The pink section was chosen quite small as well, because of superimpositions with the white and red regions.

This approach was chosen, because the possibility that a particle is detected is higher if there are more particles in the bed. Of course not everything will be categorised, but the sum of the percentages per category for yellow and green is greater than 100 percent. In conclusion there are more detections on the end.

3.2.3 Algorithm Limitation

Particles close to the edge of the video are not categorised correctly, because the contour is not closed. As result the contour mask cannot be filled and runs by itself through the object detection algorithm, producing many small particles. In case these objects can be classified, multiple particle are extracted.

This problem was neglected, because if something is very close to the wall it will be removed anyway during the wall check. Furthermore the size of detected particles is checked. Therefore it should be removed as well, because their sizes are much smaller.

		particle colour						
		red	green	yellow	pink	white	unpainted	no
	amout of used particles	27	10	10	6	6	6	0
classified as	red	12647	0	0	19	7	0	0
	green	0	4938	145	0	0	0	0
	yellow	0	66	10462	0	0	0	0
	pink	0	0	0	4121	69	0	0
	white	101	12	4	33	10734	0	0
	not categorised	1320	5023	8408	1657	931	8	0
	total amount of detected	14068	10039	19019	5830	11741	8	0
	amount of categorised	12748	5016	10611	4173	10810	0	0
	amount of not categorised	1320	5023	8408	1657	931	8	0
	percentage of detected particles per category							
classified as	red	89.90	0.00	0.00	0.33	0.06	0	0
	green	0.00	49.19	0.76	0.00	0.00	0	0
	yellow	0.00	0.66	55.01	0.00	0.00	0	0
	pink	0.00	0.00	0.00	70.69	0.59	0	0
	white	0.72	0.12	0.02	0.57	91.42	0	0
	particle categorised	90.62	49.97	55.79	71.58	92.07	0	0
	particle not categorised	9.38	50.03	44.21	28.42	7.93	100	0
	percentage of categorised particles per category							
classified as	red	99.21	0.00	0.00	0.46	0.06	0	0
	green	0.00	98.44	1.37	0.00	0.00	0	0
	yellow	0.00	1.32	98.60	0.00	0.00	0	0
	pink	0.00	0.00	0.00	98.75	0.64	0	0
	white	0.79	0.24	0.04	0.79	99.30	0	0

Table 3.1: Colour border verification results

3.3 Analysis Models

In this work two different analysis methods were developed. Both of them are described in this section.

3.3.1 Single Particle Tracking

The aim of this method is to follow a single particle during a long time. Based on its movements the dispersion coefficient is calculated with Eq. (2.3.2) (page 11).

In a fluidised bed the particle is not always on the surface and can therefore not be followed by a video camera, all the time. The only way to compute the movement is to use its coordinates and the time difference whenever it appears.

Some of these assumed movements are not correct, because the particle movement might intersect with a wall. In other words, it maybe would like to move through a wall. As a result of this intersection the particle will be detected somewhere else. To reduce the influence of this, those movements are removed during the calculation ("wall-check"). This is done by computing a mean dispersion coefficient of all valid movements. Based on the current value of the dispersion coefficient and the time needed for each movement, the Einstein equation is used again to compute a mean expected distance. If one point (centre coordinate of a detected particle) of a movement is closer to the wall than this distance, then both movements, using this point, are removed. As it can be seen in Fig. 3.17 (page 40) the movement is only removed for one coordinate, because it could be valid for the other.

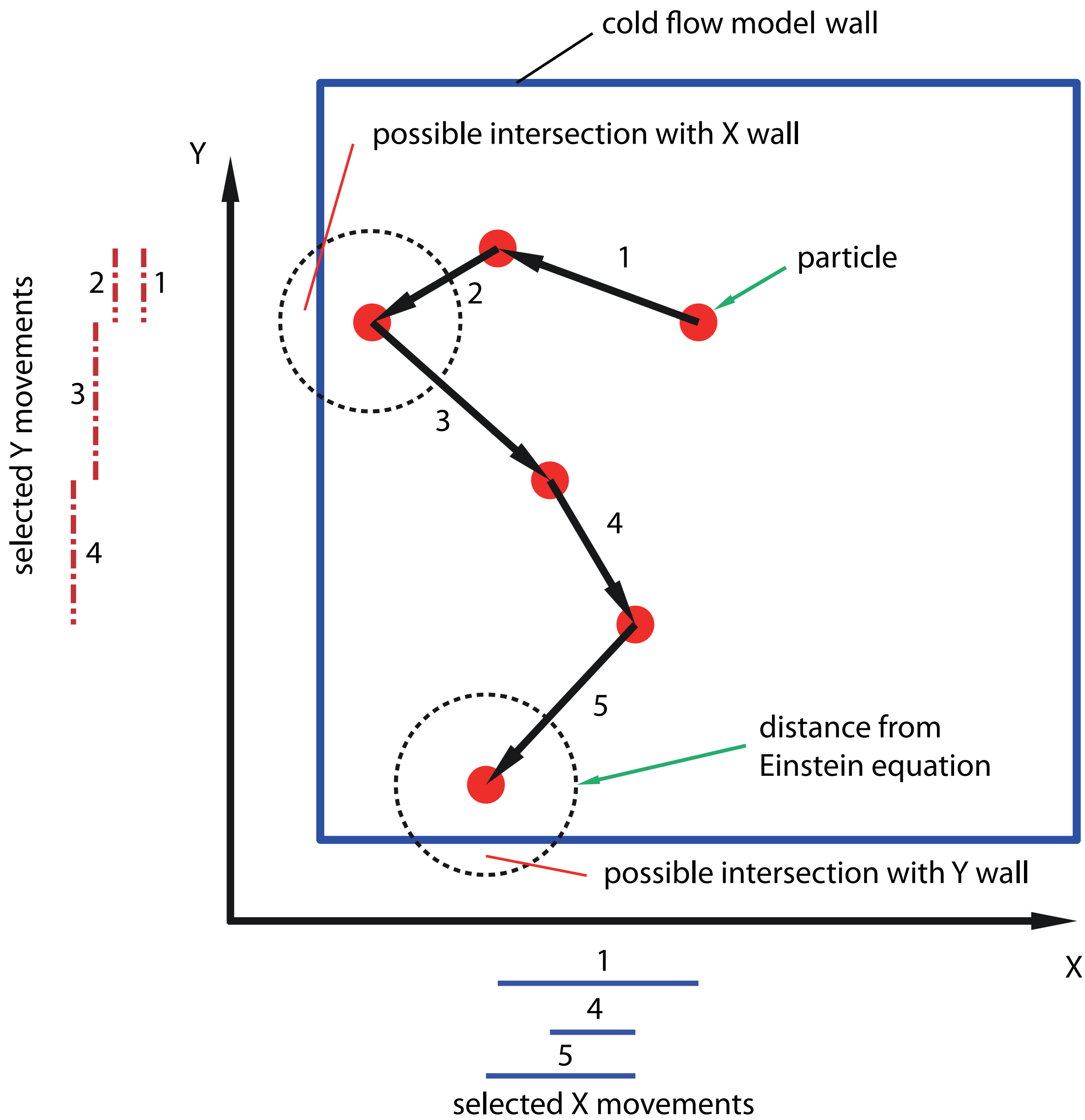

Figure 3.17: Selected movements during wall check

To reduce the influence of large dispersion coefficients based on points close to the wall the following model was developed. As already described before, the mean value of the dispersion coefficient is used to compute the expected distance between observations. In case of a large coefficient the corresponding distance would be quite big. If this happens many points close to the walls are removed. If the mean dispersion coefficient without these movements is much lower than the distance is shorter and some of the removed movements might be valid. To avoid this effect, the mean dispersion coefficient is increased whenever nothing was removed. This means that it is checked (e.g. with 10 percent of D_{mean}) if something is too close to a wall. In case it is, these movements are removed and the mean value is calculated again. Otherwise the percentage is increased. This should prevent that too many movements are removed by the algorithm. Figure 3.18 (page 42) shows the implementation of this. It is executed for every colour and direction. The percentage values used are predefined with 0.0001, 0.005, 0.01, 0.05, 0.1, 0.2, 0.3, 0.4, 0.5, 0.6, 0.7, 0.8, 0.9 and 1 times D_{mean}.

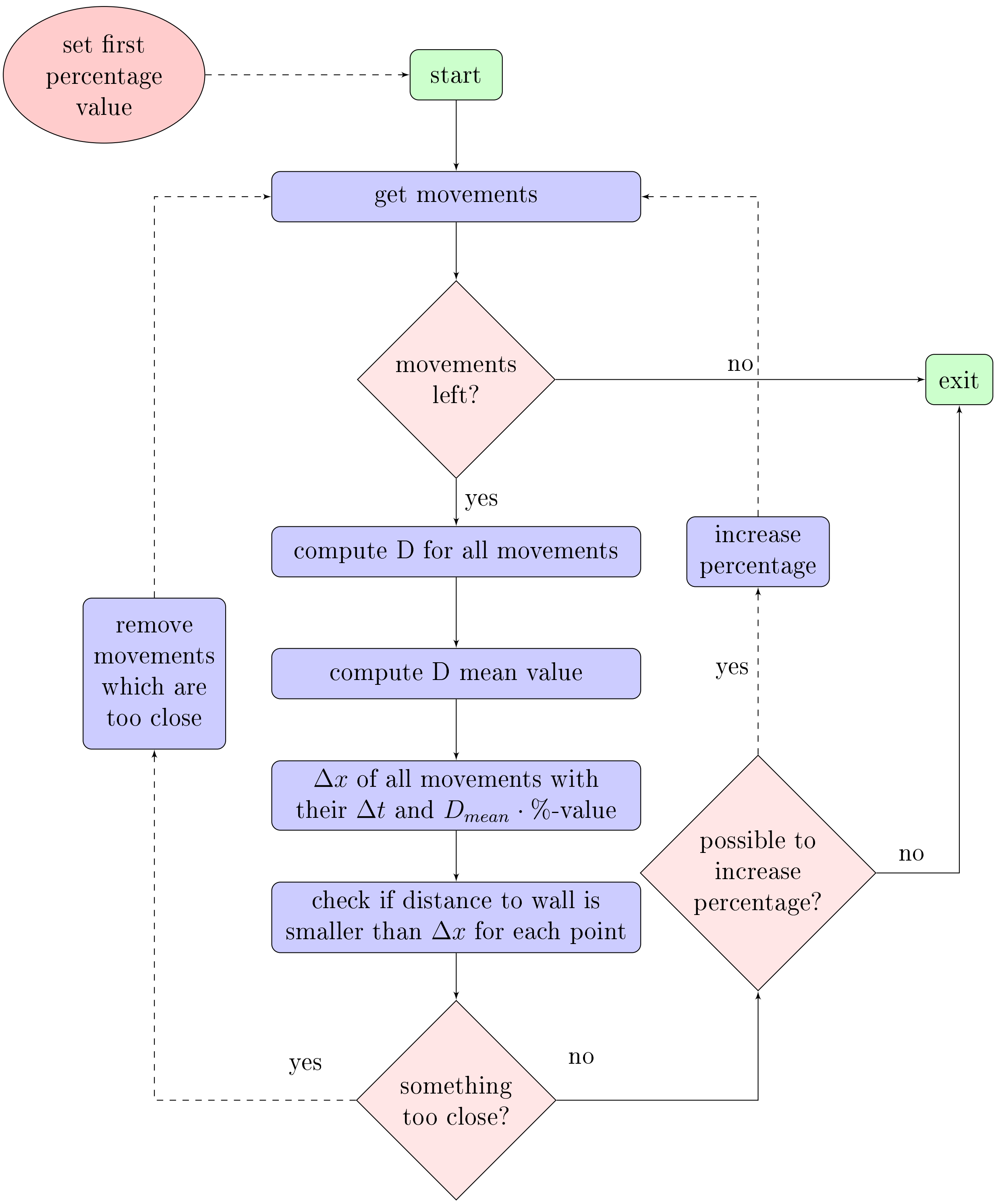

Figure 3.18: Algorithm to remove wall effects per direction

According to the mixing cell theory (see Sect. 2.3.2 (page 11)) only those movements from one mixing cell into another are interesting. It is checked, if the distance of a movement is larger than 50 percent of the mixing cell distance. Just half of the length is used, because it could move into two mixing cells (left and right or top and bottom side), depending on the direction (remember that the dispersion coefficient is computed per dimension). In case the distance is smaller, the end point of the movement is dropped and the distance is checked with the starting point and the next point.

Figure 3.19 (page 43) shows the implementation. The distance between point two, three, four and five to point one is checked. Only distance one to five is long enough. The horizontal distance and the time between point one and five is used as movement.

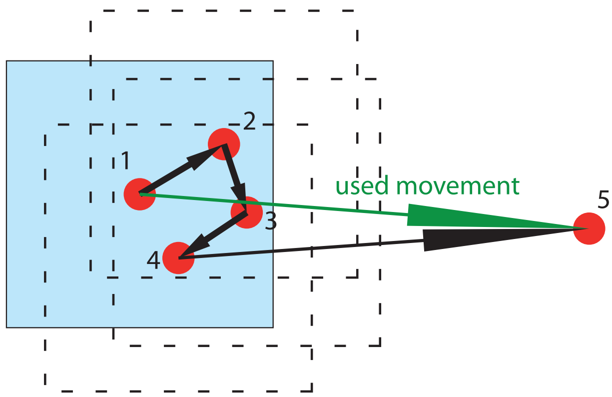

Figure 3.19: Used movement into another mixing cell

It is very important to use the time difference between point one and five and not the one between four and five, otherwise the dispersion coefficient would be completely different, because the time needed for a long distance is too short.

It is essential that the first detection point is used. Otherwise a particle always visible during a long movement would not generate any usable movement. This happens, because the particle must be quite fast to travel a certain distance in a very short time, otherwise the movement is removed all the time.

3.3.2 Multiple Particle Spreading

The idea of this analysis method is, that a batch (e.g. 70) of similar particles are dropped at once. The dispersion coefficient is computed by using the distance from every point to the drop point and the time difference to the dropping time.

Due to Eq. (2.3.2) (page 11) the dispersion coefficient converges to zero for a limited length and an increasing time. This means in theory that after a certain time the particles are homogeneously mixed.

Figure 3.20 (page 44) illustrates an experiment. The particles are dropped in one corner and spread over time into all directions. As shown the drop point is not always directly in the corner and the particles are not dropped at a single point, but close to each other. Especially the second point has a great influence on the results.

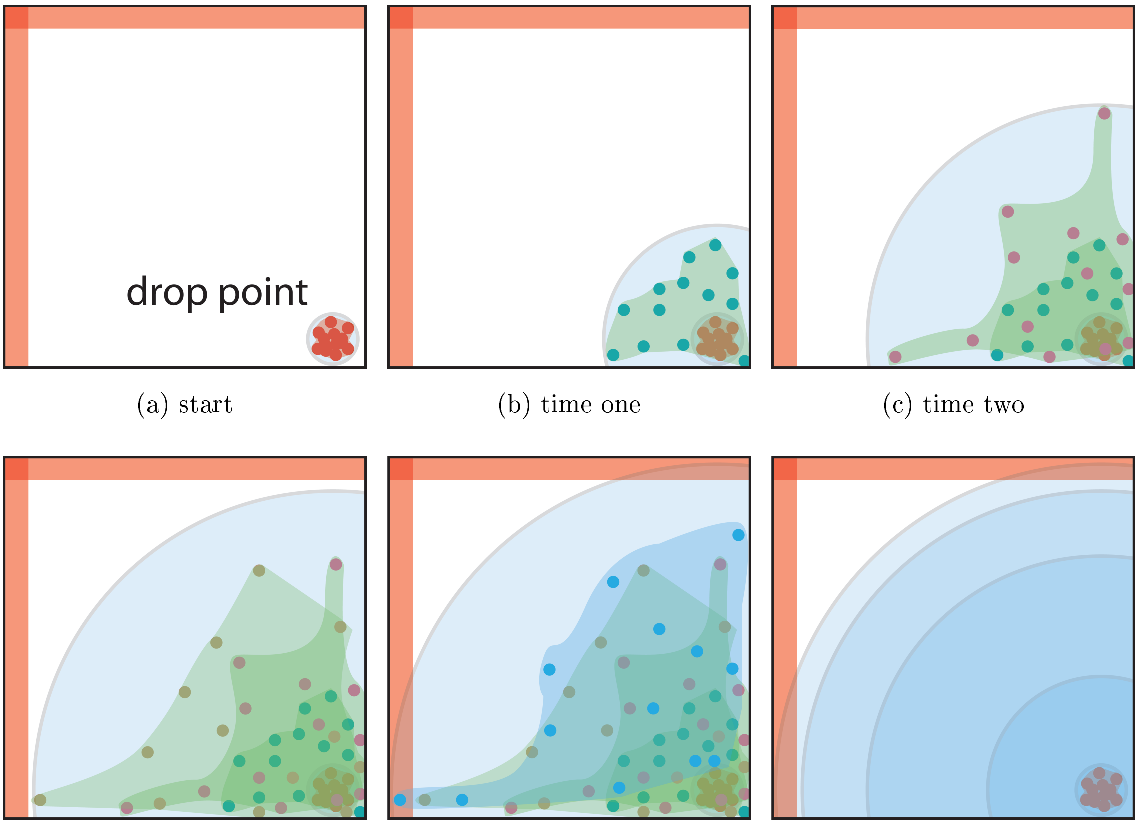

(a) start (b) time one (c) time two

(d) time three (e) horizontal end (f) summary

Figure 3.20: Illustration of a multiple particle spreading experiment. Stop areas are marked in red on the top and left side.

The dispersion coefficient is calculated (per direction) with the distance between each particle centroid coordinate and the drop point, together with their time difference. In case not everything is dropped at exactly one point, the dispersion coefficient calculated in the second frame is quite high (very low time).

In the first frame, where something is detected, the mean centroid coordinate of all particles is computed and used as reference afterwards. In the second frame, where something is detected, each new coordinate is checked with the reference.

In case the particles have not moved from their drop points they will produce dispersion coefficients in the second frame as well (distance from each centroid coordinates to the drop point is calculated and used). The distance is quite low, but the time is extremely short. If something is detected in the second frame, it is 1/24 second. Subsequently the produced dispersion coefficient is unreasonable high (e.g. see start point in Fig. 5.10 (page 82)).

This effect could be avoided if only those particles are counted which leave the drop area, but this results in the question which reference point should be used.

In theory the computation of the dispersion coefficient should be stopped when the first particle reaches an opposite wall. Practically the possibility that a particle is detected directly at the wall is quite low, therefore a so called "stop area" is defined. This is an area close to the wall and marked in red in Fig. 3.20 (page 44). This "stop area" is used to stop the algorithm. Further investigation is needed to determine the question if it should stop at the first detection in the stop area or at a certain detection frequency.

The dispersion coefficient is only calculated if something is detected. To compute mean values of multiple experiments, data for every time step is needed. In case nothing was detected at a certain time (frame), the data is linearly interpolated.

3.4 Parameter Investigation

Parameters had to be chosen during the analysis. This section gives some background information about the influence of these parameters.

3.4.1 Lower Greyscale Image Border

Between the steps of converting an image into greyscale and detecting the edges some dark sections are removed. This is necessary to remove almost black areas and increase the quality of the detected particles. Otherwise it is possible that some black intensities are slightly different (keyword image noise) and they are detected as objects. By looking on Fig. 3.5a (page 26) it can be seen that there are some small changes in intensity which are not related to coloured particles. These sections are just cut out, by defining a certain level and removing everything below it.

The impact from this step is displayed in Fig. 3.21 (page 47). From top to bottom the level is increased from 0 (nothing) up to 150. For the used data type (uint8, defined from 0 to 255) 150 is about 58.82 %.

The applied mask is printed on white instead of black background. This helps to see the mask area. Everything connected, and not white, will be detected as object (particle) and run through the classification process (described in Sect. 3.1.3 (page 27)).

In Fig. 3.22 (page 48) the remaining particles are classified. It can be seen that the amount of particles and their sizes decreases by increasing the limit value.

Dark colours on the particles edges are removed by increasing the parameter. Nevertheless these pixels are not categorised anyway. In case they are not removed before, the particle size is different and influences the ratio "categorised pixels to total amount of pixels" per particle. Based on this ratio it is decided if a particle is in one, multiple or non-categories.

The decreasing size can be seen in Fig. 3.21h (page 47). Two particles, on the right bottom side, close to each other, are not connected any more. The categorisation (see Fig. 3.22c (page 48)) is still the same. With a lower limit the same particle is sorted into multiple categories (same size and same coordinates). In contrast, with higher levels, the particles are treated as two single ones, with different coordinates and areas.

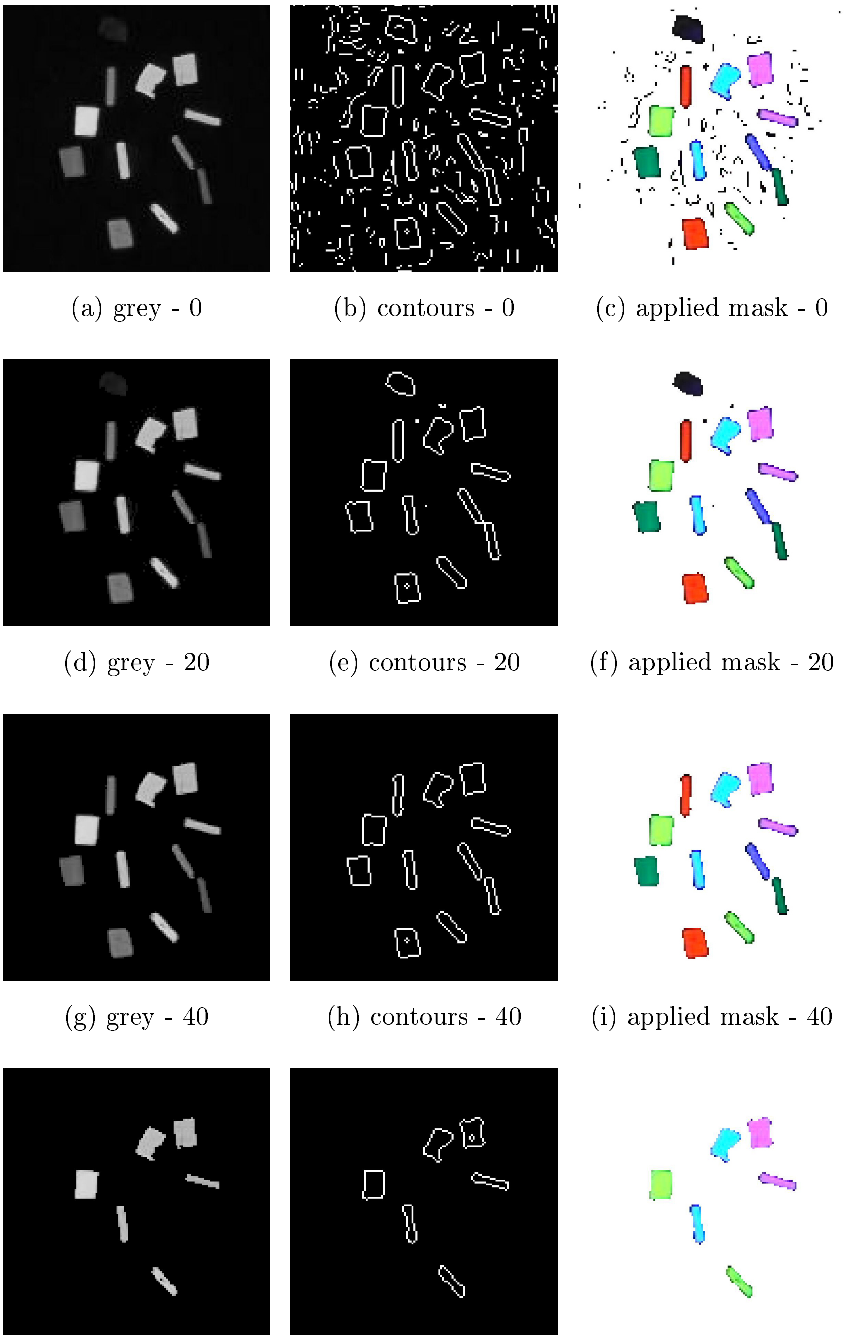

(a) grey - 0 (b) contours - 0 (c) applied mask - 0

(d) grey - 20 (e) contours - 20 (f) applied mask - 20

(g) grey - 40 (h) contours - 40 (i) applied mask - 40

(j) grey - 150 (k) contours - 150 (l) applied mask - 150

Figure 3.21: Influence of lower greyscale border limit (0 to 150) on particle detection. Applied mask is printed on white background for presentation purpose.

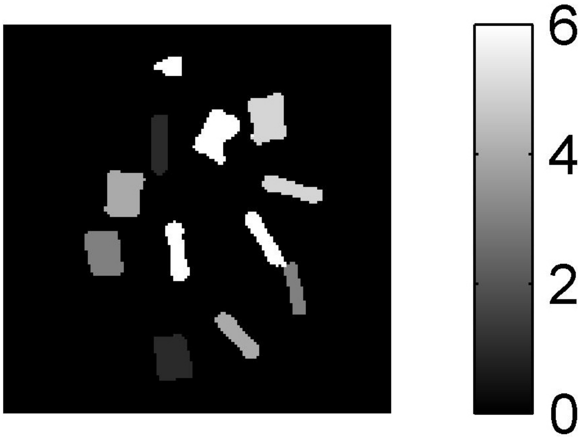

(a) limit 0

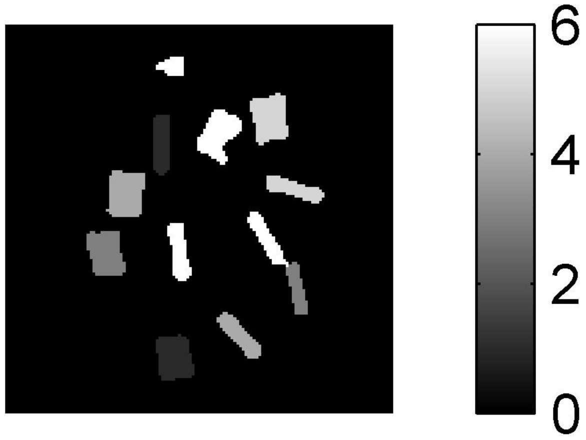

(b) limit 20

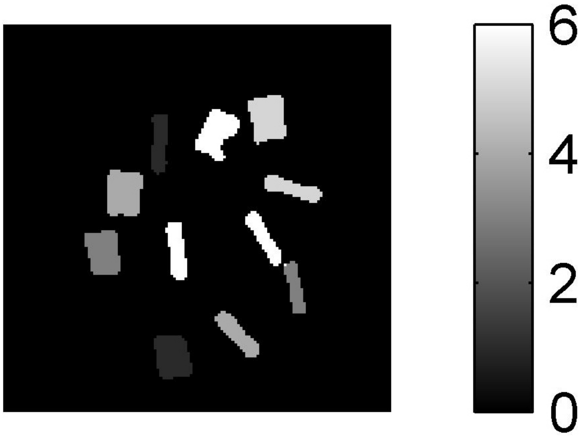

(c) limit 40

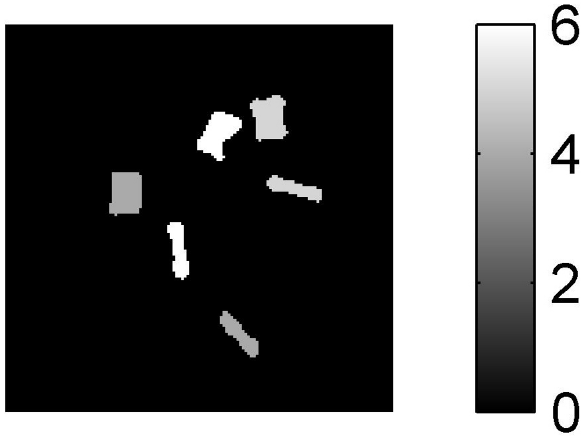

(d) limit 150

Figure 3.22: Influence of lower greyscale border limit (0 to 150) on particle categorisation

All results in this work are produced with a limit of 20. Larger values result in smaller particles, because dark pixels on the edges are removed. In case particles lying close to each other a higher level helps to split them. This increases the quality of the detected centroid coordinate. However, if the level is set too high, dark particles (for example covered with a thin layer of bed material) are removed.

A small value does not split connected particles and therefore two different particles are extracted with the same coordinate and area. By not using the parameter (=0) image noise is detected as particle. In the worst case the edge detection algorithm does not work. If it does, the amount of detected particles is higher. Therefore more time is needed to classify them. During the classification process they are dropped anyway, so this is just wasted computation time.

A good balance between the previous mentioned effects was found with a value of 20 which is 7.84 %[2]. By looking at Fig. 3.5a (page 26) it can be seen that most of the image noise is below 20.

3.4.2 Pixel-Length Ratio

The video recorded by the camera is in pixel. Nevertheless, the wanted dispersion coefficient is a length based unit. Therefore the pixels must be converted into a certain length. If the distance to the object, the focal distance and some camera parameters (e.g. physical size of sensor pixel is 5.5 µm) are known then it is possible to calculate the detected horizontal distance. This calculations are difficult and, as already mentioned, many parameters are needed, which are hard to get. Especially the distance to the object is unknown.

Thus it is done by detecting the cold flow model edges (in the video) at a certain bed height (not fluidized). This amount of pixels is proportional to the dimensions of the model (30 cm × 30 cm). With this ratio the pixels are converted into metres. In case the edge detection is not correct the results are influenced.

The resolution of the used videos is 424 pixel × 640 pixel. For a perfect camera setup 30 cm are 424 pixels. A setup is perfect when the distance from one wall to its opposite is fully covered by the camera but walls are not visible

$$\frac{0.3\,\mathrm{m}}{424\,\mathrm{pixel}} = 7.0755 \times 10^{-4}\,\mathrm{m/pixel} \tag{3.4.1}$$

In case the setup is not perfect (e.g. more recorded than needed), a different ratio is used (e.g. 400 px instead of 424), because the outer part has to be excluded. This is necessary, because otherwise there might be some reflections on the walls.

With a different ratio the sensitivity changes. For instance a movement of one pixel and a ratio based on 400 pixels will be 0.75×10^{-3} m. In contrast it is 0.71×10^{-3} m for a perfect setup (424 pixel).

This means that lower resolutions increase the sensitivity of coordinates. For lower resolutions the error of common centroid coordinates of multiple particle ascent. The

[2]Used data type, uint8, is defined from 0 to 255

dispersion coefficient is based on square distance, therefore the error increases by square. Larger dispersion coefficients induce a higher particle removal rate during the wall check. Subsequently the amount of left over movements decline.

In conclusion the effect can be decreased by increasing the video resolution, but higher resolution results in more data (longer analysis time).

3.4.3 Mixing Cell Width

The mixing cell width is a chosen parameter. Based on it the dispersion coefficient is computed. The results sensitivity to this parameter can be studied in Fig. 3.23 (page 50).

It can be seen that it has a great influence on the results. On the left side it is continually increasing. On the right side the dispersion coefficient fluctuates. This could have several reasons. One could be a physical one, that the wall effects are already dominating, because long distance movements in a small model have to be detected close to a wall. The more reasonable is, that this has some statistical reasons. The amount of movements, the dispersion coefficient is based on, is very limited. By increasing the mixing cell width the amount of movements goes exponentially down, as it can be seen in Fig. 3.24 (page 51). The displayed amount is the sum of all movements for all categories and five videos divided by the amount of video clips (five).

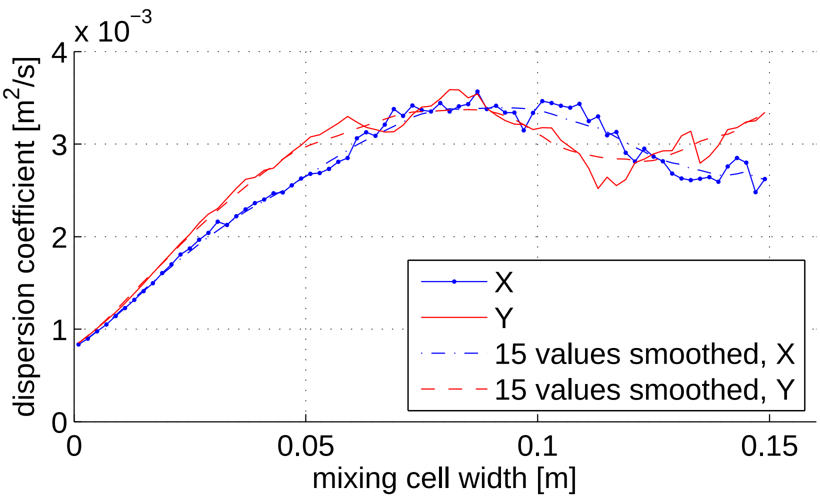

Figure 3.23: Dispersion coefficient for different mixing cell widths (7 cm bed height, large pellets, superficial velocity of 0.185 m s^{-1}). Values are movement weighted mean values of five 20 min videos and five different coloured particles

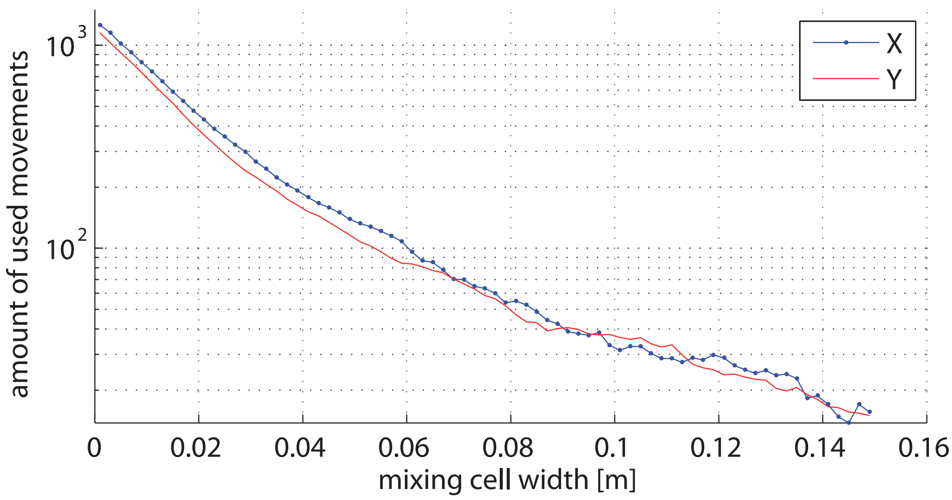

Figure 3.24: Finally used movements (7 cm, $0.185\,\mathrm{m\,s^{-1}}$, large pellets)

The importance of the mixing cell length leaded to the perception that a method to determine it, in an more accurate way than it was done before, is needed. In previous work the distance between the bubbles was measured with a ruler.

In theory the particles should accumulate between the bubble paths, if they float. Therefore it should be possible, by analysing very long videos with many particles, to see these spots.

These spots should be extractable if the detections are categorised in a grid and the amount of elements per cell is displayed.

The results of two different superficial velocities can be seen in Fig. 3.25 (page 52) and Fig. 3.26 (page 53).

With these images it was not possible to find any pattern to draw some conclusions about the mixing cell distance. Presumable the amount of used data is too limited. With the technical equipment it was not possible to record long run videos (e.g. of several hours or days).

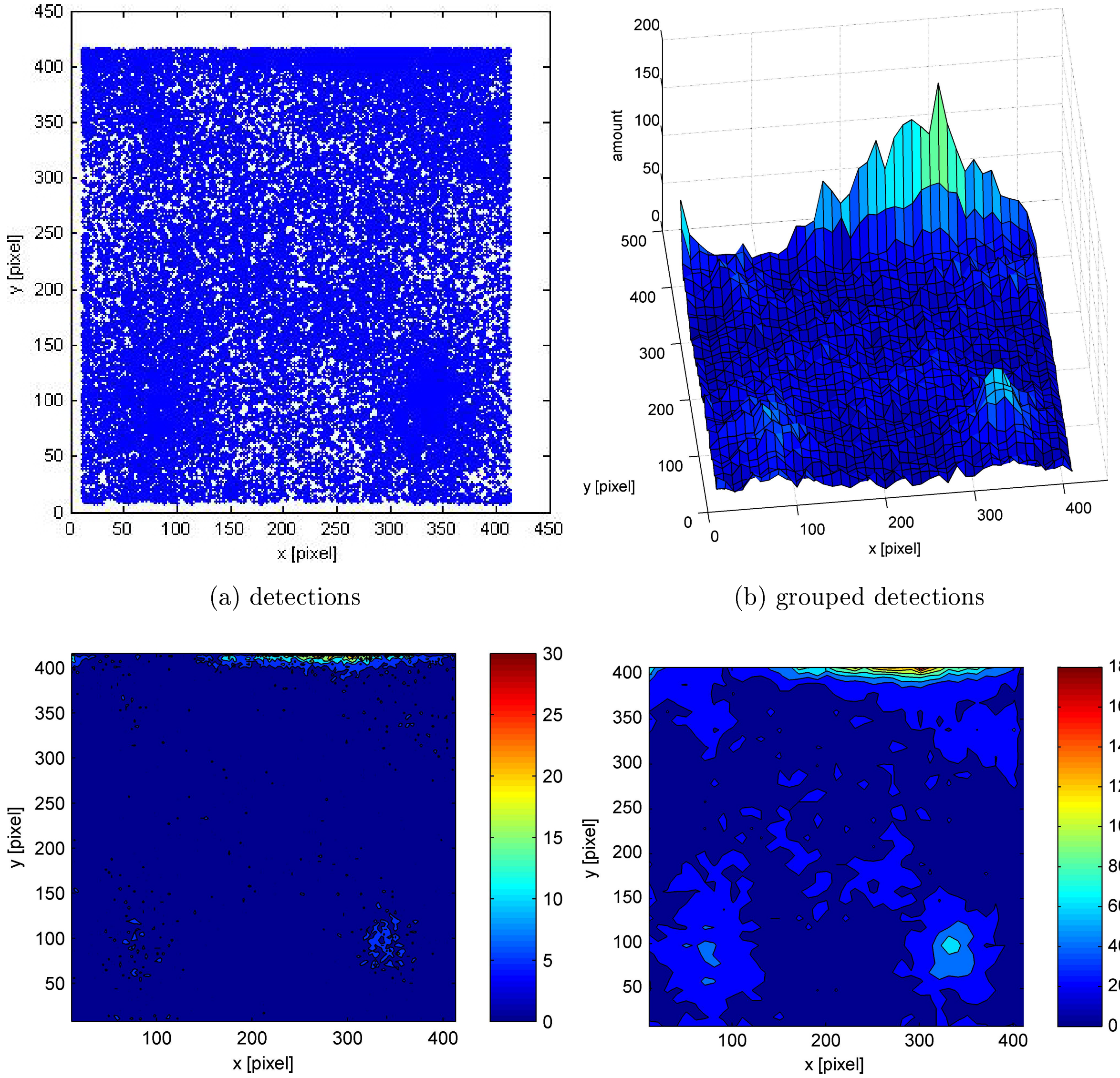

(a) detections

(b) grouped detections

(c) grouped detections (cell width: 3)

(d) grouped detections (cell width: 10)

Figure 3.25: Detections and their amount (bed height: 3 cm, superficial velocity: $0.185\,\mathrm{m\,s^{-1}}$)

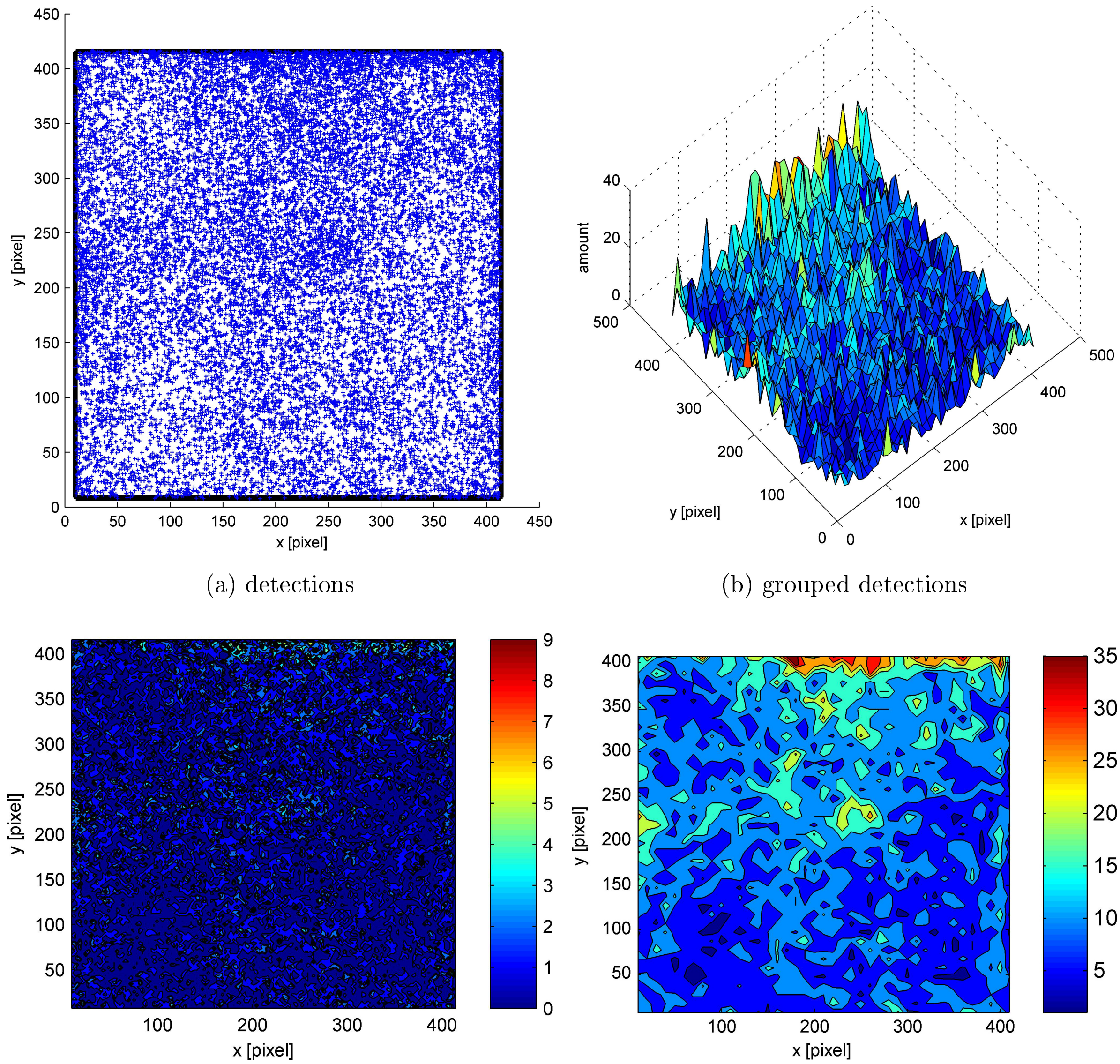

(a) detections

(b) grouped detections

(c) grouped detections (cell width: 3)

(d) grouped detections (cell width: 10)

Figure 3.26: Detections of 13 videos and their amount (bed height: 7 cm, superficial velocity: $0.375\,\mathrm{m\,s^{-1}}$)

Theoretically the dispersion coefficient discovered with both methods should be the same. Therefore it must be possible to extract it from the multiple particle spreading method when the stop area is reached. With this value the mixing cell length can be extracted from the single particle tracking plots.

This was tried for two cases. In case of low mixing (3 cm, $0.185\,\mathrm{m\,s^{-1}}$) and high mixing (7 cm, $0.375\,\mathrm{m\,s^{-1}}$). In the first case the found values are much smaller than the nozzle distance[3] (18 mm). Details to the used cold flow model can be found in Sect. 4.1 (page 60). For the second instance nothing was found, because the extracted dispersion was smaller than all values from the single particle tracking method. The comparison was done with and without movement weighted mean values.

If the chosen mixing cell width is too low, a microscopic view has been applied, but the model is only valid for a macroscopic one. In case of larger assumed mixing cells the established dispersion coefficient should be the same (without statistical effects). Figure 3.27 (page 54) visualises this idea. The red area marks the section where the defined mixing cell is too small.

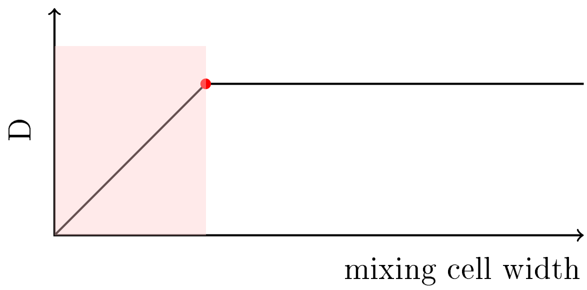

Figure 3.27: Change between microscopic to macroscopic view

[3]distance between the holes in the distribution plate

3.5 Scaling-up the Results

To compare cold flow model results with those from large industrial applications they have to be scaled-up according to the scaling laws (see Sect. 2.2.2 (page 9)). The model is just artificial (for operation conditions and the used materials see Table 4.1 (page 62)), therefore not based on an existing reactor. Nevertheless the results can be scaled-up.

In this work scaling factors are provided for combustion (see Table 3.2 (page 55) and Table 3.3 (page 56)) and gasification (see Table 3.4 (page 57)) processes by choosing a fluid at a certain temperature.

	fluid properties			
fluid	dry air			
temperature [°C]	700	800	900	1000
density [$kg\,m^{-3}$]	0.363	0.329	0.301	0.277
kinematic viscosity [$m^2\,s^{-1}$]	1.154×10^{-4}	1.348×10^{-4}	1.551×10^{-4}	1.780×10^{-4}
	reactor dimensions			
scalingfactor [–]	3.887	4.311	4.734	5.189
width x [m]	1.166	1.293	1.420	1.557
width y [m]	1.166	1.293	1.420	1.557
	fuel properties			
density [$kg\,m^{-3}$]	813.361	737.178	674.440	620.664
	bed material properties			
density [$kg\,m^{-3}$]	2681.079	2429.959	2223.154	2045.892
mean particle size [m]	2.915×10^{-4}	3.233×10^{-4}	3.550×10^{-4}	3.892×10^{-4}

Table 3.2: Chosen and computed large scale conditions and their physical properties (dry air properties from (Kothandaraman and Subramanyan; 2004, page 24)) used for combustion

	fluid properties			
fluid	oxygen			
temperature [°C]	700	800	900	1000
density [$kg\,m^{-3}$]	0.402	0.363	0.333	0.306
kinematic viscosity [$m^2\,s^{-1}$]	1.170×10^{-4}	1.380×10^{-4}	1.610×10^{-4}	1.840×10^{-4}
	reactor dimensions			
scalingfactor [−]	3.923	4.379	4.853	5.305
width x [m]	1.177	1.314	1.456	1.591
width y [m]	1.177	1.314	1.456	1.591
	fuel properties			
density [$kg\,m^{-3}$]	900.747	813.361	746.141	685.643
	bed material properties			
density [$kg\,m^{-3}$]	2969.129	2681.079	2459.502	2260.083
mean particle size [m]	2.942×10^{-4}	3.284×10^{-4}	3.640×10^{-4}	3.979×10^{-4}

Table 3.3: Chosen and computed large scale conditions and their physical properties (oxygen properties from (Kothandaraman and Subramanyan; 2004, page 25)) used for combustion

	fluid properties			
fluid	steam			
temperature [°C]	700	800	900	1000
density [$\mathrm{kg\,m^{-3}}$]	0.226	0.204	0.187	0.172
kinematic viscosity [$\mathrm{m^2\,s^{-1}}$]	1.220×10^{-4}	1.470×10^{-4}	1.740×10^{-4}	2.040×10^{-4}
	reactor dimensions			
scalingfactor [−]	4.034	4.567	5.111	5.682
width x [m]	1.210	1.370	1.533	1.705
width y [m]	1.210	1.370	1.533	1.705
	fuel properties			
density [$\mathrm{kg\,m^{-3}}$]	506.390	457.095	419.004	385.394
	bed material properties			
density [$\mathrm{kg\,m^{-3}}$]	1669.212	1506.722	1381.162	1270.373
mean particle size [m]	3.025×10^{-4}	3.425×10^{-4}	3.833×10^{-4}	4.262×10^{-4}

Table 3.4: Chosen and computed large scale conditions and their physical properties (steam properties from (Kothandaraman and Subramanyan; 2004, page 29)) used for gasification

By choosing a fluid, bed material density, fuel density and reactor dimensions are fixed and have to be calculated. This is done by using the rearranged version of Eq. (2.2.2) (page 9) and Eq. (2.2.4) (page 9) in combination with Eq. (2.2.1) (page 9). The index M stands for model and L for large. The used material for the down scaled fuel particles is aluminium. More on this can be found in Sect. 4.1.2 (page 63).

$$\rho_{sL} = \rho_{fL} \cdot \left(\frac{\rho_s}{\rho_f}\right)_M \tag{3.5.1}$$

$$L_L = L_M \cdot \left(\frac{u_{0L}}{u_{0M}}\right)^{2/3} \tag{3.5.2}$$

Based on these values the superficial velocity (with a rearranged version of Eq. (2.2.1) (page 9)) and the scaling factor for the dispersion coefficient are calculated.

$$u_{0L} = \sqrt{\frac{u_{0M}^2 \cdot L_L}{L_M}} \tag{3.5.3}$$

Results for the scaled-up superficial velocities, for low (left) and high (right) fluidization[4], are shown in Table 3.5 (page 59).

The dispersion coefficients unit is $m^2 s^{-1}$, which is the same as if a velocity is multiplied with a length.

$$\frac{D_L}{D_M} = \frac{u_{0L} \cdot L_L}{u_{0M} \cdot L_M} \tag{3.5.4}$$

This equation rearranged and in combination with Eq. (2.2.1) (page 9) provides Eq. (3.5.5) (page 58) needed to scale up the results from the experiments.

$$D_L = D_M \cdot \frac{\sqrt{g \cdot L_L} \cdot L_L}{\sqrt{g \cdot L_M} \cdot L_M} = D_M \cdot \underbrace{\left(\frac{L_L}{L_M}\right)^{1.5}}_{DSF} \tag{3.5.5}$$

Table 3.6 (page 59) shows factors from Eq. (3.5.5) (page 58) for the different cases.

A short-cut factor (for Eq. (3.5.5) (page 58)) to scale-up the dispersion coefficient is provided in Table 3.6 (page 59).

[4] more on this see Sect. 4.3 (page 68)

fluid	temperature [°C]	superficial velocity [m s^{-1}]	
air	20	0.185	0.370
dry air	700	0.365	0.730
dry air	800	0.385	0.769
dry air	900	0.403	0.806
dry air	1000	0.422	0.844
oxygen	700	0.367	0.734
oxygen	800	0.388	0.775
oxygen	900	0.408	0.816
oxygen	1000	0.427	0.853
steam	700	0.372	0.744
steam	800	0.396	0.792
steam	900	0.419	0.837
steam	1000	0.441	0.883

Table 3.5: Superficial velocities at cold conditions and their scaled-up values for different cases

	dry air	oxygen	steam
temperature [°C]	DSF [–]		
700	7.66	7.77	8.10
800	8.95	9.16	9.76
900	10.30	10.69	11.55
1000	11.82	12.22	13.55

Table 3.6: Computed scaling factor DSF for Eq. (3.5.5) (page 58) to multiply cold flow model dispersion coefficient results with

Chapter 4

Experiments

4.1 Experimental Setup

A setup considering the perspective view (see Sect. 2.6 (page 17)) as illustrated in Fig. 4.1 (page 60) has been chosen for the experiments. The distance between camera and distribution plate was always the same during different experiments, thus the distance between camera and bad surface varied.

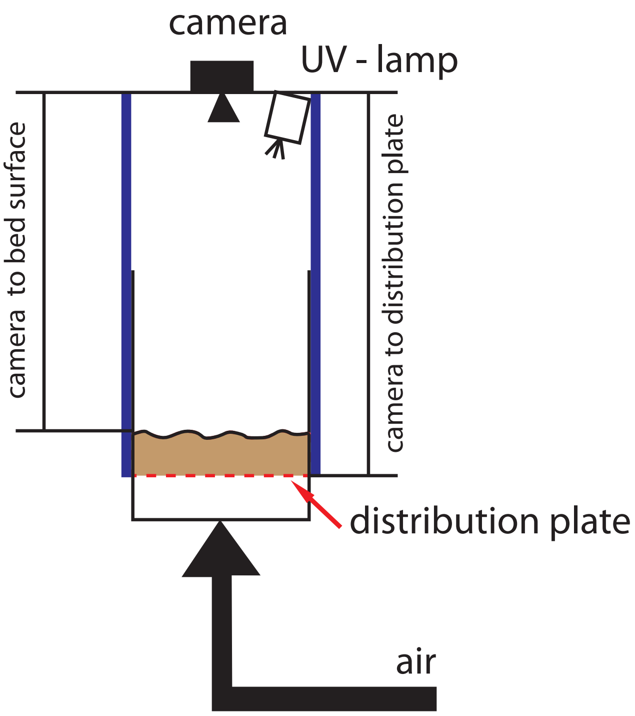

Figure 4.1: Experimental setup

4.1.1 Cold Flow Model

The cold flow model used in this work has an area of 0.3 m × 0.3 m. To ensure the same fluidization over the whole area a distribution plate with an appropriate pressure drop was chosen. This model supports several different kinds of plates. Nevertheless in this study only the plate displayed in Fig. 4.2 (page 61) was used. The distance between the holes is 18 mm.

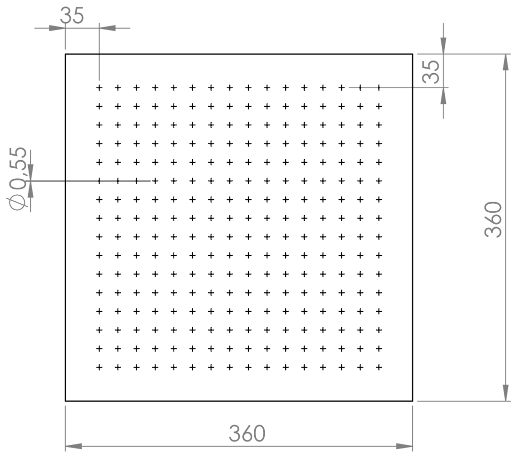

Figure 4.2: Distribution plate

To prevent bed material falling through the holes of the distribution plate a tight-knit mesh is added on top of the plate. The measured pressure drop of distribution plate and net without bed material is displayed in Fig. 4.3 (page 61).

The used bed material is bronze powder with an average particle diameter of 75 µm. This size represents the average diameter of bed material particles under hot conditions and is in the same Geldart group (B).

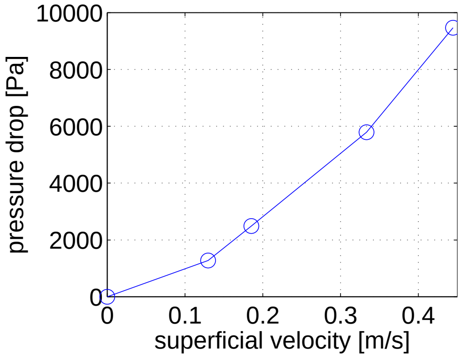

Figure 4.3: Distribution plate pressure drop

As already mentioned in Sect. 3.5 (page 55) the used fluid is air at 20 °C. To avoid electrostatic effects the walls are painted with Larostat® 519.

Table 4.1 (page 62) gives a summary of the used materials, their physical properties and the particle sizes.

bed material		
material	bronze	
density	$8900\,\mathrm{kg\,m^{-3}}$	
particle size	$75\,\mathrm{\mu m}$	
fluid (air)		
temperature	$20\,^{\circ}\mathrm{C}$	
density	$1.205\,\mathrm{kg\,m^{-3}}$	1
kinematic viscosity	$15.06 \times 10^{-6}\,\mathrm{m^2\,s^{-1}}$	1
fuel particles		
material	aluminium	
density	$2700\,\mathrm{kg\,m^{-3}}$	2
diameter	$3\,\mathrm{mm}$	
length, large pellet	$15\,\mathrm{mm}$	
length, small pellet	$5\,\mathrm{mm}$	
length, chip	$12\,\mathrm{mm}$	
width, chip	$9\,\mathrm{mm}$	
height, chip	$2.5\,\mathrm{mm}$	

Table 4.1: Operation conditions and chosen materials. [1] data from (Kothandaraman and Subramanyan; 2004, page 24), [2] data from (Hatch et al.; 1984, page 202)

4.1.2 Particle Preparation

To increase the contrast between bed material and particles, only ultraviolet light is used. This means that only UV active substances are visible and anything else is black or at least very dark.

The used particle material is aluminium. This material was chosen to mimic wood primary chips. According to (Kaltschmitt et al.; 2009, page 373) the raw density of dry wood is between 400 and $750\,\mathrm{kg\,m^{-3}}$. As it can be seen in Table 3.2 (page 55), Table 3.3 (page 56) and Table 3.4 (page 57) this in good agreement with the scaled up particle density.

The same material is used with a cylindrical shape to analyse the geometry influence on the results. Moreover this shape models pellets.

In case of pellets the density is increased during the manufacturing process. According to the Ö-Norm M7135 standard it has to be at least $1120\,\mathrm{kg\,m^{-3}}$ with a maximum water content of 10%.

This higher density requires a different particle material to model pellets properly. Reasons why the material is used for both particle types describes Sect. 5.3 (page 89).

The chosen dimensions of the fuel particles represents wood chips (size is depending on scaling factor and goes for the provided factors from $47 \times 35 \times 10$ mm to $68 \times 51 \times 14$ mm) and pellets. The size of the scaled up pellets is also depending on the scaling factor that has to be used. For the provided factors the diameter range goes from 12 mm to 17 mm. The length for small pellets goes from 19 mm to 28 mm and the one for large pellets from 58 mm to 85 mm.

According to the standard CEN/TS 14 961 (*CEN/TS 14961:2005: Feste Biobrennstoffe - Brennstoffspezifikationen und -klassen.*; 2005) and relating to (Kaltschmitt et al.; 2009, page 364) the small modelled pellets are in category D12 and D25 (larger particle slightly to long to fit the same categories). The modelled pellets are on the upper side of the limits. The reason is that the resolution of the used camera is quite low and therefore the amount of pixels is limited. The small quantity of categorised pixels makes it statistically insufficient to categorise them. This, combined with low surface times, makes it very hard to detect and extract small particles. Therefore the amount of data per 20 minutes video clip is quite limited.

To detect a particle under UV light conditions it has to interact with UV radiation. Thus the particles are painted with UV active paint. The paint is lowering the density of the particles slightly. The amount is unknown, but is increasing for smaller particles (keyword volume/surface ratio).

To follow more than one particle at the same time the colour "footprint" has to be unique. To ensure this, numerous analyses with different colours and their combinations were executed.

Based on the given colours a plethora of mixing has been done to create colours with a good detection rate. More on the detection rate and its quality is described in Sect. 3.2 (page 29). On the end five different colours were found and used in single particle tracking experiments. For the multiple particle spreading method only red particles were used, but multiple colours would be possible.

4.1.3 Design of Internals

In previous work (Larsson and Olsson; 2013) the effect of internals was investigated, primarily through modelling and measuring in a smaller cold flow model.

To measure the effect of internals on the results in a larger model a flexible system was designed. With these new created parts it is possible to add different kind of wall and pipe combinations. The new system contains rods (which should model pipes), walls and beams. These parts can be combined as displayed in Fig. 4.4 (page 65). It is possible to vary the amount of levels and rods, change the distance between them and add walls at different positions. Furthermore they can be used under stationary and circulation conditions.

The red marked part visualises a wall, going from the top to the bottom of the package. As it can be seen, the position can be varied. Additionally a whole layer could be rotated by 90 degree. With this combination a kind of grid is possible.

The chosen combination in this study is displayed in Fig. 4.5 (page 65). It shows three layers with a distance between the holes per row of 34.8 mm horizontally and 15 mm vertically.

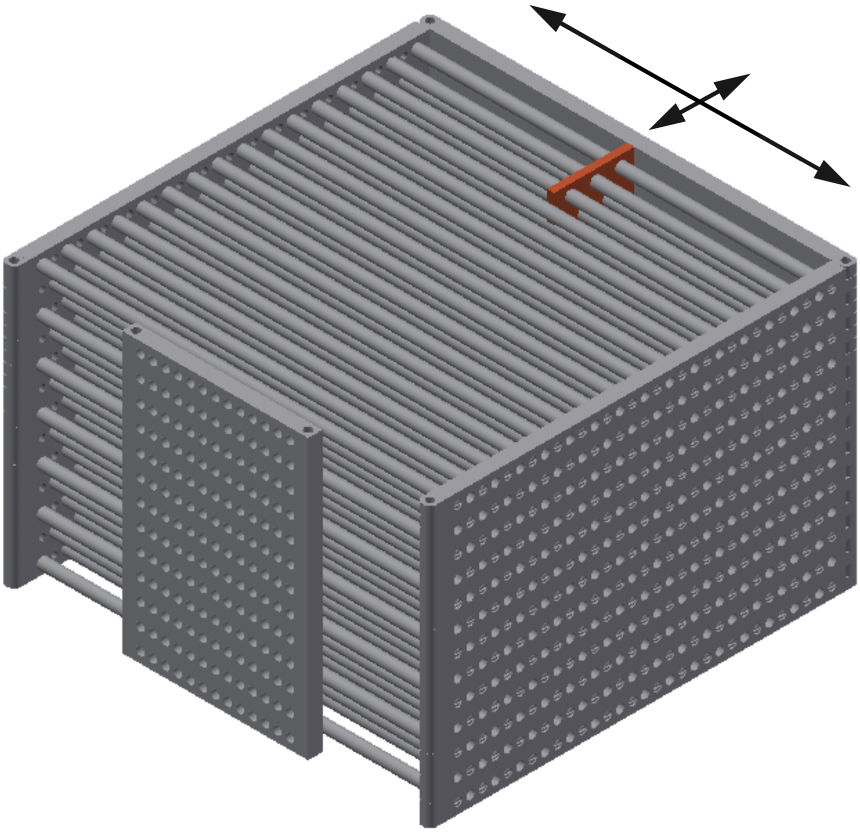

Figure 4.4: Overview about possible internals

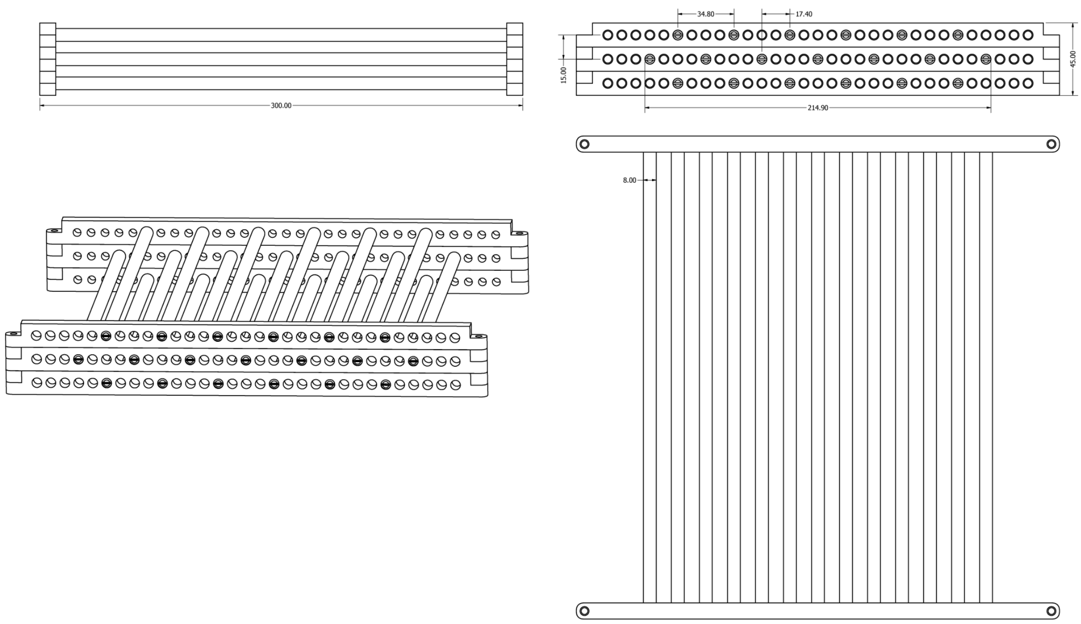

Figure 4.5: Selected tubes setup for the experiments

One important problem with these tubes are reflections. The internals are made of PMMA which is reflecting shiny particles. In case the particles are close to the tubes the reflection and the particle might be connected and everything will be detected as a single large particle (with wrong centroid coordinate). In case they are not connected, two particles will be detected. The question is, which the correct one is.

This effect is already well known for the reactor walls. There the reflections are cut out by defining the detection area.

The same method is very hard to apply for the tubes. Due to the perspective view (see Sect. 2.6 (page 17)) rods which are on top of each other might be visible in the video. In case all positions are well known, it has to be ensured, that they do not change for a video clip. As long as no one touches the camera frame this is ensured for the camera. On the contrary for the cold flow model, it was observed that it starts vibrating at higher bed heights and fluidizations.

Another problem with cutting out pipe areas is, that the remaining detection area is quite low, because the tubes of two levels have different offsets.

A different approach is to avoid the reflections. This can be done by covering the pipes with not reflecting paint. To get the same wall effects the roughness from the paint and pipes should be the same. Additionally the paint has to be abrasion-resistant. In an optimum case it would be something that lowers the electrostatic effect as well.

4.2 Parameters to Vary

In the previous sections many parameters that could be varied in experiments are explained. A summary and additional ideas are given in the following list:

- particle density/material
- particle size
- particle shape (e.g. pellets, chips)
- fluidization
- bed height
- bed material/density
- circulating/stationary fluidized bed
- internals (yes, no, different combinations)
- distribution plate

The number of possible combinations is quite high. Therefore just some of them were varied and the others were kept constant.

4.3 Chosen Combinations

In this work, particle size and type as well as different bed heights and fluidizations were investigated. Additionally some experiments with tubes were carried out.

Experiments were carried out with two superficial velocities (u_0) which are, according to Fig. 2.2 (page 6) (for $Ar^{1/3}$ and U^* see Table 4.2 (page 68)), both in the bubbling fluidization regime. All the combinations are shown in Table 4.3 (page 68).

u_{mf}	m s^{-1}	0.0237	
$Ar^{1/3}$	–	6.574	
u_0	m s^{-1}	0.185	0.375
U^*	–	0.2037	0.4074
u_0/u_{mf}	–	7.8	15.6

Table 4.2: Fluidized bed key figures $u_{mf} = \mu_f/(\rho_f \cdot d_{sv}) \cdot (\sqrt{33.7^2 + 0.0408 \cdot Ar} - 33.7)$ and $U^* = Re/Ar^{1/3}$

bed height	tubes	pellet, large	pellet, small	chips
3 cm	-	X	X	-
7 cm	-	X	X	X
7 cm	yes	X	-	X

Table 4.3: Experiments test matrix. Everything marked with X is analysed with superficial velocities of 0.185 m s^{-1} and 0.375 m s^{-1}

The experiments with small pellets and tubes were left out, because these small particles might stuck in the holes of the beams. For further experiments the holes must be closed. The tubes package was only used with a bed height that ensures that the tubes are fully covered. Otherwise there might be some reflections. Problems with them are mentioned in Sect. 4.1.3 (page 64).

Chapter 5

Results and Discussion

The following section shows the results and gives an interpretation. All the presented values are down-scaled.

5.1 Single Particle Tracking

Figure 5.1 (page 70) (for data see Table B.1 (page 96)) shows the time percentage of particles detected at the bed surface at different conditions. Figure 5.2 (page 70) shows the same data but grouped by the ratio particle volume per particle surface. Figure B.1 (page 97) and Fig. B.2 (page 98) shows the underlying data of a low and high mixing case.

Table B.1 (page 96) shows an increase in surface time for lower superficial velocities and bed heights. Furthermore it can be seen that larger particles are more often detected at the surface. On the one hand this could have fluid dynamical reasons, because they float better. On the other hand it could be because they are bigger and easier to detect.

The chips percentage compared to the one from large pellets is increased for high superficial velocities and tubes. A possible reason could be that they are slightly shorter and therefore their interference through the pipes is lower.

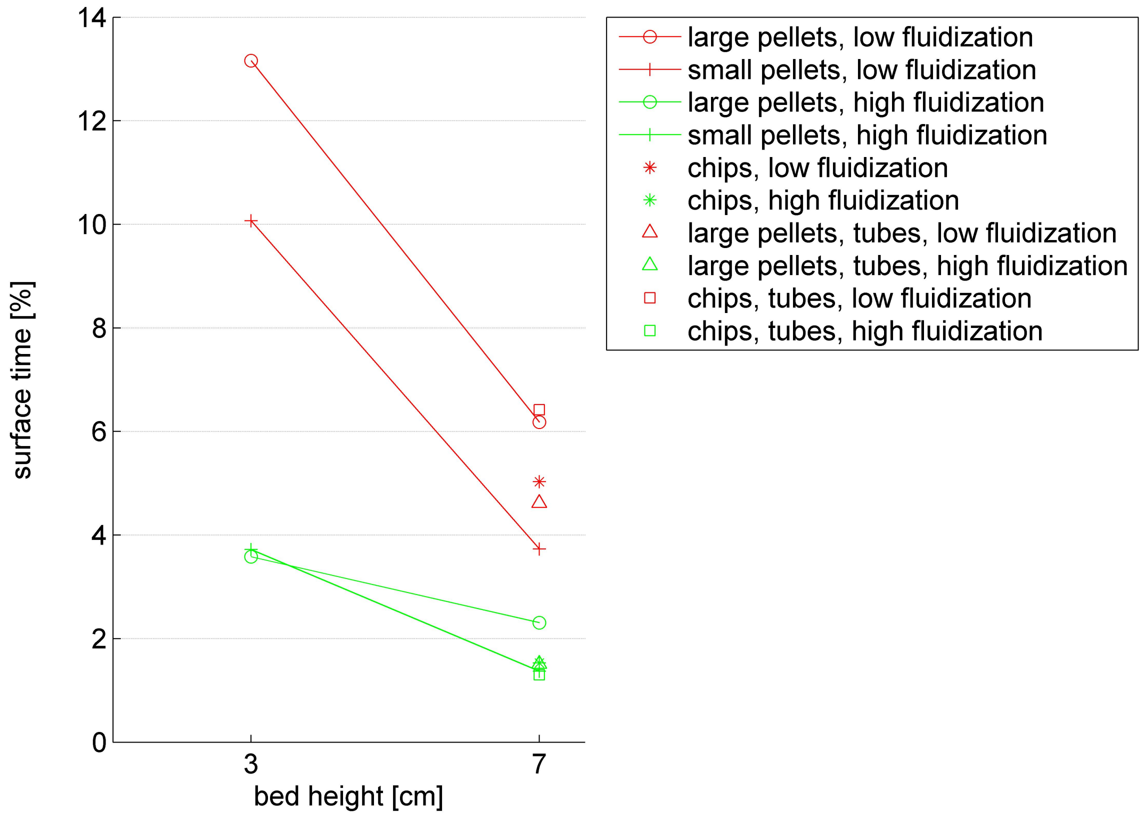

Figure 5.1: Percentage of surface time for different conditions

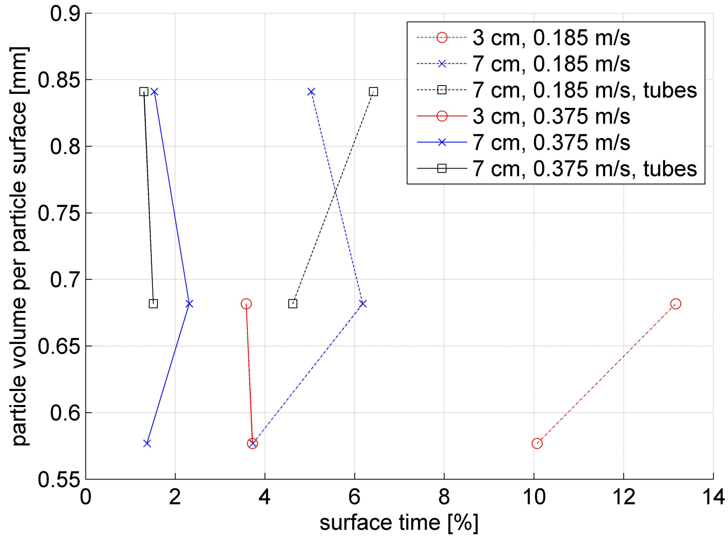

Figure 5.2: Ratio particle volume per surface area over particle surface time (in %). Volume/Surface for small pellets is 0.577 mm, large pellets 0.682 mm and for chips 0.841 mm

Figure 5.3 (page 73) as well as Fig. 5.4 (page 74) show mixing cell width variation results at different conditions (particles, tubes, fluidization). In Fig. 5.5 (page 75) and Fig. 5.7 (page 77) the results are movement weighted. Figure 5.6 (page 76) and Fig. 5.8 (page 78) display the amount of used movements for the computation of these dispersion coefficients. The values displayed are the mean values of all used movements from all video files (sum of all movements in all categories per video divided by the amount of videos). The mixing cell width is increased from 0.001 m in 0.002 m steps until the average amount of used movements is below 10. This is done to remove statistically useless points.

In general it can be seen, especially for higher bed heights, that the dispersion coefficient varies quite much. Furthermore it is higher with increased bed heights and greater fluidization. In most cases the dispersion coefficient is similar for both directions. Moreover it can be seen that the amount of used movements is higher for lower bed heights and superficial velocities.

The amount of movements is decreasing exponentially with linear increasing mixing cell width. It is higher for a lower fluidization. Therefore the result statics are more reliable and furthermore larger mixing cell widths can be investigated (because if the amount of movements is below 10 the data is removed).

For the same fluidization conditions the amount of movements for lower bed heights is higher. Additional it is higher for larger particles at lower bed heights, probably because the detection rate is better. The amount of movements for chips is slightly greater than those of small pellets, but smaller than the one of large pellets.

The dispersion coefficient found for lower bed heights and both superficial velocities over the whole mixing cell width variation is lower for large pellets than for small ones.

For low fluidization and 7 cm bed height the dispersion coefficient from large pellets is below the one from small pellets. The mean dispersion coefficient (see Fig. 5.3 (page 73)) of large pellets is lower than the small pellets and greater than the chips one. In case of higher fluidization the one for large pellets in y direction is more below the one of small pellets than in x direction.

It is found that the dispersion coefficient with tube setup is almost direction independent for low fluidization. In contrast in case of higher fluidization it is much greater in parallel (x) than cross-sectional (y, to the tubes) direction. Furthermore it has to be noted that in case of higher fluidization the dispersion coefficient is greater in x direction than in y (with and without tubes) at the same bed height (7 cm). The difference is greater with tubes. The amount of used movements is lower for the tubes combination at 7 cm and $0.375\,\mathrm{m\,s^{-1}}$. The dispersion coefficient is greater for chips at 7 cm bed height and $0.375\,\mathrm{m\,s^{-1}}$ with tubes than without. The difference in x and y is bigger without tubes.

Figure 5.3 (page 73) shows a step for small pellets, 3 cm bed height, and low fluidization. It is assumed that this could be the mixing cell length where microscopic view changes to macroscopic. The length is about 0.05 m, which is almost three times larger than the nozzles distance (18 mm). A similar, but smaller step, can be seen in the same graph for large pellets and 3 cm bed height at about 0.09 m. These steps are not visible in the movement weighted plot (Fig. 5.5 (page 75)) where the curves are not combined for both directions. It should be kept in mind that the values are smoothed values. Currently it is unknown where this effect comes from, making it very interesting for further investigation. In Fig. 5.4 (page 74) the curves from 7 cm, small pellets, large pellets and chips have a common point at 0.055, before they disperse.

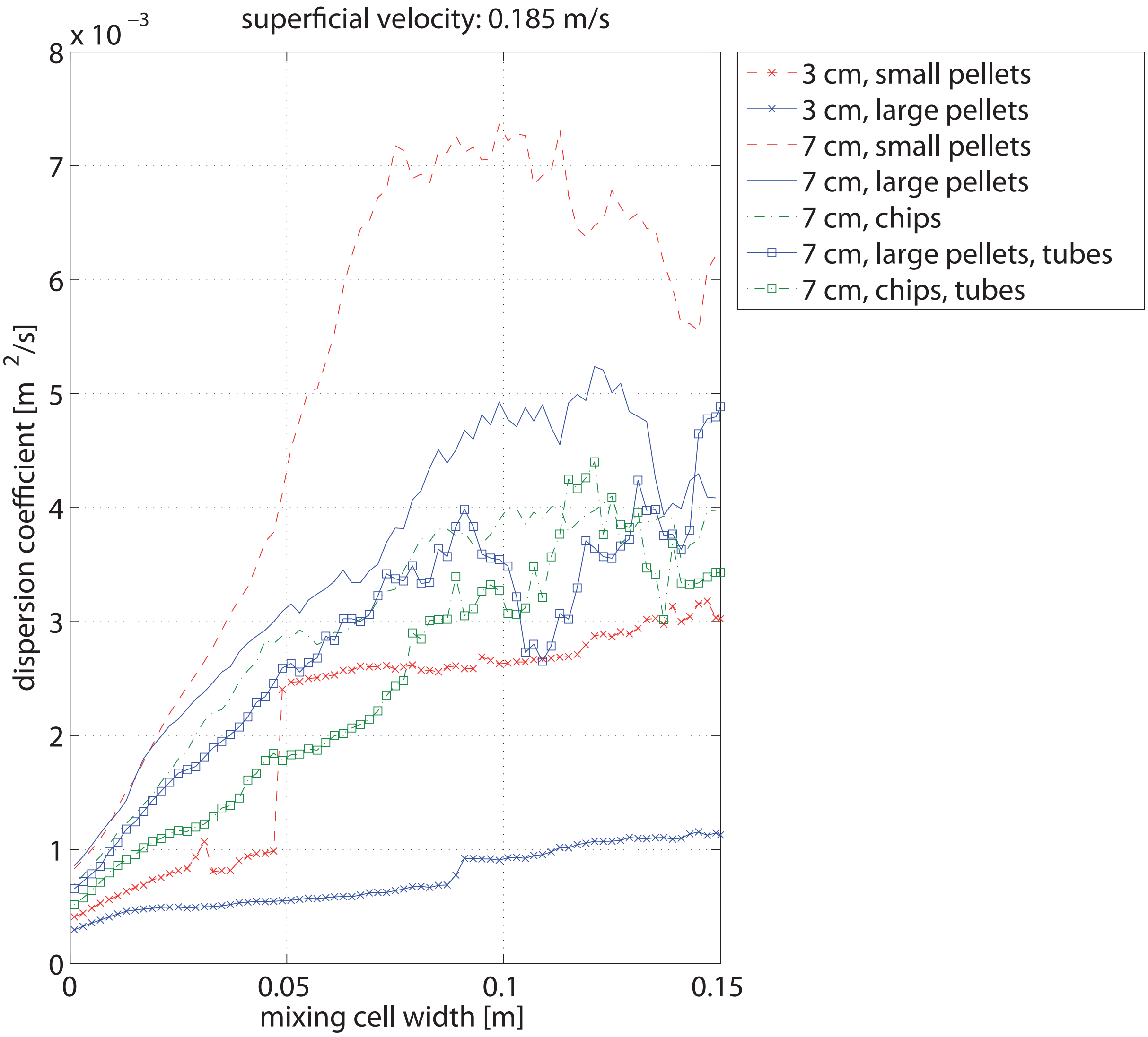

Figure 5.3: Mean dispersion coefficient from single particle tracking method for different configurations and a superficial velocity of $0.185\,\mathrm{m\,s^{-1}}$.

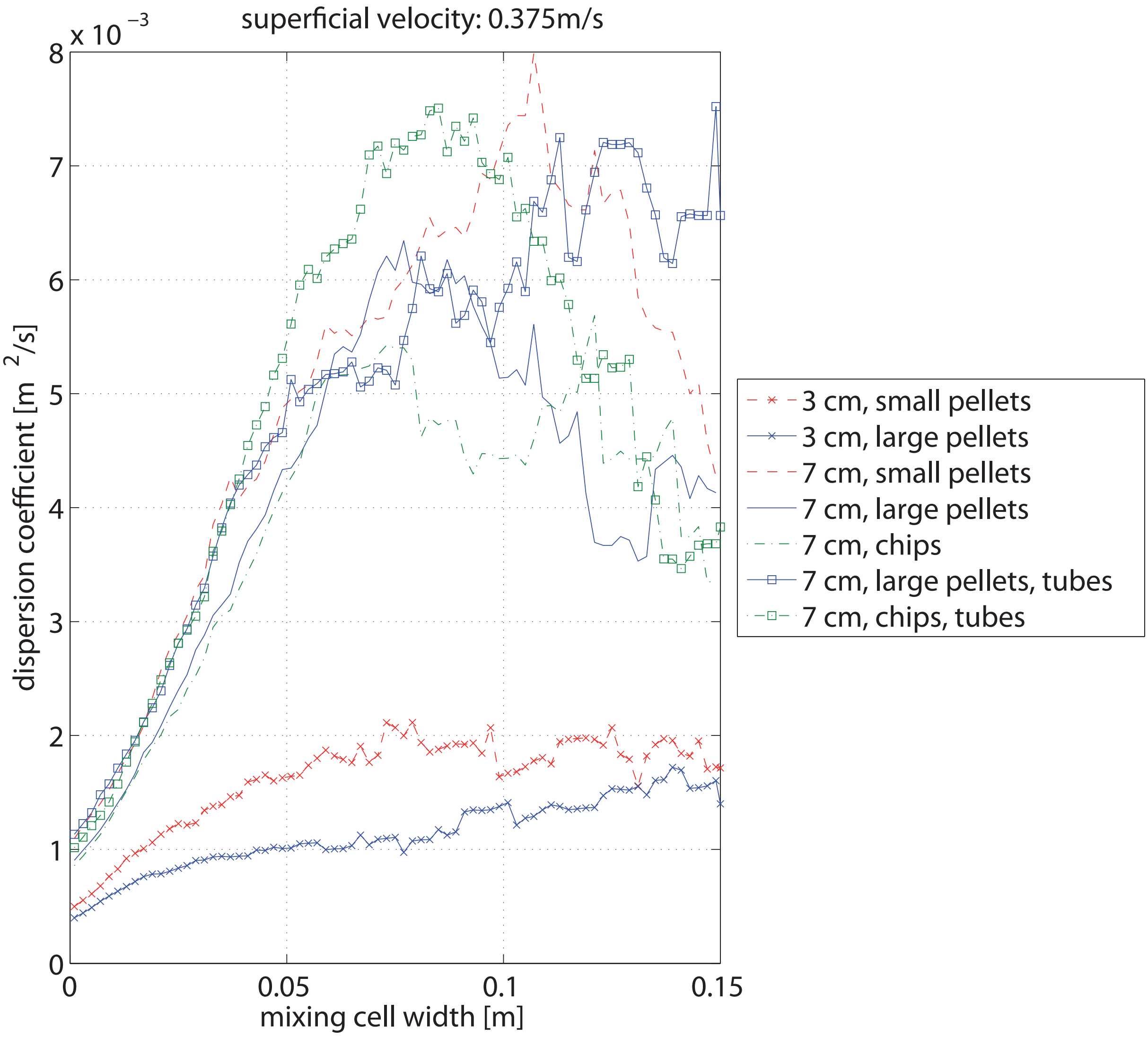

Figure 5.4: Mean dispersion coefficient from single particle tracking method for different configurations and a superficial velocity of $0.375\,\mathrm{m\,s^{-1}}$.

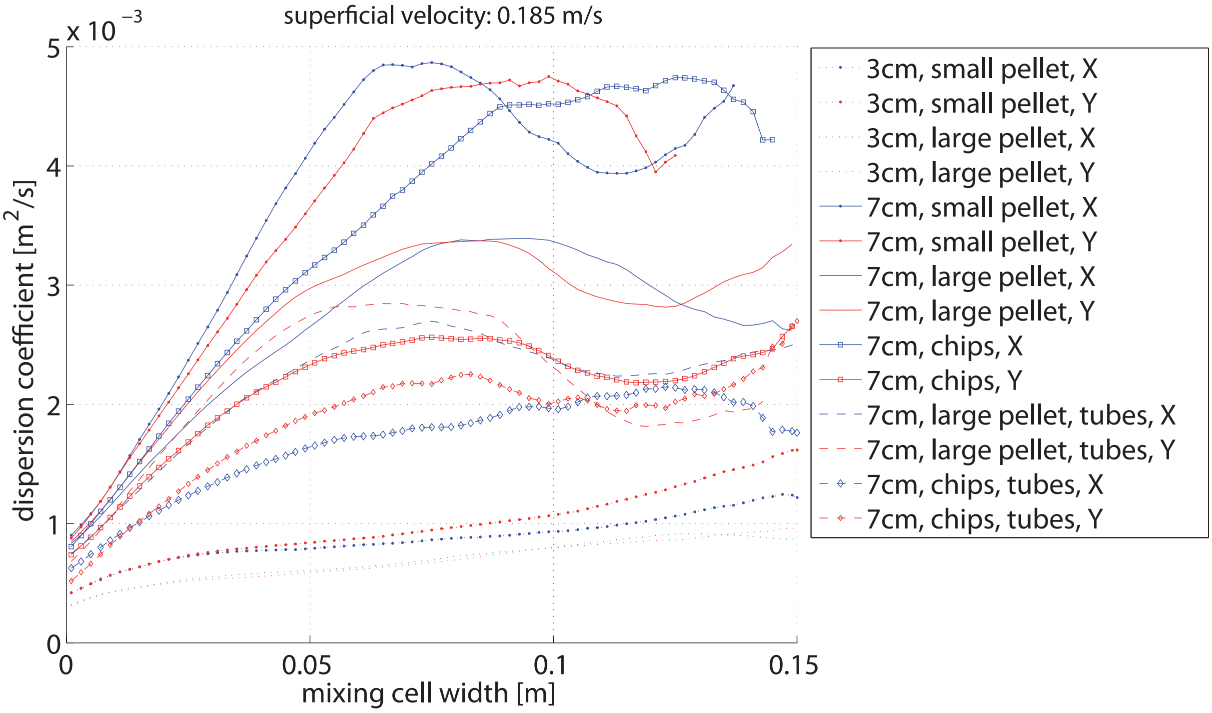

Figure 5.5: Dispersion coefficient for two directions from single particle tracking method for different configurations and a superficial velocity of $0.185\,\mathrm{m\,s^{-1}}$. Dispersion coefficients are 15 values smoothed movement weighted mean values from five (three for chips and/or tubes setup) videos with five different coloured particles each. Results with average movements below ten are removed.

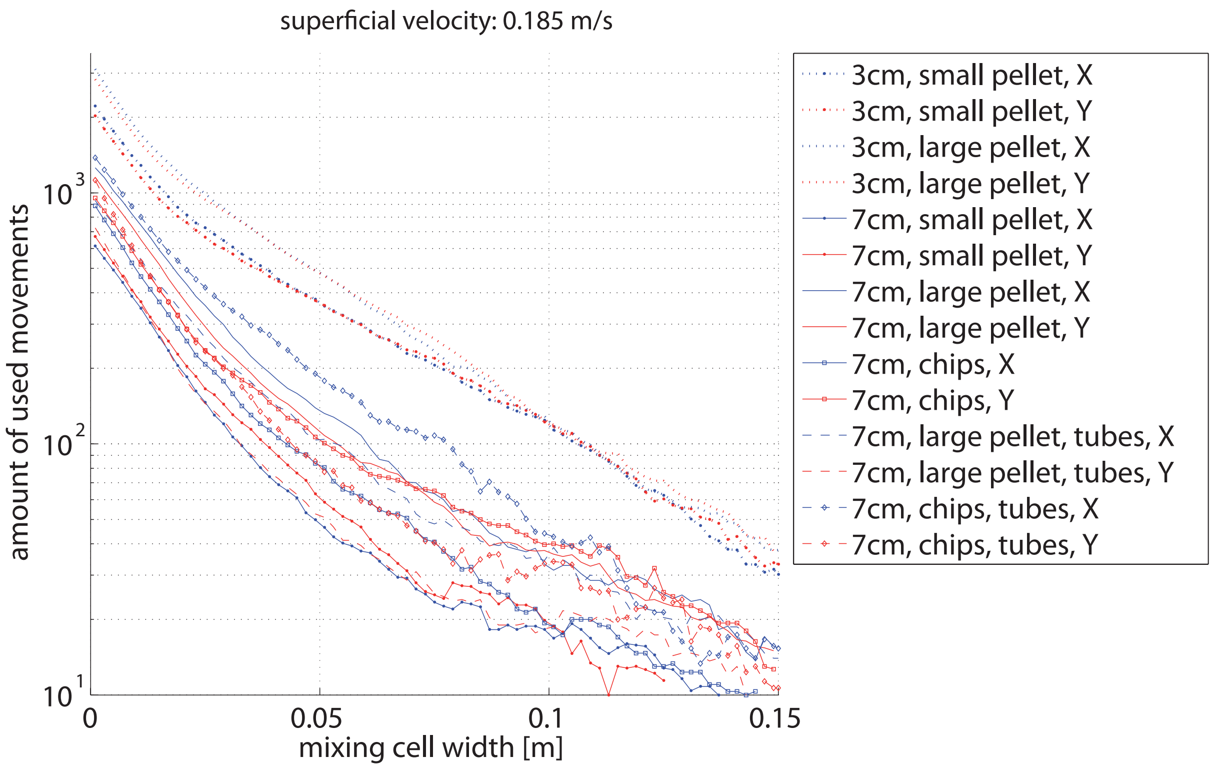

Figure 5.6: Average amount of used movements for single particle tracking method for different configurations and a superficial velocity of $0.185\,\mathrm{m\,s^{-1}}$. Results with average movements below ten are removed.

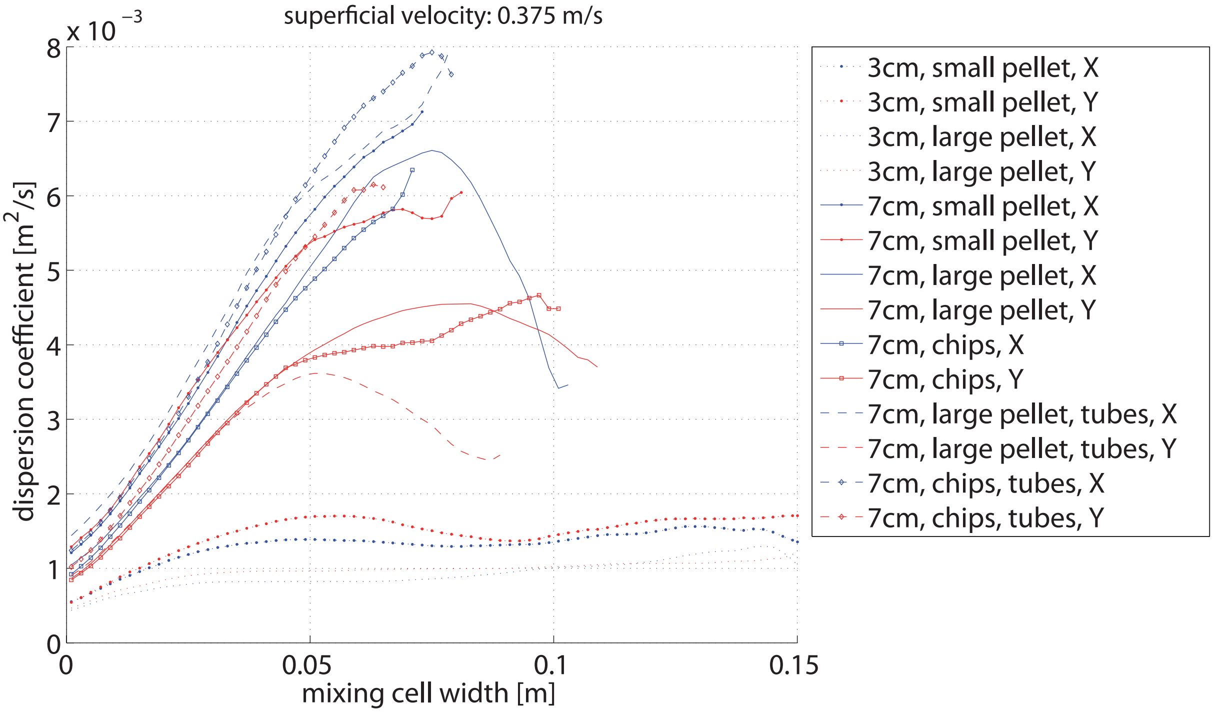

Figure 5.7: Dispersion coefficient for two directions from single particle tracking method for different configurations and a superficial velocity of $0.375\,\mathrm{m\,s^{-1}}$. Dispersion coefficients are 15 values smoothed movement weighted mean values from five (three for chips and/or tubes setup) videos with five different coloured particles each. Results with average movements below ten are removed.

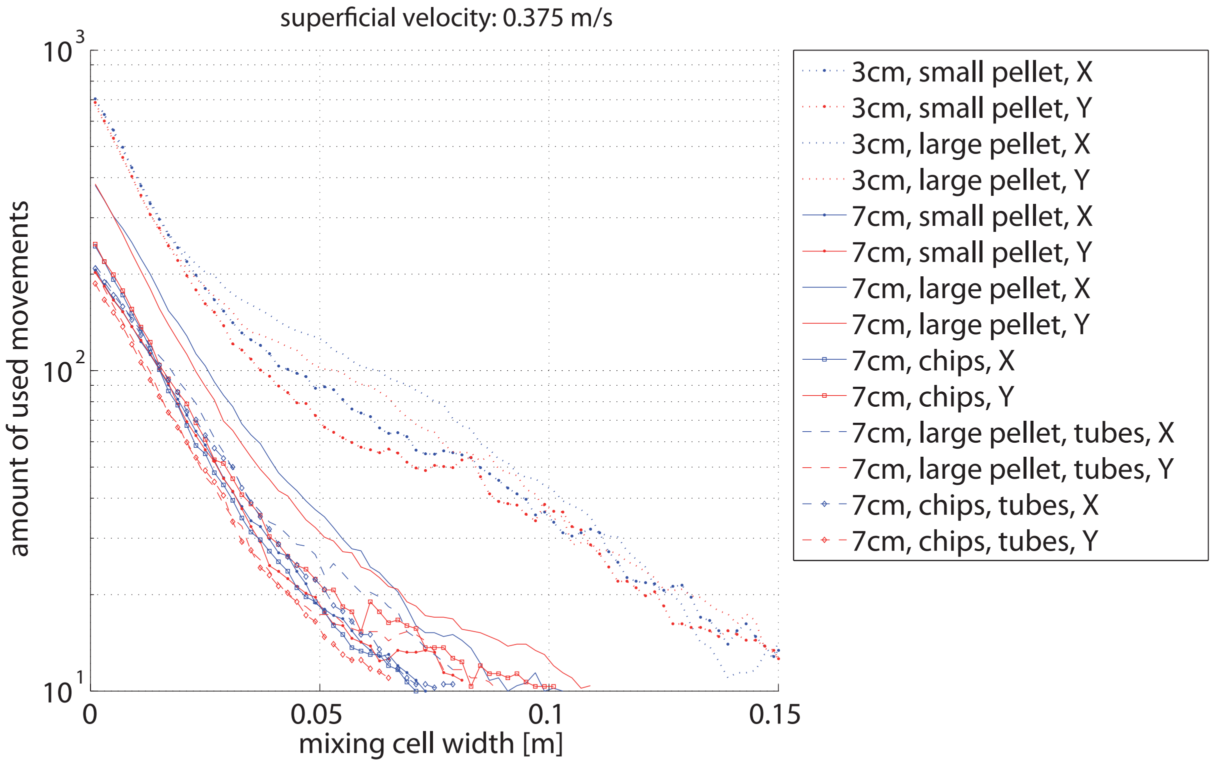

Figure 5.8: Average amount of used movements for single particle tracking method for different configurations and a superficial velocity of $0.375\,\mathrm{m\,s^{-1}}$. Results with average movements below ten are removed.

Table 5.1 (page 80) shows the maximum median dispersion coefficient values from the mixing cell width variation. Except the 7 cm, small pellets results the dispersion coefficients are large for higher fluidization. The dispersion coefficients obtained from the high bed height experiments are larger than those of the lower bed height. The values from 3 cm bed height are four to five times lower than those of the of the 7 cm bed height (bed height difference is 2.3 times). At 3 cm bed height small pellets have large dispersion coefficients than large pellets.

For 7 cm bed height and a low fluidization chips have the lowest and small pellets the highest dispersion coefficients. A double in fluidization changes this order to the highest values for chips and the lowest for large pellets.

In case of a tubes setup it can be seen that chips have lower dispersion coefficients at a superficial velocity of $0.185\,\mathrm{m^2\,s^{-1}}$ and higher ones at $0.375\,\mathrm{m^2\,s^{-1}}$.

bed height [cm]	superficial velocity [$\mathrm{m\,s^{-1}}$]	particle	option	$D_{\mathrm{median,max}}$ [$\mathrm{m^2\,s^{-1}}$]
3	0.185	large pellet		0.89×10^{-3}
3	0.375	large pellet		1.15×10^{-3}
3	0.185	small pellet		1.26×10^{-3}
3	0.375	small pellet		1.51×10^{-3}
7	0.185	chips		2.91×10^{-3}
7	0.375	chips		6.70×10^{-3}
7	0.185	large pellet		4.22×10^{-3}
7	0.375	large pellet		5.62×10^{-3}
7	0.185	small pellet		6.39×10^{-3}
7	0.375	small pellet		6.09×10^{-3}
7	0.185	chips	tubes	1.93×10^{-3}
7	0.375	chips	tubes	8.56×10^{-3}
7	0.185	large pellet	tubes	2.88×10^{-3}
7	0.375	large pellet	tubes	5.95×10^{-3}

Table 5.1: Dispersion coefficient results of single particle tracking analysis. Values are the maximum median values of the mixing cell variation from x and y

5.2 Multiple Particle Spreading

Figure 5.9 (page 81) shows the results from experiments at 7 cm bed height, superficial velocity of $0.375\,\mathrm{m\,s^{-1}}$ and 70 red large pellets.

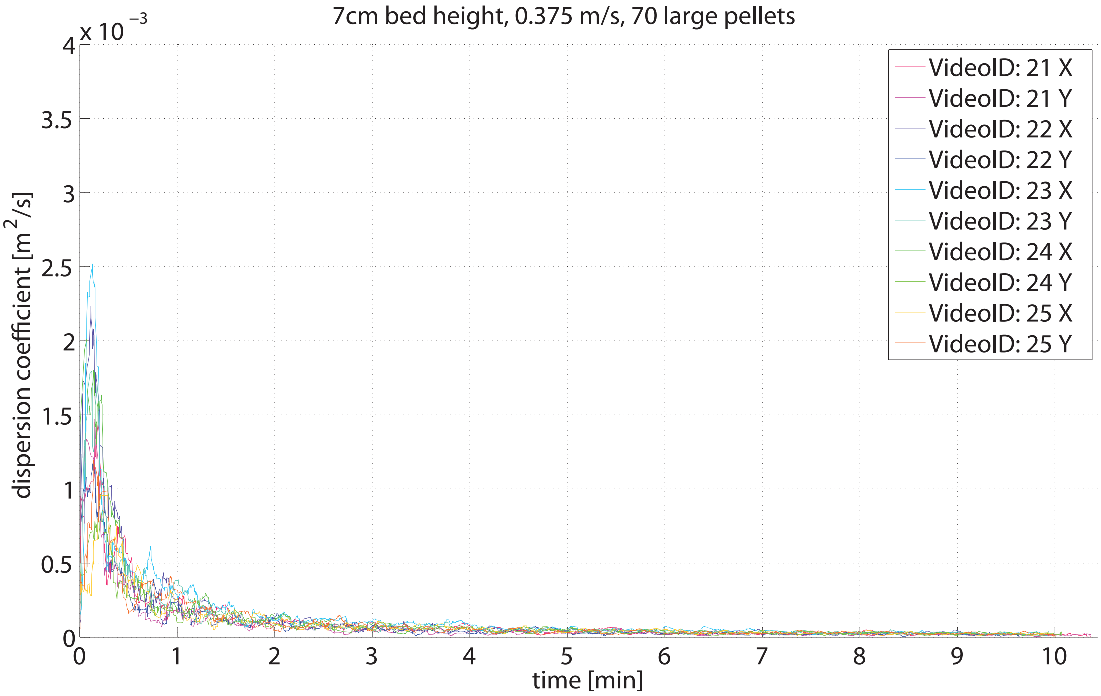

Figure 5.9: Dispersion coefficient measured with multiple particle spreading method, 7 cm bed height, $0.375\,\mathrm{m\,s^{-1}}$ and 70 large pellets from five videos

It can be seen that the trend of all video files and directions is almost the same. It is high in the beginning and decreases quite fast, before it converges to almost 0 at the end. This is in good agreement with theory. In some experiments it has been seen that the dispersion coefficient increases in the beginning, before it reaches the maximum. It is unknown where this comes from. Probably this happens because particles are close to each other so that they are detected as bigger ones.

The results displayed in Fig. 5.10 (page 82) to Fig. 5.15 (page 84) shows the mean values from the multiple particle spreading method. As already mentioned in Sect. 3.3.2 (page 44) some interpolation was needed to create mean values of several experiments. The recorded video lengths were between 10 and 20 minutes.

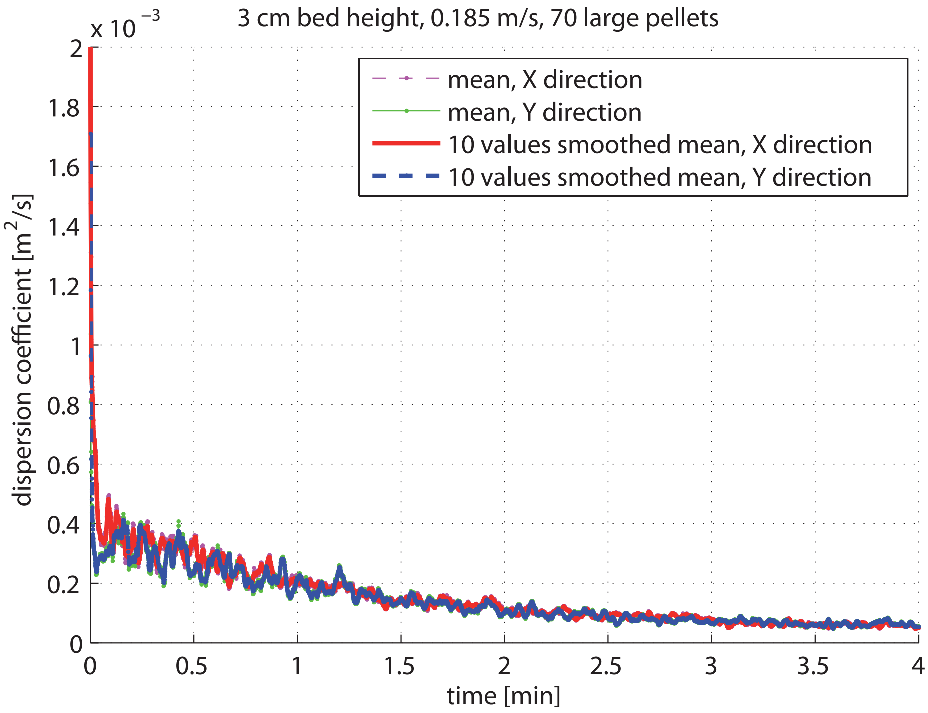

Figure 5.10: Dispersion coefficient measured with multiple particle spreading method, 3 cm bed height, superficial velocity of $0.185\,\mathrm{m\,s^{-1}}$ and 70 large pellets

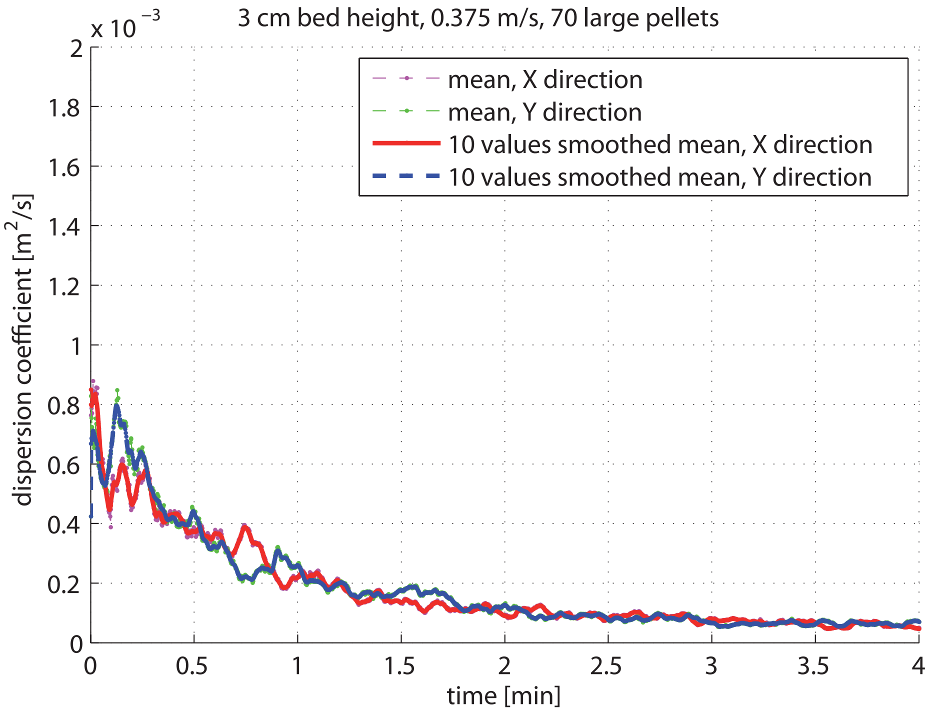

Figure 5.11: Dispersion coefficient measured with multiple particle spreading method, 3 cm bed height, superficial velocity of $0.375\,\mathrm{m\,s^{-1}}$ and 70 large pellets

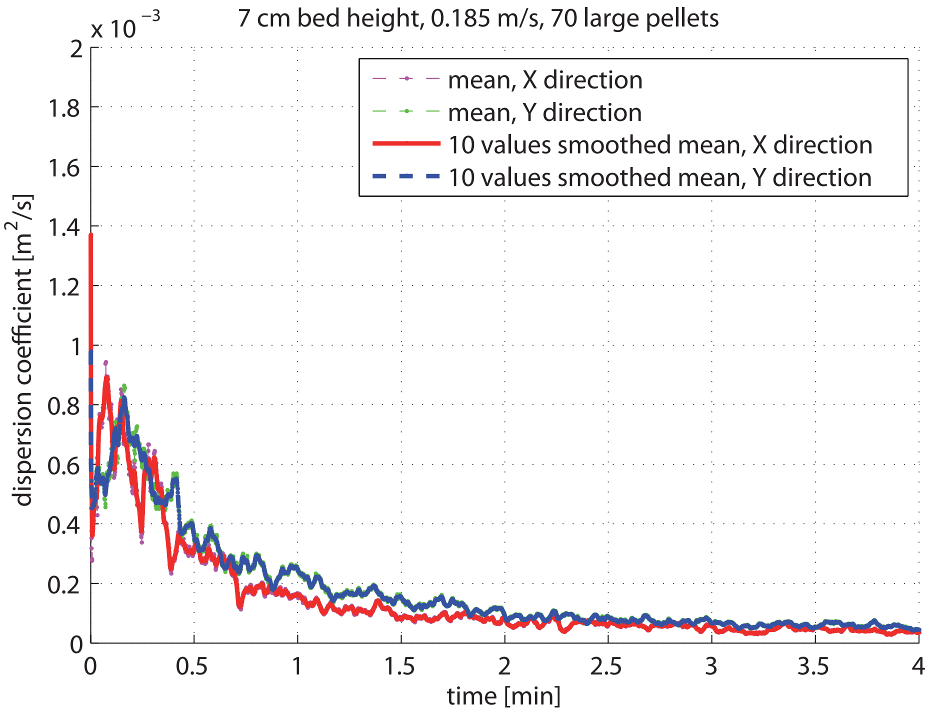

Figure 5.12: Dispersion coefficient measured with multiple particle spreading method, 7 cm bed height, superficial velocity of $0.185\,\mathrm{m\,s^{-1}}$ and 70 large pellets

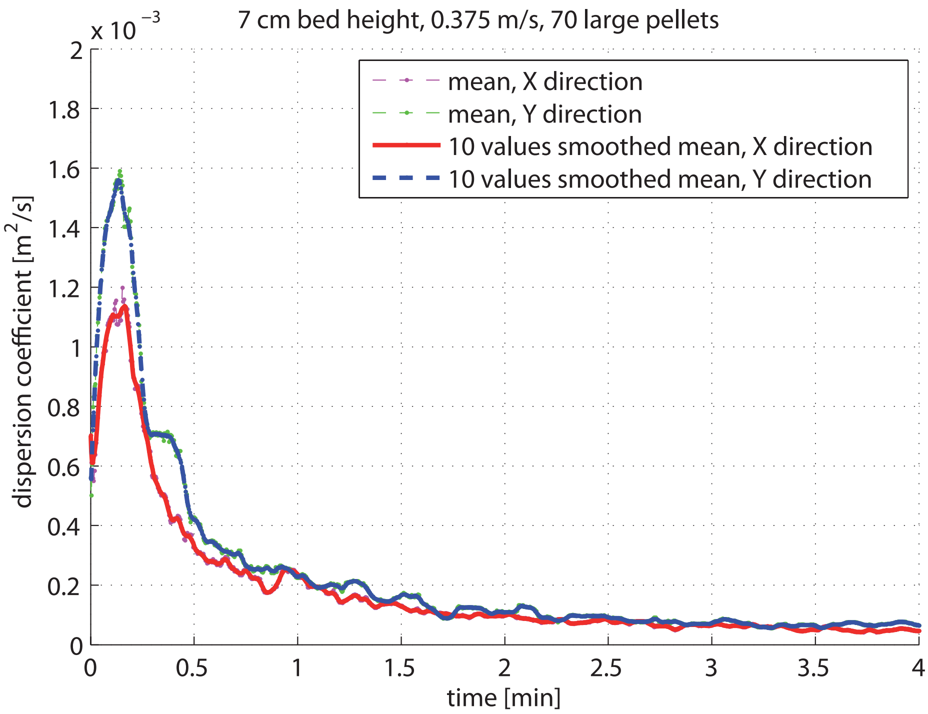

Figure 5.13: Dispersion coefficient measured with multiple particle spreading method, 7 cm bed height, superficial velocity of $0.375\,\mathrm{m\,s^{-1}}$ and 70 large pellets

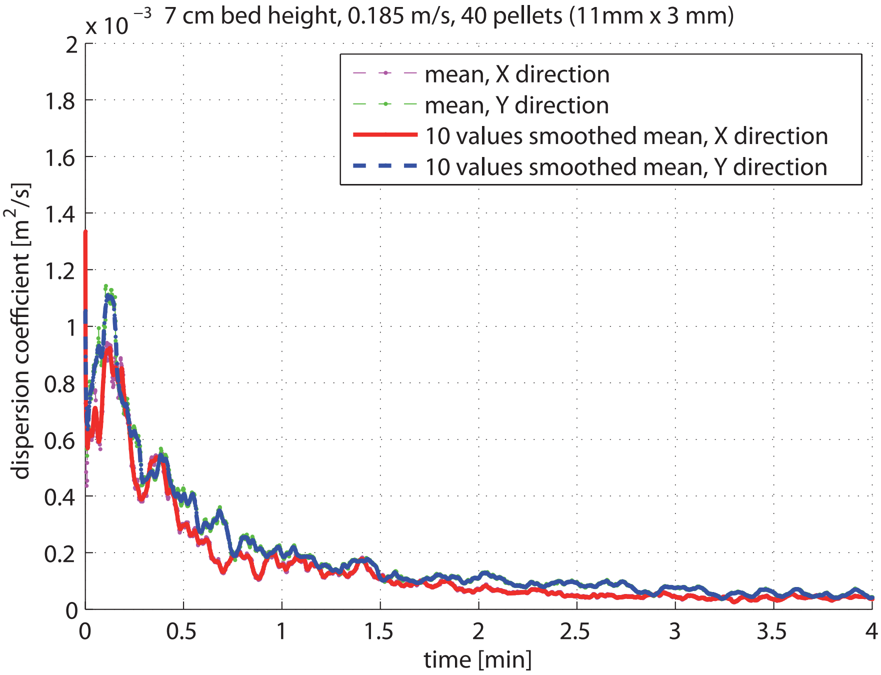

Figure 5.14: Dispersion coefficient measured with multiple particle spreading method, 7 cm bed height, superficial velocity of $0.185\,\mathrm{m\,s^{-1}}$ and 40 slightly shorter pellets (11 mm long, same diameter)

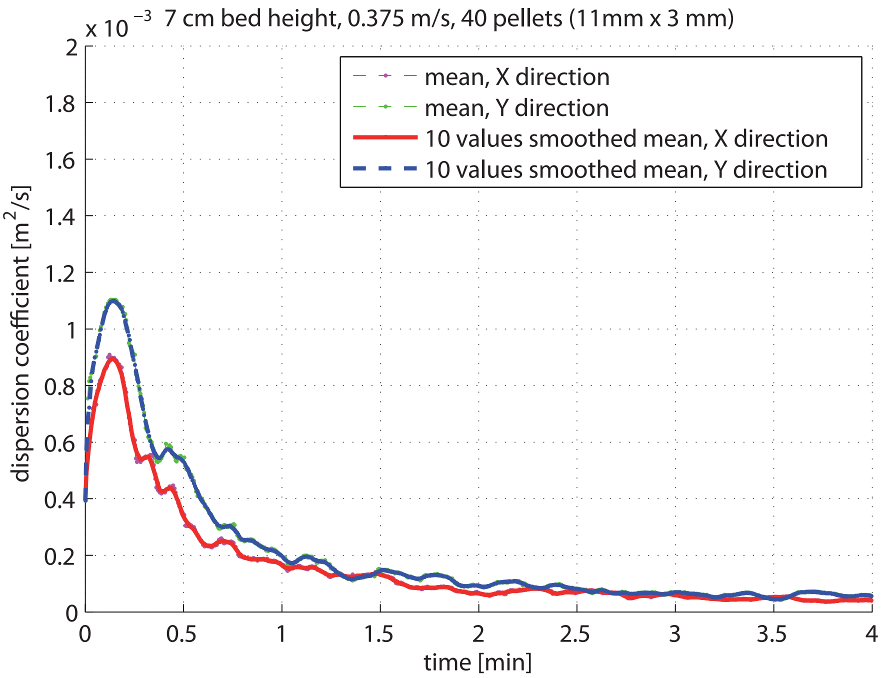

Figure 5.15: Dispersion coefficient measured with multiple particle spreading method, 7 cm bed height, superficial velocity of $0.375\,\mathrm{m\,s^{-1}}$ and 40 slightly shorter pellets (11 mm long, same diameter)

The results show that all cases reach a dispersion coefficient of $0.2 \times 10^{-3}\,\mathrm{m}^2\,\mathrm{s}^{-1}$ after one minute. For a better comparison mean values from these plots from both directions are calculated. This can be done, because the mixing should be the same (symmetric bed, no tubes, no internals, dropped in one corner). The expressiveness of these plots is increased by reducing the maximum displayed time to half a minute (see Fig. 5.16 (page 85)).

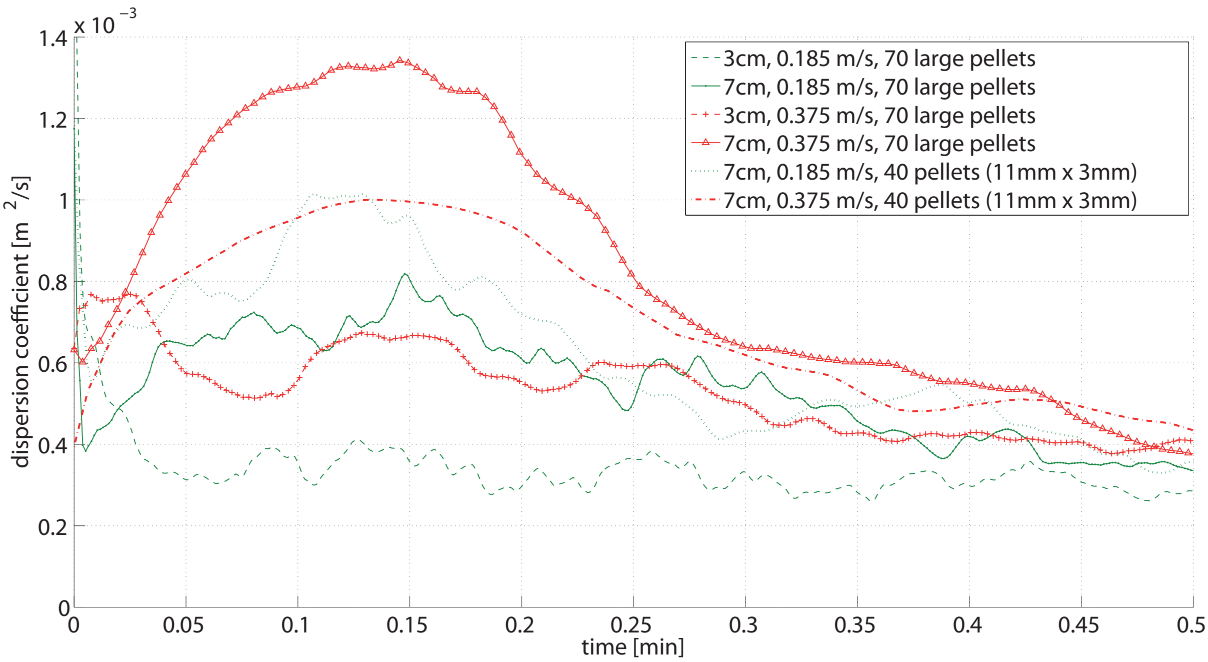

Figure 5.16: Dispersion coefficient measured with multiple particle spreading method for different cases. Displayed data is a five values smoothed mean value from all experiments and both directions for each case (different bed heights, superficial velocities and particle types).

The first detections in the stop areas are expressed by box plots. Figure 5.17 (page 88) displays the values for the combined graph. Those for each direction are listed in Appendix D (page 114). Mean values are displayed in Table 5.2 (page 86).

Figure 5.16 (page 85) shows that an increase in bed height and superficial velocity indicate higher dispersion coefficients. All the different combinations convert to the same value after a long time, therefore the interesting time is in the beginning, before something hits the opposite wall.

Table 5.2 (page 86) shows that the first detections in the stop area are generally, except one outlier, already after round six seconds (depending on the case).

bed height [cm]	superficial velocity [$\mathrm{m\,s^{-1}}$]	particle	time [min]		
			x	y	combination
3	0.185	70 large pellets	0.36070	0.19238	0.27654
3	0.375	70 large pellets	0.18638	0.31470	0.25054
7	0.185	70 large pellets	0.12584	0.10541	0.11563
7	0.375	70 large pellets	0.12057	0.21460	0.16758
7	0.185	40 pellets	0.16098	0.13709	0.14903
7	0.375	40 pellets	0.23344	1.86906	1.05125

Table 5.2: Mean detection times of first detections in stop area for different conditions

Figure D.1 (page 114) and Fig. D.2 (page 115) shows that the results different are for both directions. This could happen, because the surface time for particles is quite low and therefore they are not on the surface if they reach the stop areas. Extending the stop are from the chosen 10 % (of the reactor length) should decrease this effect. A side effect of increasing this parameter is, that the time before reaching this stop area is decreased (due to shorter distances). All in all it is a fast process. To increase the results quality many particles and runs are needed to ensure good statistics.

Times are larger for lower fluidization and bed heights. In case of higher bed heights and higher fluidization they are slower, most likely because they are not detected.

40 slightly smaller pellets have the same trend as the longer ones. The detection times are increased for less particles, probably because the probability that something is detected at the surface is lower since the amount of particles is 42 % less.

The huge time difference of 94.2 seconds between x and y for 40 pellets at 7 cm bed height and $0.375\,\mathrm{m\,s^{-1}}$ leads to the question if mixing is really symmetrical and combinations from x and y are allowed. Further work needs to investigate if it is possible to combine data from both directions and extract the dispersion coefficient or, extract it for both directions and create mean values afterwards.

The dispersion coefficient computed from the 40 pellets experimental data needs further investigation to explain why it is partially greater for a lower fluidization than for higher one (compare 40 pellets curves).

The trend of the highest mixing environments (7cm, $0.375\,\mathrm{m\,s^{-1}}$) suggests that larger pellets mix better than smaller under these conditions. In contrast, for lower superficial velocity it is the other way round (see 7cm, $0.185\,\mathrm{m\,s^{-1}}$).

It has been observed, that paint was missing on many particles after a couple of experiments. Therefore the particles had to be repainted. This effect has not been observed by long single particle tracking runs. Therefore it is assumed that the particles interact with each other and scratch off the paint. Additionally it is likely that the sharper edges (compared to the particles used for single particle tracking) are the reason for this, or at least increasing this effect. The sharper edges come from the particle preparation. The particles created for single particle tracking have smoothed edges, the other still have the pliers cut face. As already mentioned in Sect. 3.2.1 (page 29), the unpainted parts are not a problem. Nevertheless the colour pieces are. They are much lighter than the particles and therefore better floating on the bed material. In case they are big enough they are detected as particles, categorised and used in subsequently calculations. This effect needs further investigation.

Figure 5.17 (page 88) shows the distribution of the first detections. It can be seen, that lower bed heights data is wider spread. Further on, smaller particles produce larger median values.

In conclusion the whole analysis is very various. Therefore many runs are needed to achieve good statistics. The time until the first detections in the stop area is quite short, but is extendable with a larger cold flow model.

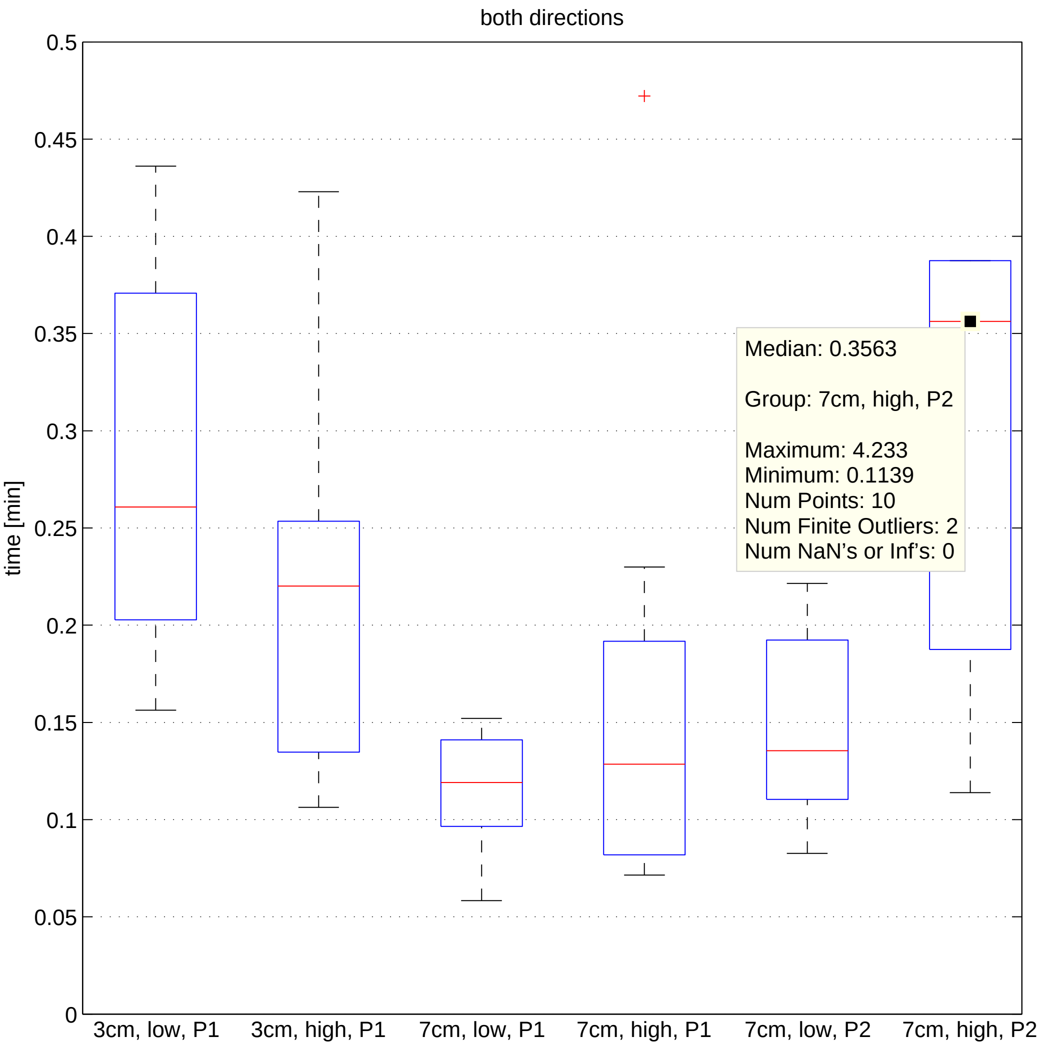

Figure 5.17: Zoomed in box plot off first detections in stop area (x and y direction) of all experiments for different conditions. P1 stands for 70 large pellets and P2 for 40 slightly smaller pellets. Low stands for a superficial velocity of $0.185\,\mathrm{m\,s^{-1}}$ and high for $0.375\,\mathrm{m\,s^{-1}}$.

5.3 Scaling Inaccuracies

The results quality by not fitting all scaling laws is unknown. The errors occur from deviations during the scaling process. For instance, if no bed material with needed density exists or is too difficult to handle, a different has to be chosen. Thereby divergences of several tenths of percentages are committed. In former work (e.g. see (Johnsson et al.; 1999)), with the same derivation, it has been shown that the cold flow model data agrees relatively well with them of the original large-scale application.

If the bed material under hot conditions is sand with an average density of $2600\,\mathrm{kg\,m^{-3}}$ the densities (see Sect. 3.5 (page 55)) differ up to 51%. The effect of this on the results is unknown. If the used bed material is lighter, it can be assumed, that the material is ejected more far away (during the eruption). Further on this might overestimate the dispersion coefficient.

Table 3.4 (page 57) shows the highest deviation for the bed material densities.

The chosen fuel particle material covers (depending on the scale up case) the density range of wood chips.

In case of pellets (and the scale-up case) it is 19.6 % to 65.6 % too low. By comparing the deviation of bed material density and particle density it can be seen that the lowest difference can be found at the case with the highest bed material deviation. Subsequently the cases (mostly gasification conditions) with high density deviation are those representing pellets (based on the closest density ratio).

Pellets used in the down-scaled unit are lighter and therefore float better. Subsequently this should overestimate the mixing. To verify this assumption experiments with different fuel particle materials are needed. It should be kept in mind, that the developed detection algorithm only detects something on the bed surface. Therefore heavy particles require very long recording times to ensure a certain amount of data. The percentages of surface time are depending on the conditions. As it can be seen in Table B.1 (page 96) the range goes from 1.3 to 13.16 %.

5.4 Influence of Perspective View on Results

Particle positions are influenced by the perspective view. The effect does not exist in the centre, but is increasing to the sides. Raising bed height and superficial velocity results in rougher conditions. This means that the bubble eruptions are growing and therefore the influence increases. Higher bed heights decrease the distance between camera and bed, which leads to a different focal distance and therefore to a wider angle of view. Further on the particle position could have an increased distance from the focus level due to the higher bed height. This results in unsharpness and subsequently in a different particle size.

In case of single particle tracking, movements using coordinates close to the wall are often removed anyway. Therefore the effect should be lower for these results.

For large mixing cell lengths the effect might be higher, since longer distances are needed, which results in coordinates closer to walls. In general, shorter movements are more likely effected by wrong coordinates.

The effect is decreasing by increasing the distance to the camera (as described in Sect. 2.6 (page 17)). In case no wide angle lens is used it can be assumed that the error is less, compared to those from scaling inaccuracies.

Chapter 6

Conclusion

The new detection algorithm detects and classifies particles correctly. The colour sensitivity of the detection algorithm is reduced. Additionally the categorisation is optimised. As result five instead of three particles can be used, increasing the amount of extracted information. Furthermore the algorithm is suitable for parallel computing.

During this work, two different theoretical models (single particle tracking, multiple particle spreading) were implemented. Parameter investigations lead to the knowledge of the importance of the mixing cell length (single particle tracking) and its major influence. Some ideas to figure it out were tried, but none was successful. Subsequently this parameter needs further investigation to achieve dispersion coefficients that could be compared with industrial applications.

Both ways show that dispersion coefficients are higher by increasing bed heights and fluidizations. However the results order of magnitude is different.

For low mixing cell lengths the results of different conditions are in the same range. In case of higher values the results fluctuate considerably. Beside wall effects it is assumed that this has some statistical reasons. Therefore more data is needed (more videos and/or a much larger cold flow model).

For repeatable results from the multiple particle spreading method much more data is needed.

Without knowledge of the mixing cell length the dispersion coefficients ($0.8 \times 10^{-3}\,\mathrm{m^2\,s^{-1}}$ to $8.56 \times 10^{-3}\,\mathrm{m^2\,s^{-1}}$) had to be estimated from the maximum median values.

Chapter 7

Further Work

This thesis gives several ideas where further work is needed. The most important one is the investigation of the mixing cell width. Further on the models have to be compared. Therefore much more data is needed to make it statistically reliable. For the use of different internal combinations a way must be found to remove the reflections. Moreover the algorithm must be extended by adding the possibility to add internal walls and include them in the "wall-check"[1].

[1] see Sect. 3.3.1 (page 39)

Appendix A

Colour Classification - RGB Plots

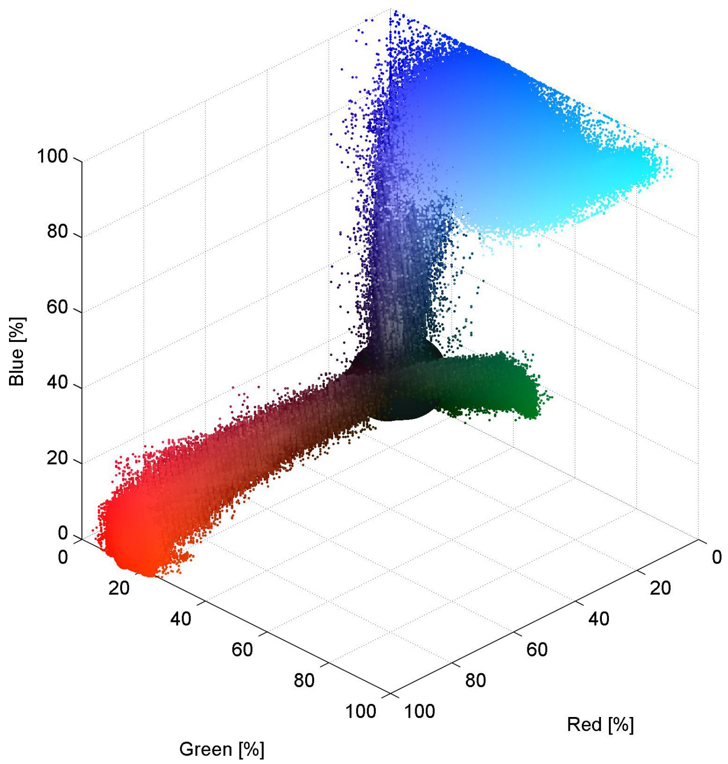

Figure A.1: Colours detected in videos with red, white or green particles - 3d view

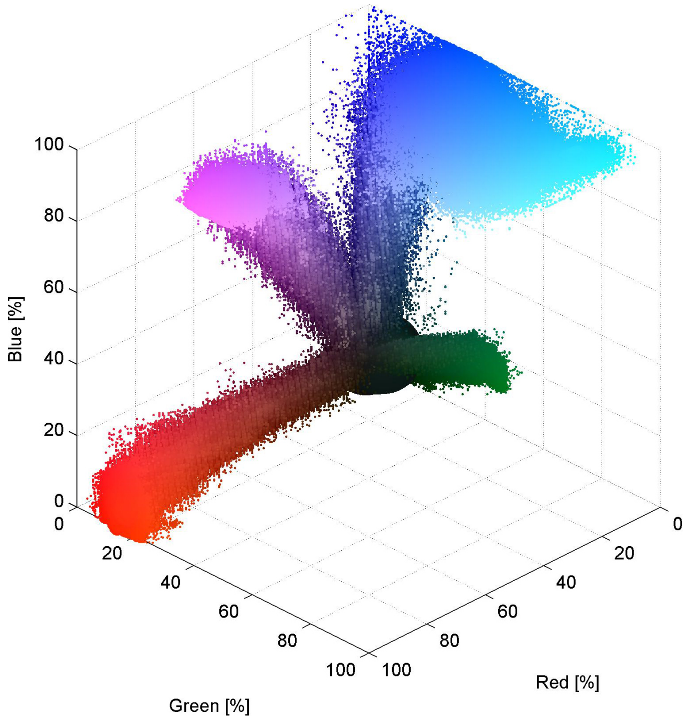

Figure A.2: Colours detected in videos with red, white, green or pink particles - 3d view

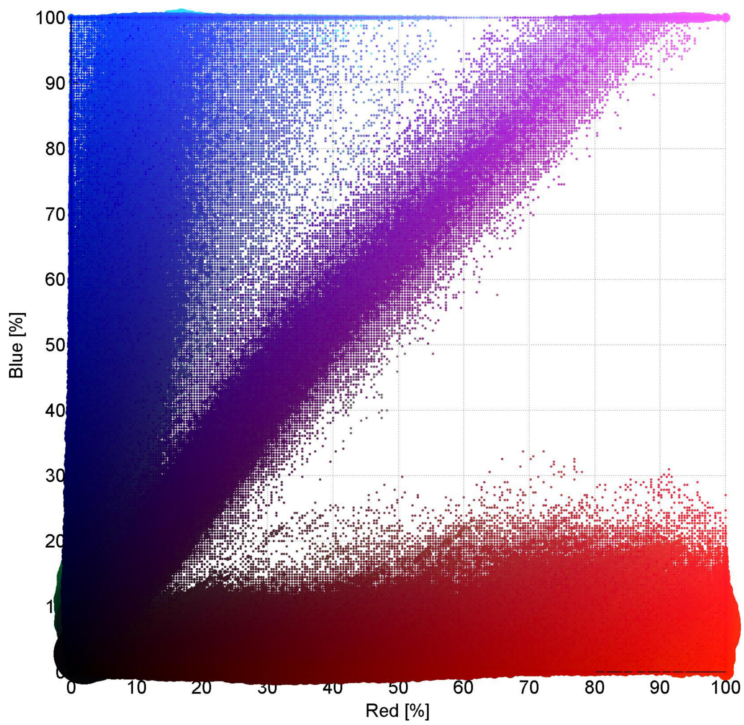

Figure A.3: Colours detected in videos with red, white, green or pink particles - 2d view

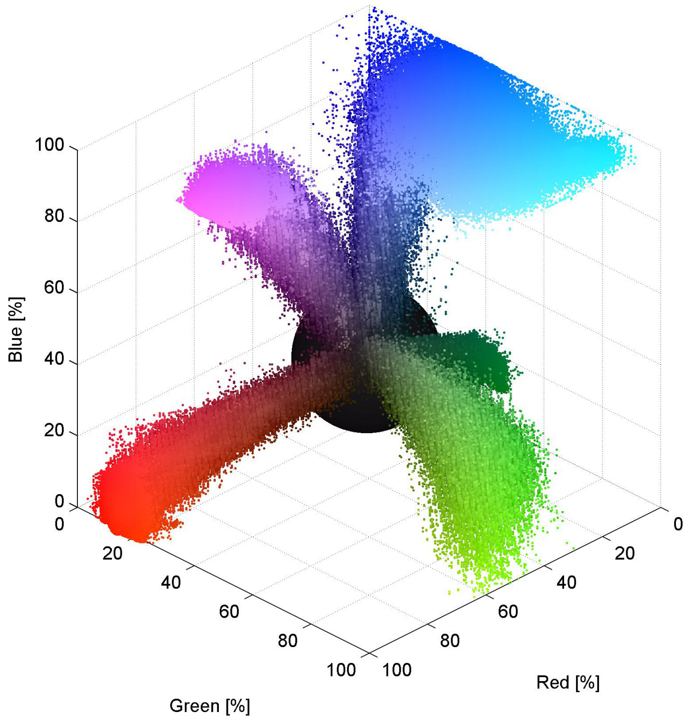

Figure A.4: Colours detected in videos with red, white, green, pink or yellow particles - 3d view

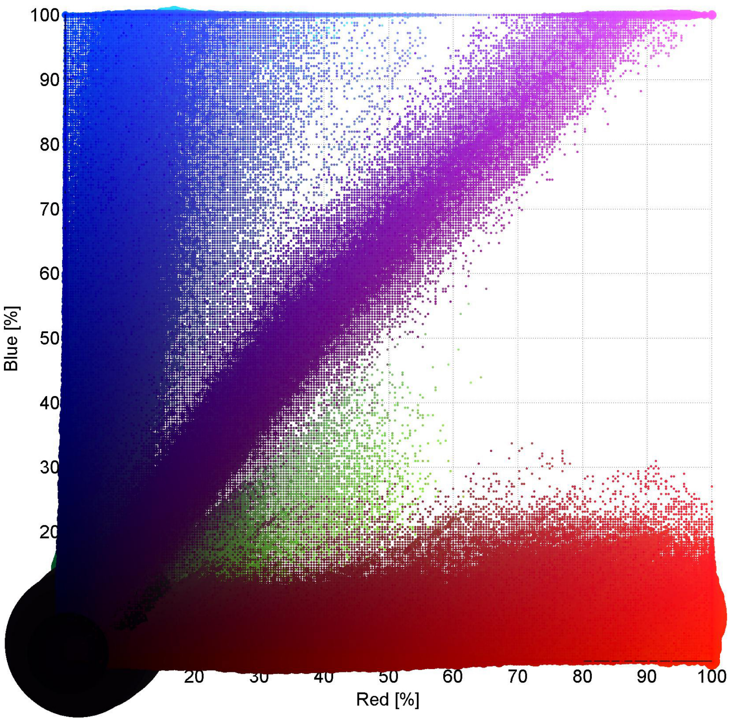

Figure A.5: Colours detected in videos with red, white, green, pink or yellow particles - 2d view

Appendix B

Surface Time

bed height [cm]	superficial velocity [$\mathrm{m\,s^{-1}}$]	particle	option	surface time [%]
3	0.185	small pellet		10.07
3	0.375	small pellet		3.72
3	0.185	large pellet		13.16
3	0.375	large pellet		3.58
7	0.185	small pellet		3.73
7	0.375	small pellet		1.37
7	0.185	large pellet		6.18
7	0.375	large pellet		2.31
7	0.185	chips		5.03
7	0.375	chips		1.53
7	0.185	large pellet	tubes	4.62
7	0.375	large pellet	tubes	1.51
7	0.185	chips	tubes	6.42
7	0.375	chips	tubes	1.30

Table B.1: Percentage of surface time for different conditions

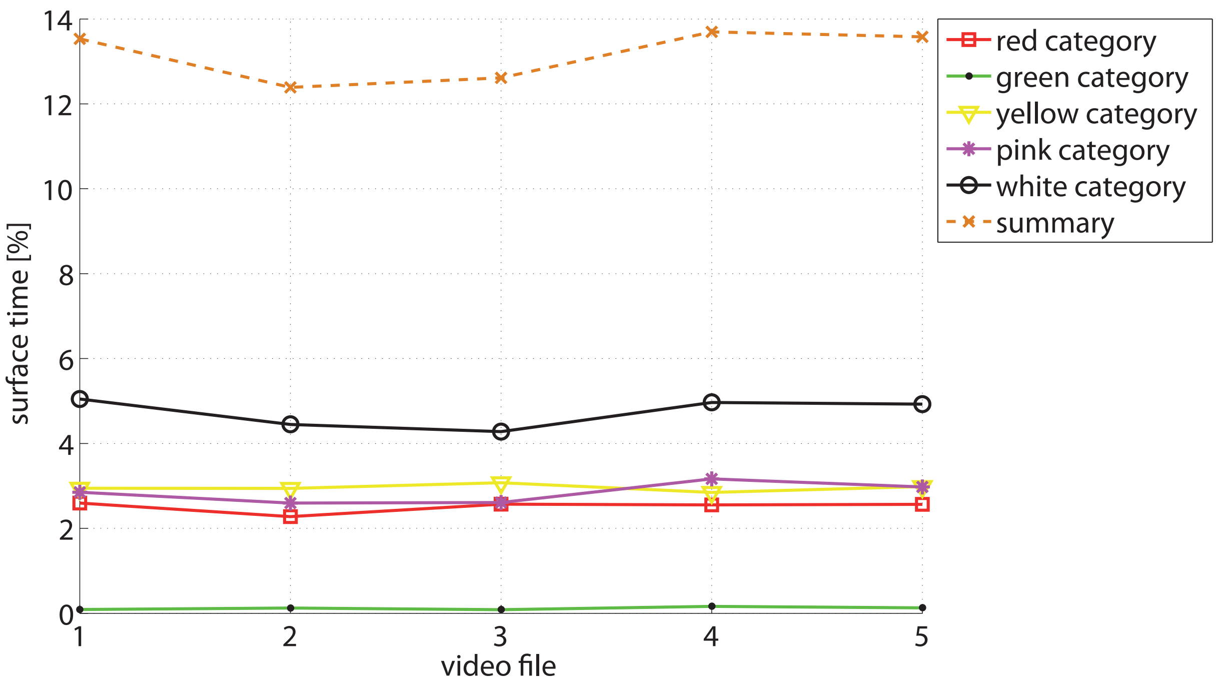

Figure B.1: Percentage of time, particles are on the surface (3 cm, $0.185\,\mathrm{m\,s^{-1}}$, large pellets)

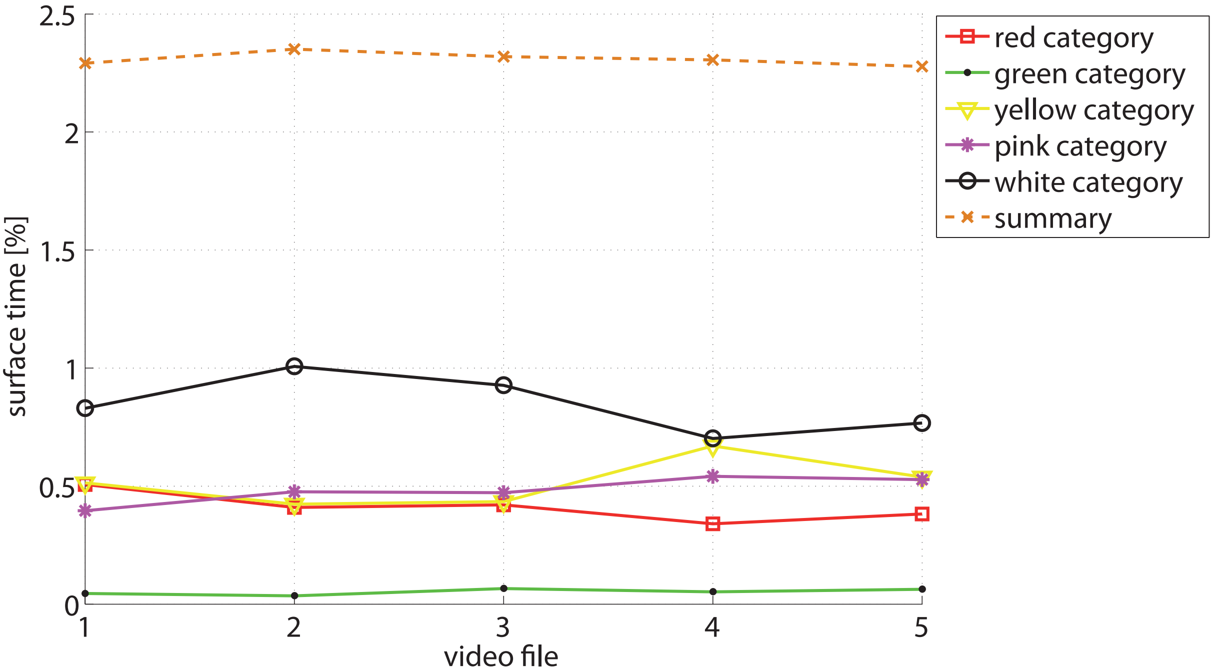

Figure B.2: Percentage of time, particles are on the surface (7 cm, $0.375\,\mathrm{m\,s^{-1}}$, large pellets)

Appendix C

Mixing Cell Variation Statistical Plots

Figure C.1 (page 100) to Fig. C.14 (page 113) show statistics from dispersion coefficients extracted for x, y and both directions. The bright red area marks all values (from minimum to maximum). The darker red goes from 25 to 75 percent quantiles. The used data is from all videos and categories with movements and dispersion coefficients greater 0.

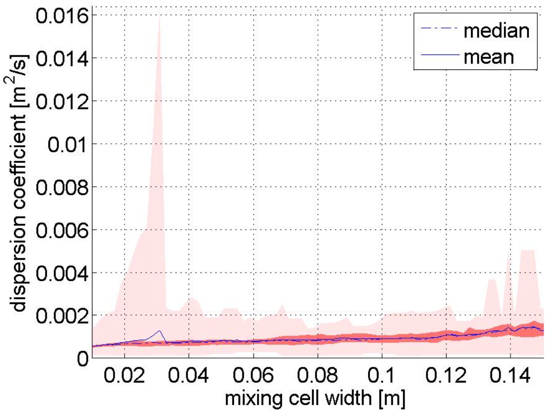

(a) x direction

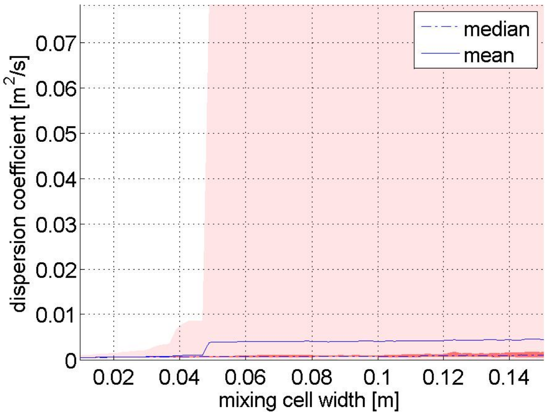

(b) y direction

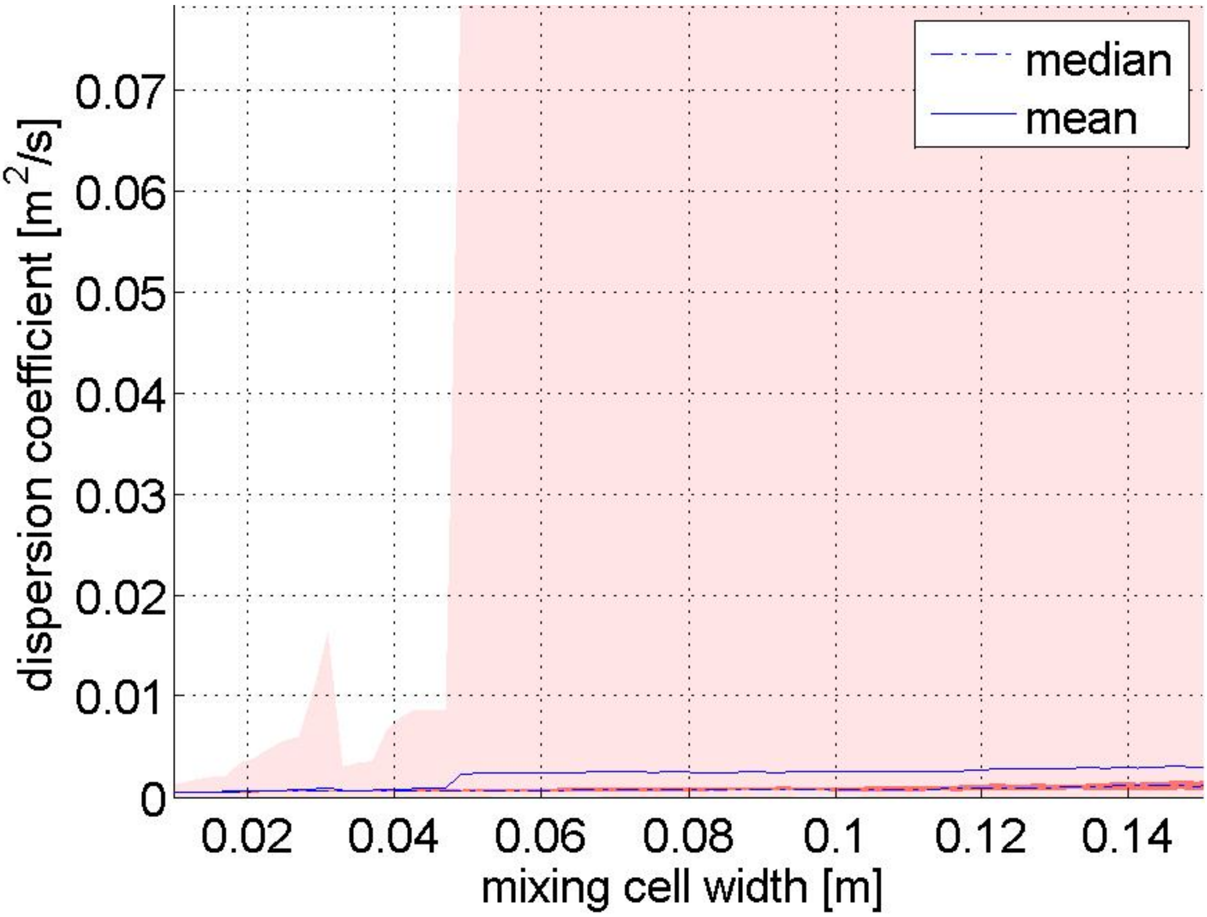

(c) x and y direction

Figure C.1: Dispersion coefficients for different mixing cell lengths at 3 cm bed height, superficial velocity of $0.185\,\mathrm{m\,s^{-1}}$ and small pellets

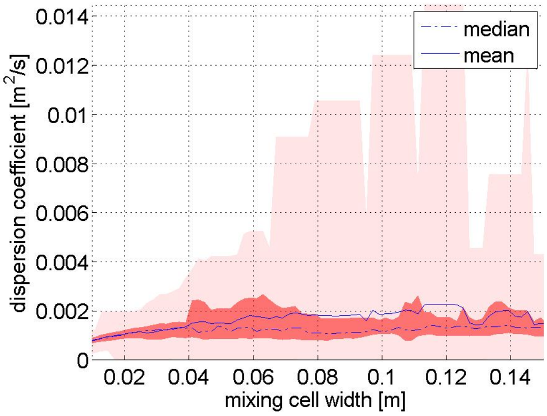

(a) x direction

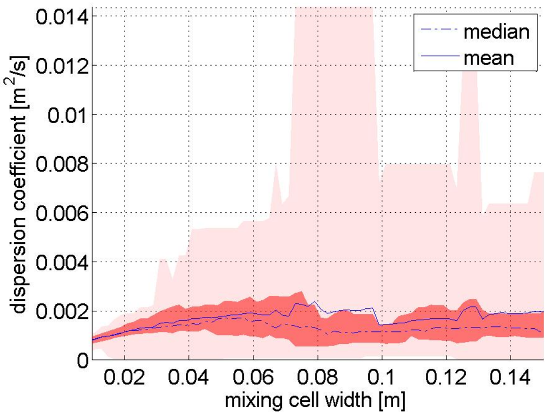

(b) y direction

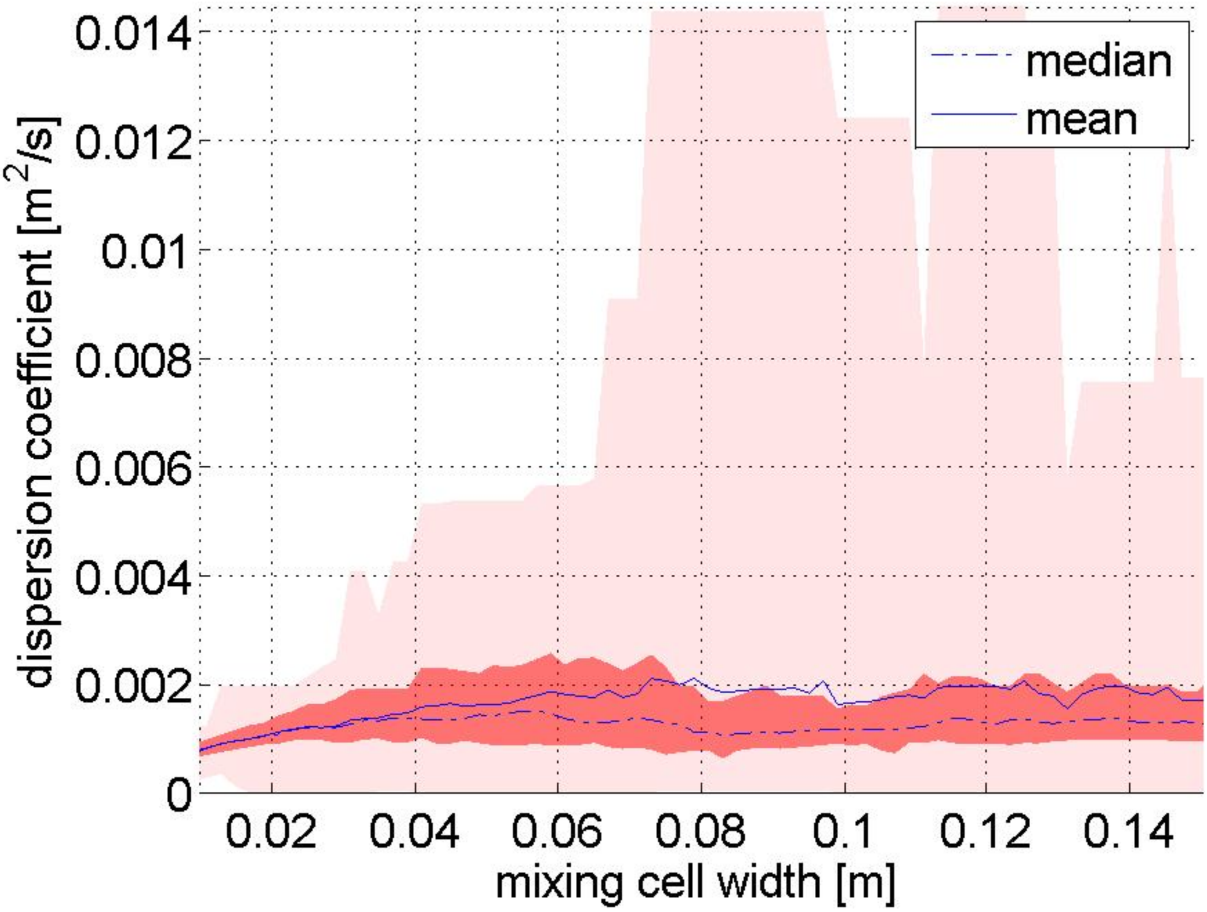

(c) x and y direction

Figure C.2: Dispersion coefficients for different mixing cell lengths at 3 cm bed height, superficial velocity of $0.375\,\mathrm{m\,s^{-1}}$ and small pellets

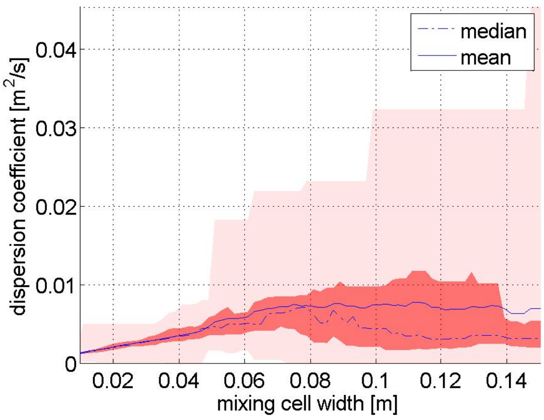

(a) x direction

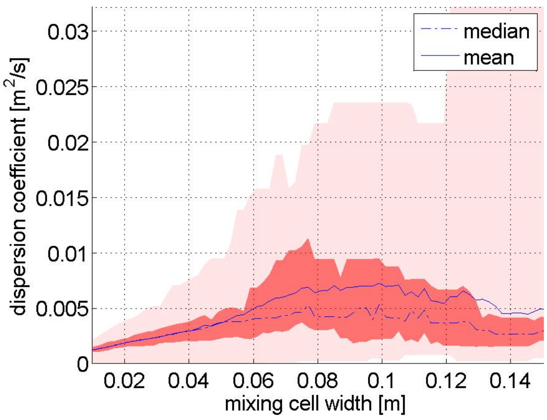

(b) y direction

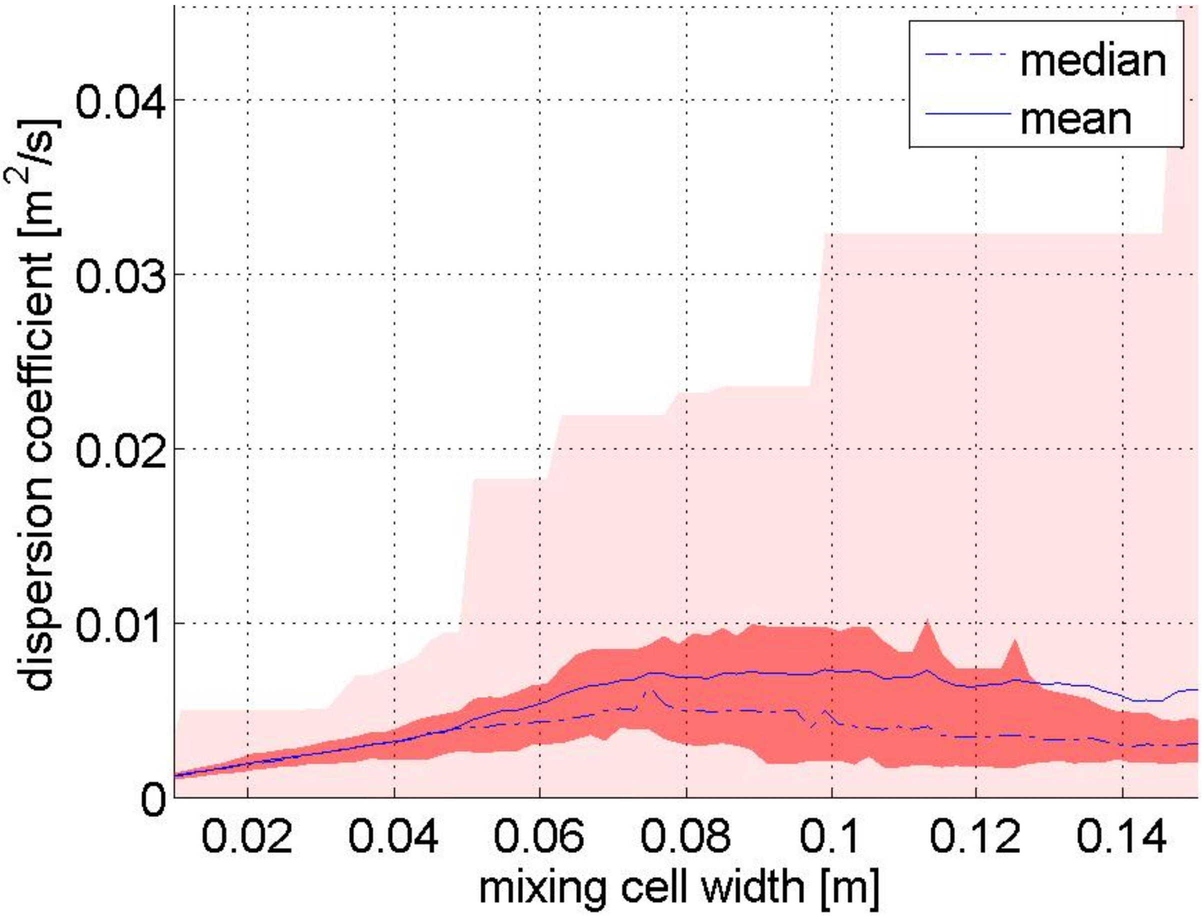

(c) x and y direction

Figure C.3: Dispersion coefficients for different mixing cell lengths at 7 cm bed height, superficial velocity of $0.185\,\mathrm{m\,s^{-1}}$ and small pellets

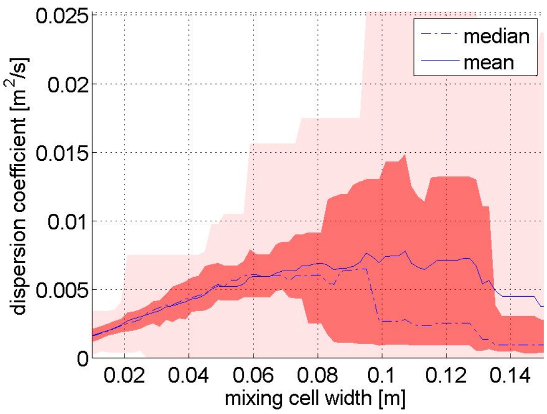

(a) x direction

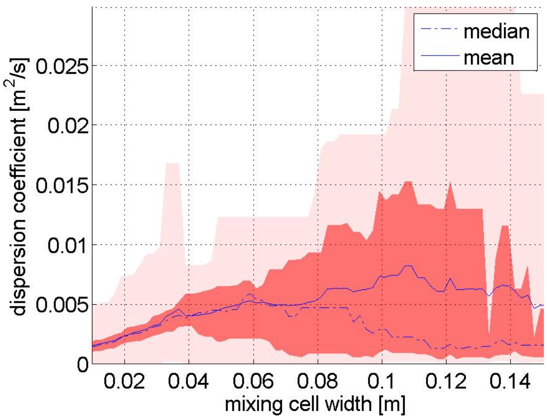

(b) y direction

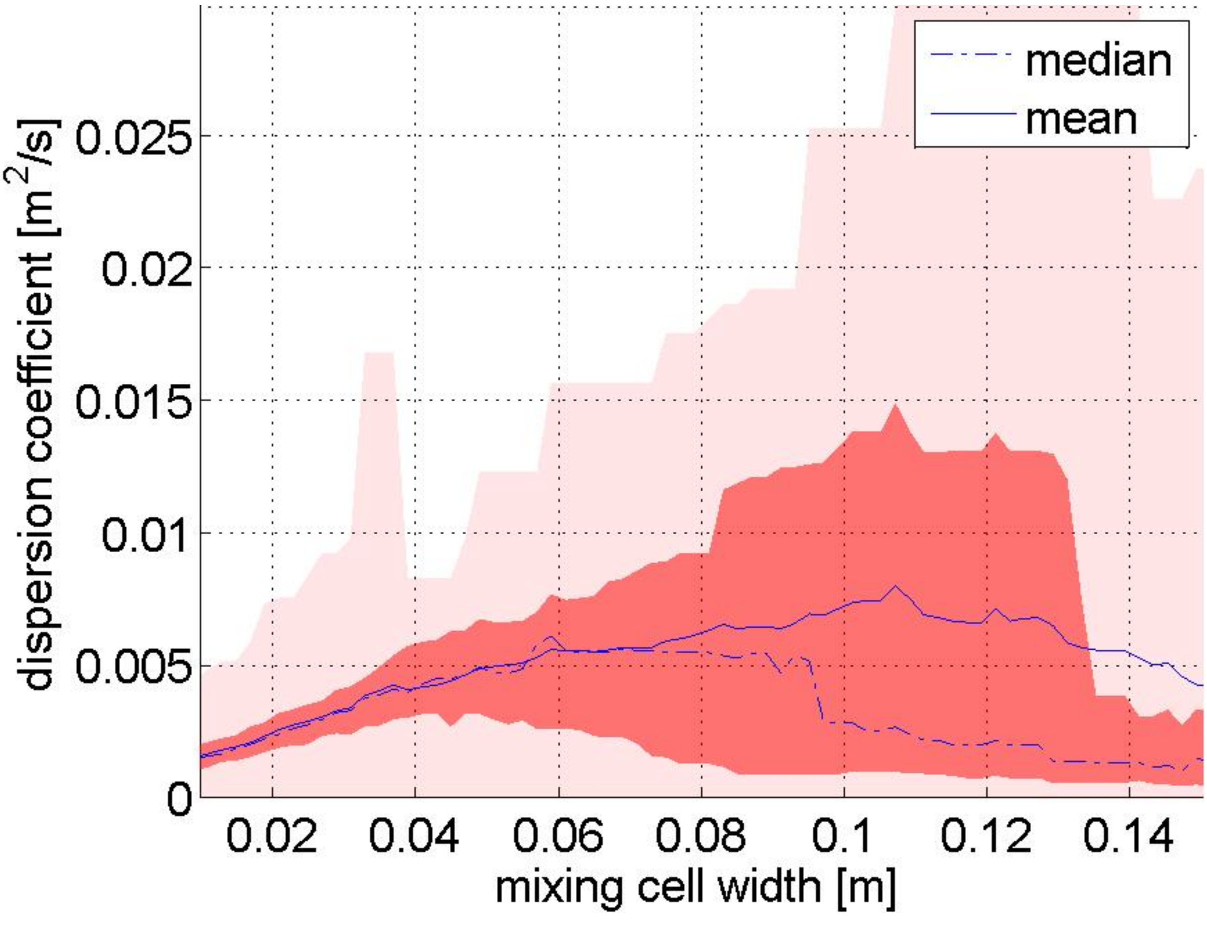

(c) x and y direction

Figure C.4: Dispersion coefficients for different mixing cell lengths at 7 cm bed height, superficial velocity of $0.375\,\mathrm{m\,s^{-1}}$ and small pellets

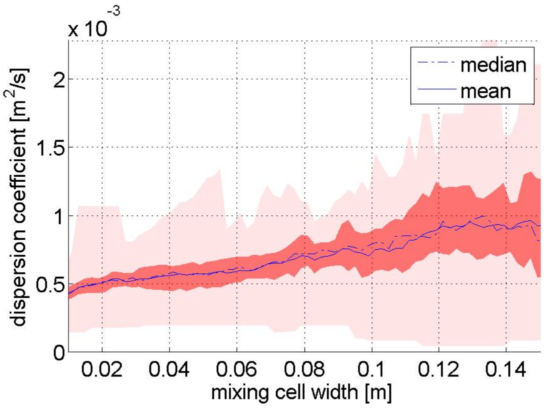

(a) x direction

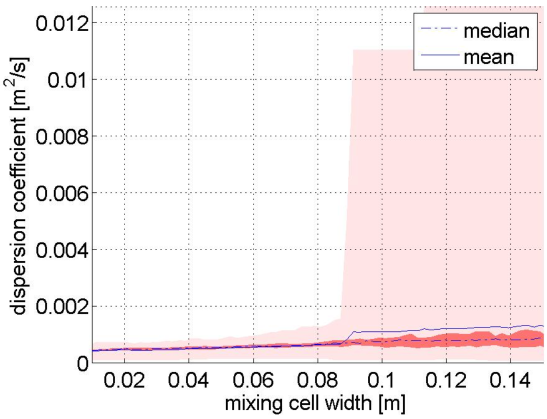

(b) y direction

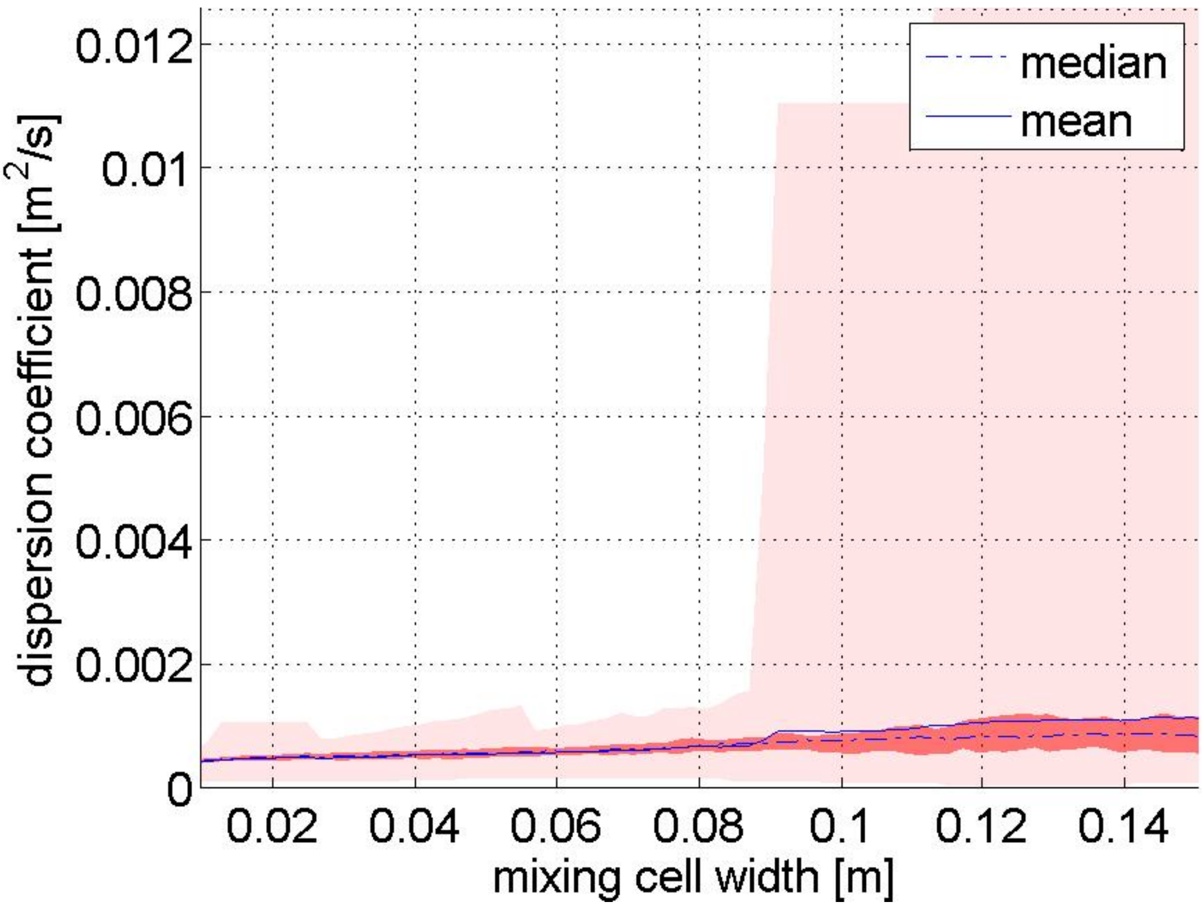

(c) x and y direction

Figure C.5: Dispersion coefficients for different mixing cell lengths at 3 cm bed height, superficial velocity of 0.185 $m\,s^{-1}$ and large pellets

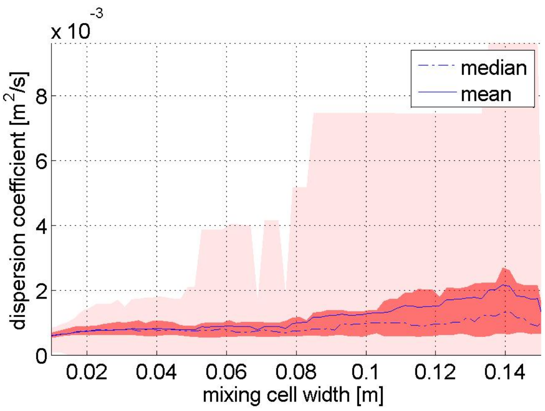

(a) x direction

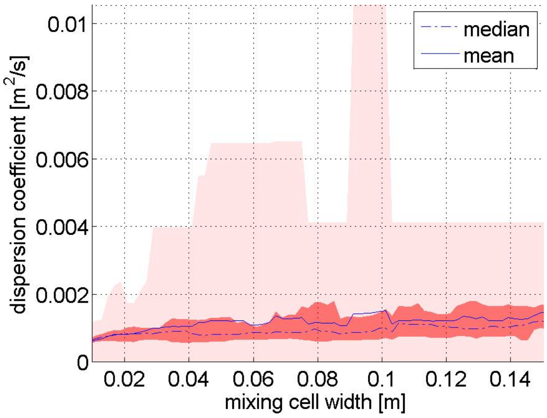

(b) y direction

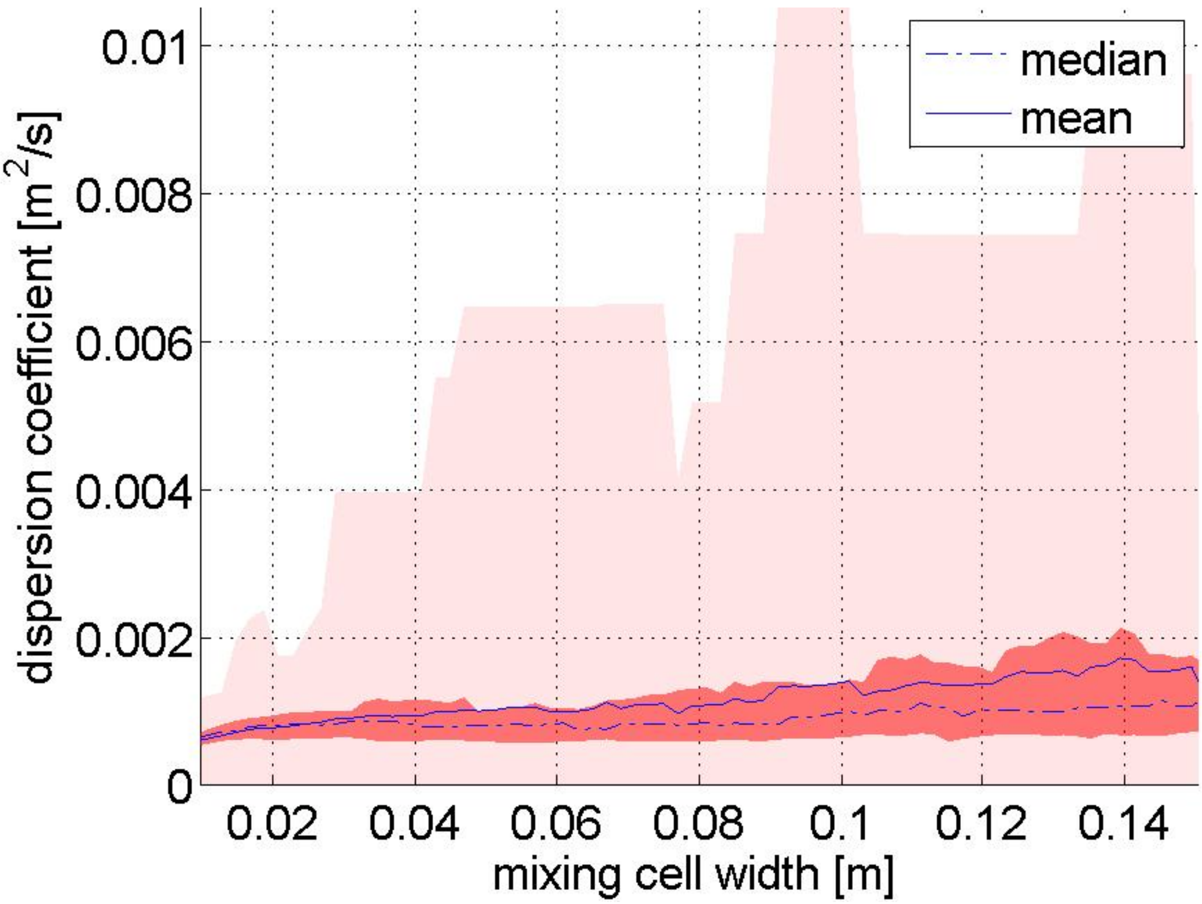

(c) x and y direction

Figure C.6: Dispersion coefficients for different mixing cell lengths at 3 cm bed height, superficial velocity of $0.375\,\mathrm{m\,s^{-1}}$ and large pellets

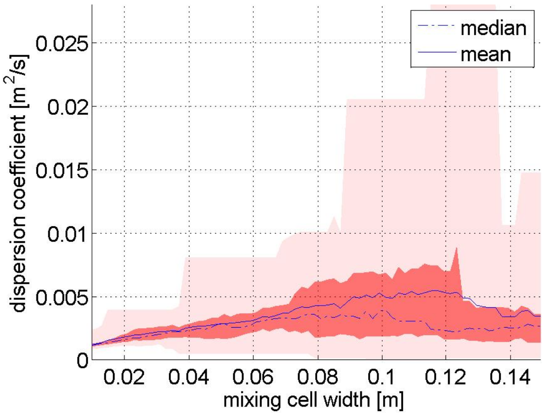

(a) x direction

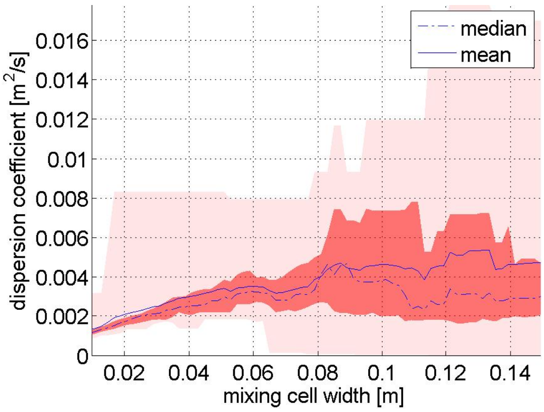

(b) y direction

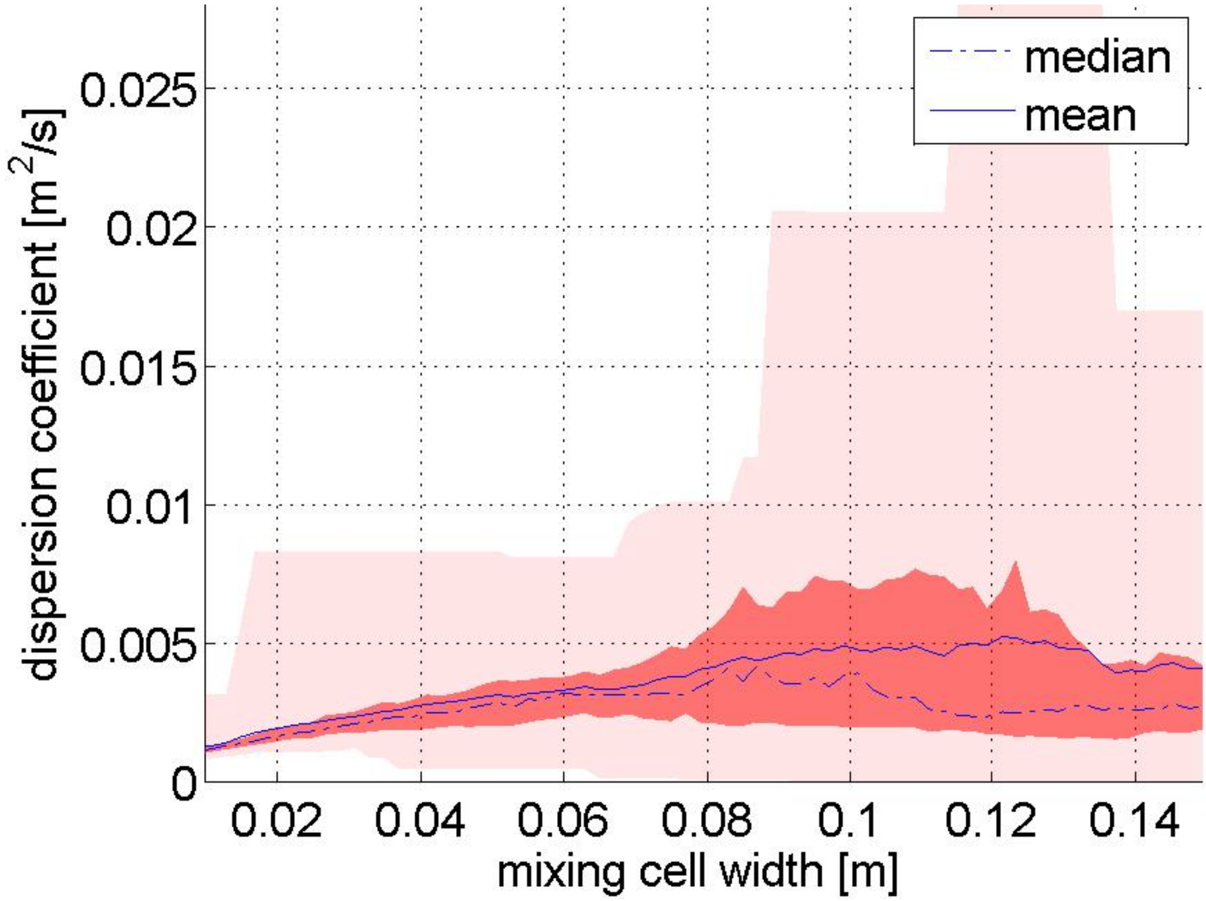

(c) x and y direction

Figure C.7: Dispersion coefficients for different mixing cell lengths at 7 cm bed height, superficial velocity of 0.185 m s^{-1} and large pellets

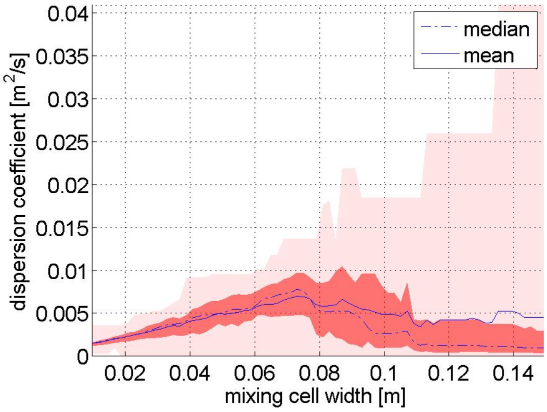

(a) x direction

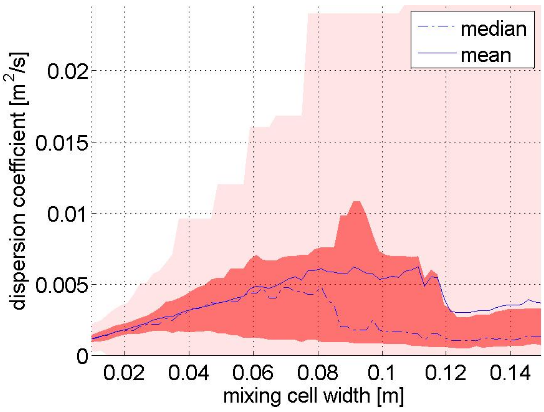

(b) y direction

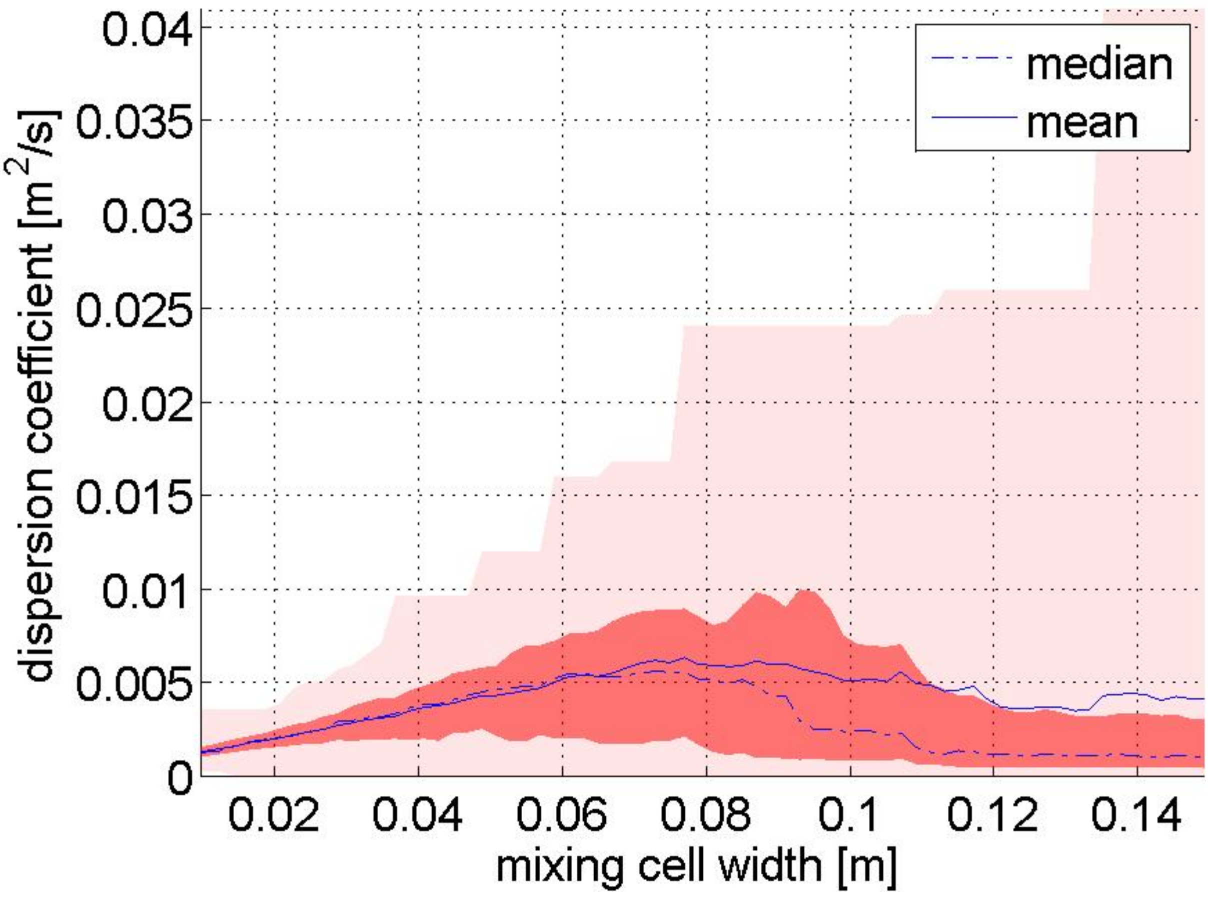

(c) x and y direction

Figure C.8: Dispersion coefficients for different mixing cell lengths at 7 cm bed height, superficial velocity of $0.185\,\mathrm{m\,s^{-1}}$ and large pellets

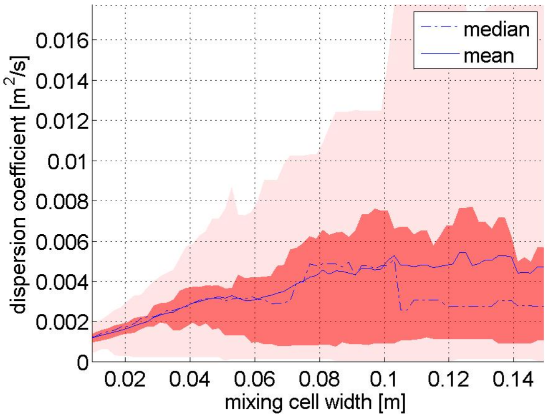

(a) x direction

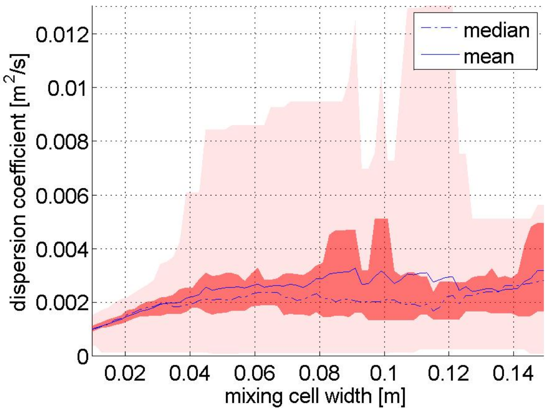

(b) y direction

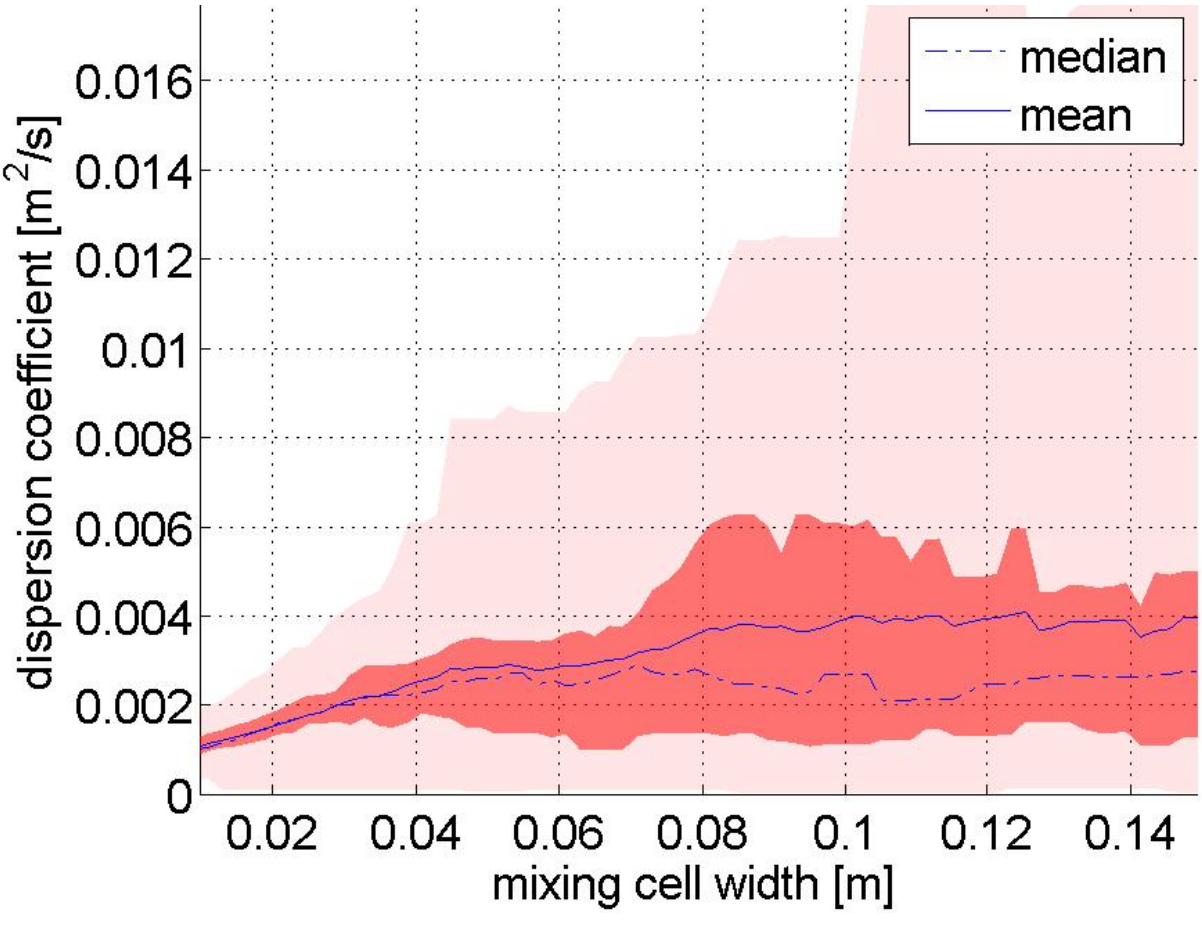

(c) x and y direction

Figure C.9: Dispersion coefficients for different mixing cell lengths at 7 cm bed height, superficial velocity of $0.185\,\mathrm{m\,s^{-1}}$ and chips

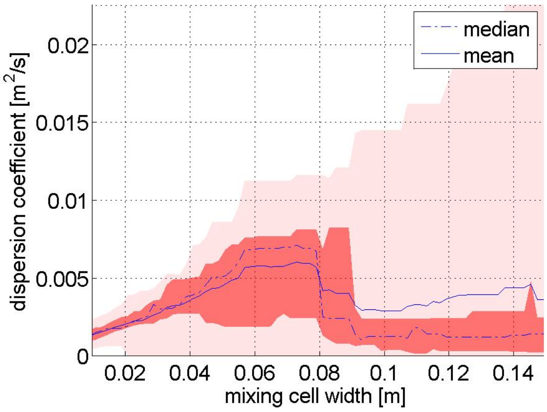

(a) x direction

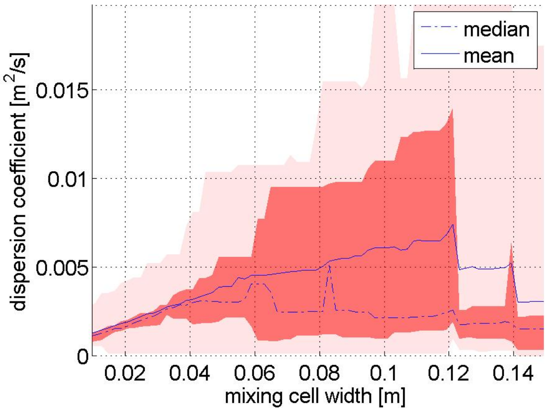

(b) y direction

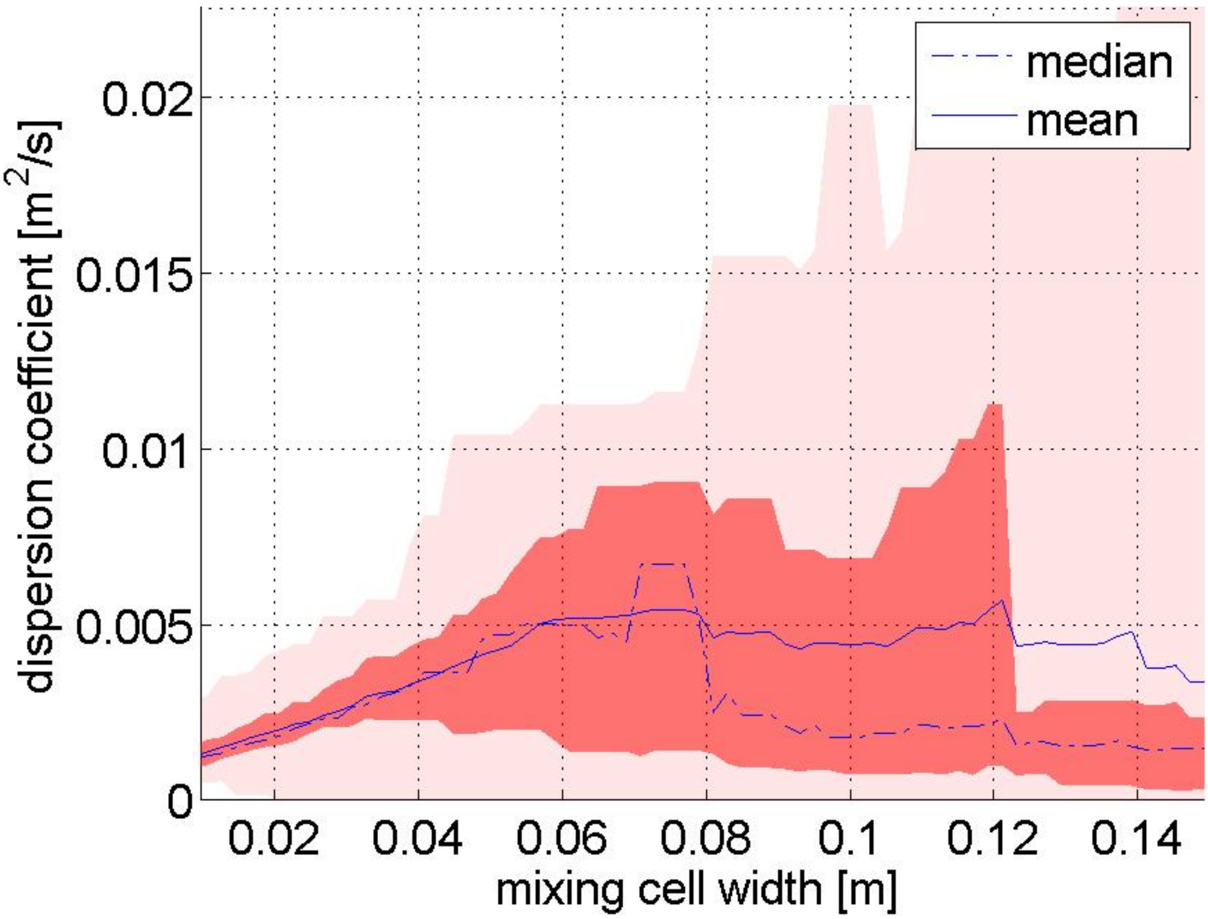

(c) x and y direction

Figure C.10: Dispersion coefficients for different mixing cell lengths at 7 cm bed height, superficial velocity of $0.375\,\mathrm{m\,s^{-1}}$ and chips

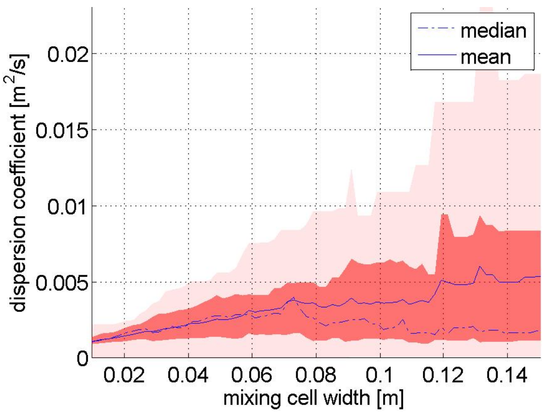

(a) x direction

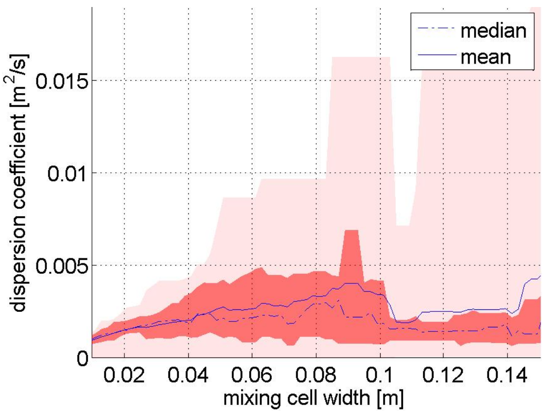

(b) y direction

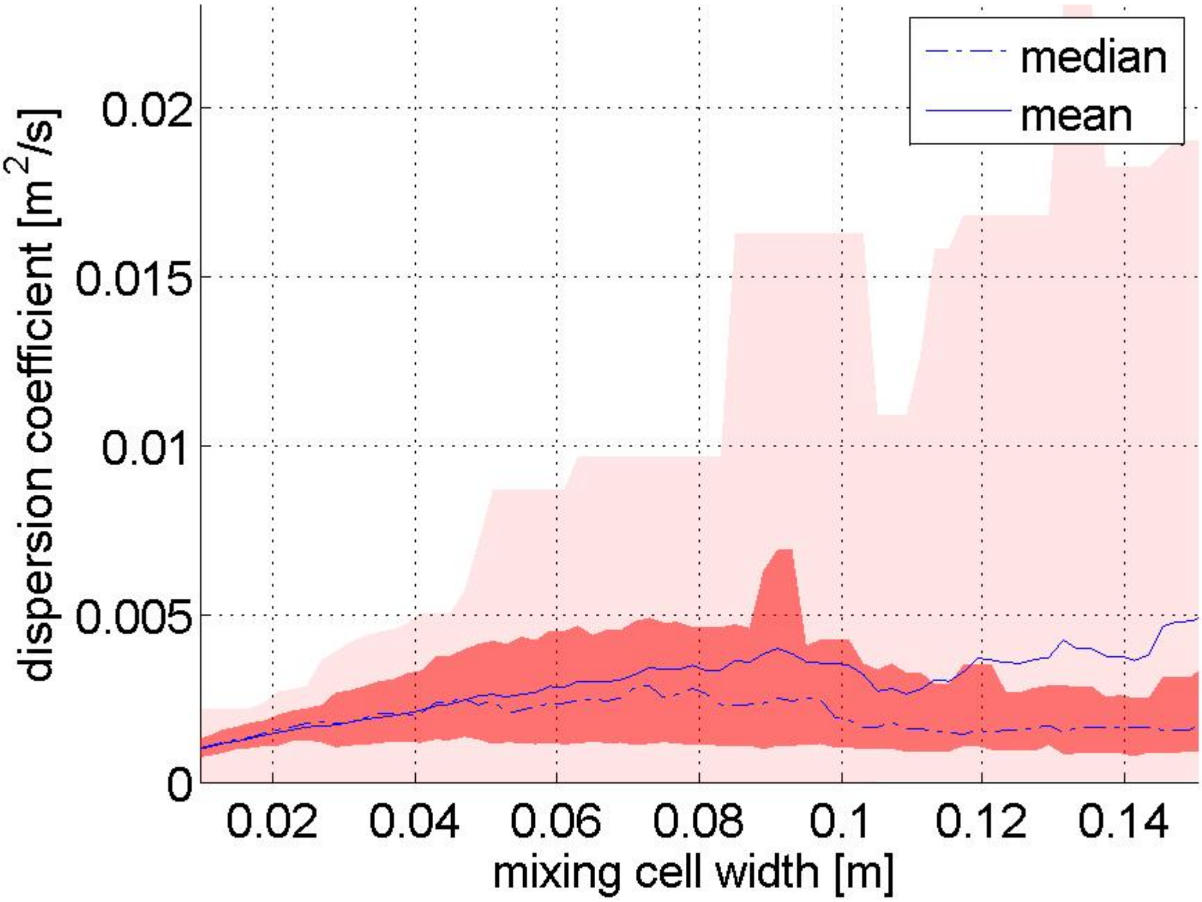

(c) x and y direction

Figure C.11: Dispersion coefficients for different mixing cell lengths at 7 cm bed height, superficial velocity of $0.185\,\mathrm{m\,s^{-1}}$, large pellets and tubes

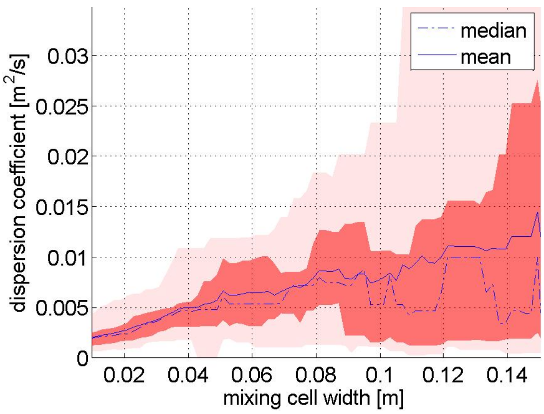

(a) x direction

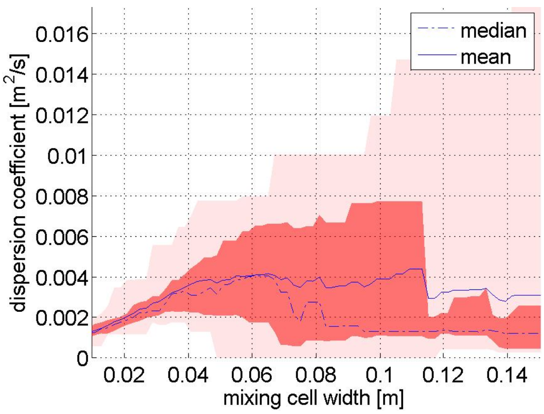

(b) y direction

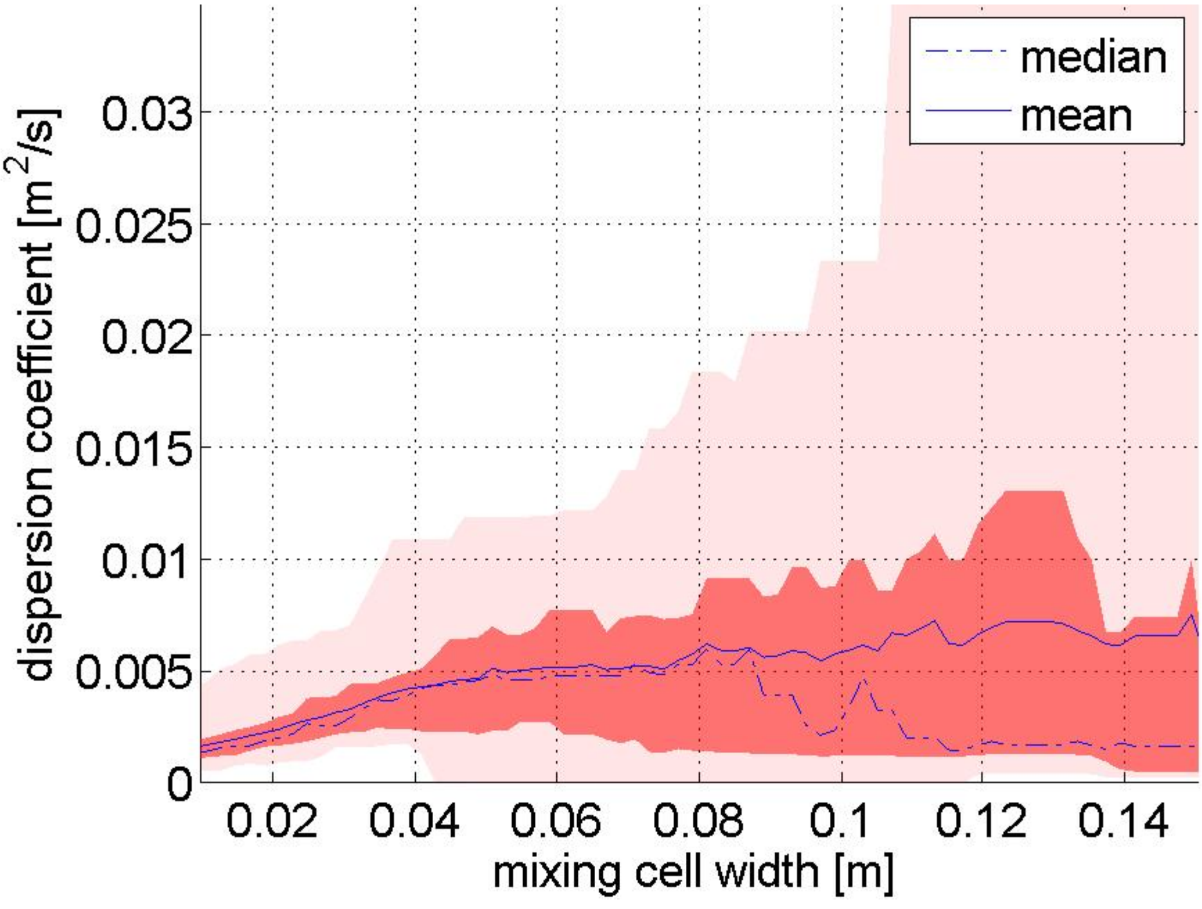

(c) x and y direction

Figure C.12: Dispersion coefficients for different mixing cell lengths at 7 cm bed height, superficial velocity of $0.375\,\mathrm{m\,s^{-1}}$, large pellets and tubes

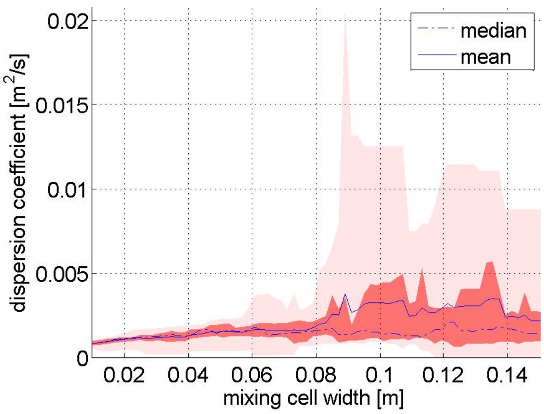

(a) x direction

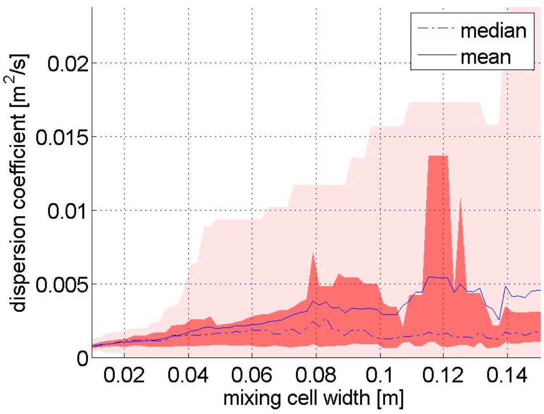

(b) y direction

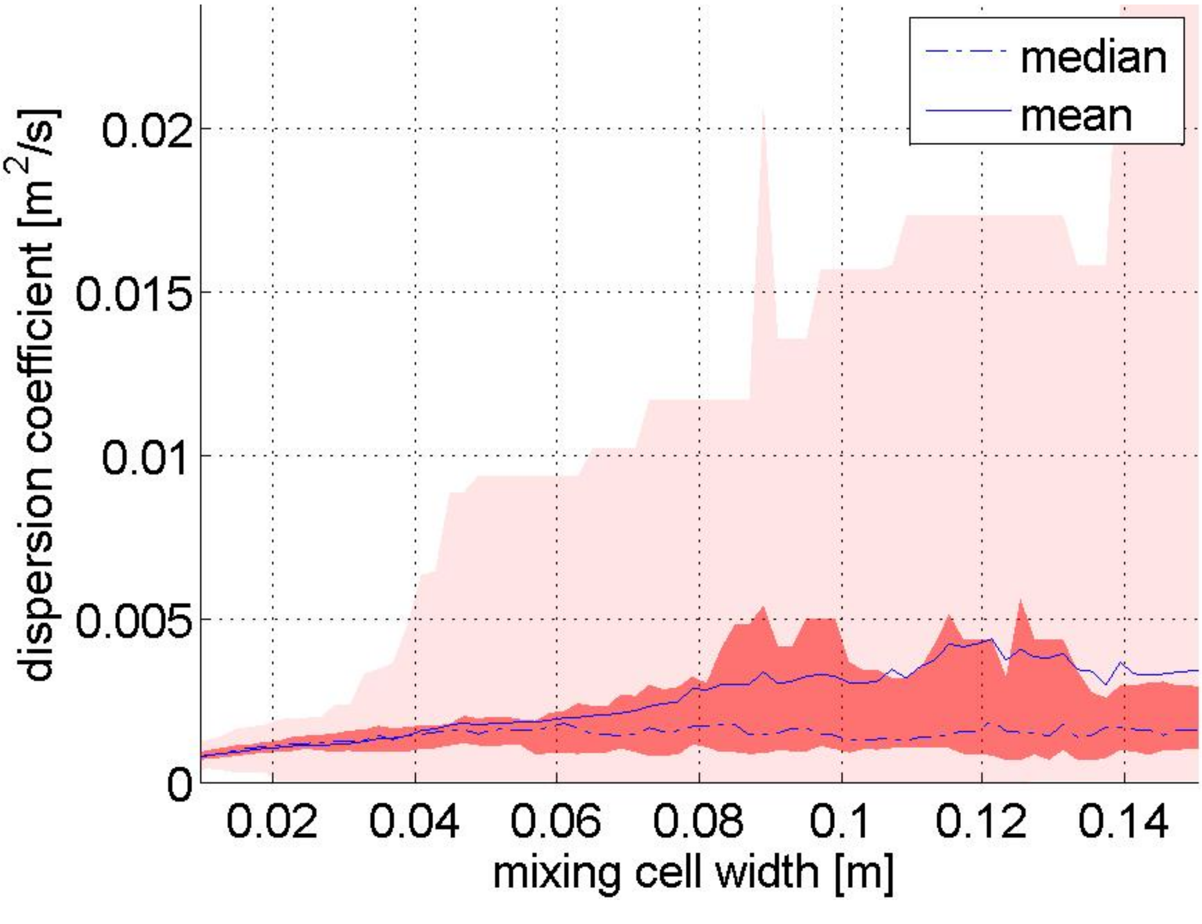

(c) x and y direction

Figure C.13: Dispersion coefficients for different mixing cell lengths at 7 cm bed height, superficial velocity of $0.185\,\mathrm{m\,s^{-1}}$, chips and tubes

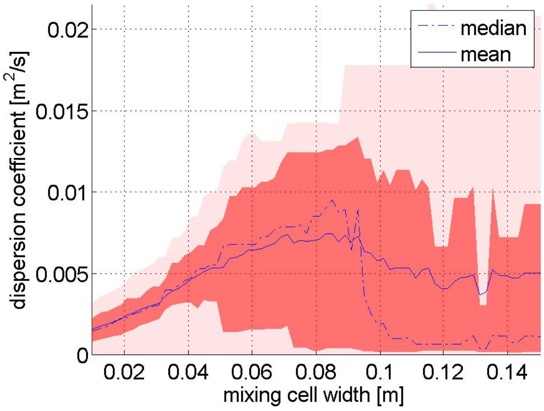

(a) x direction

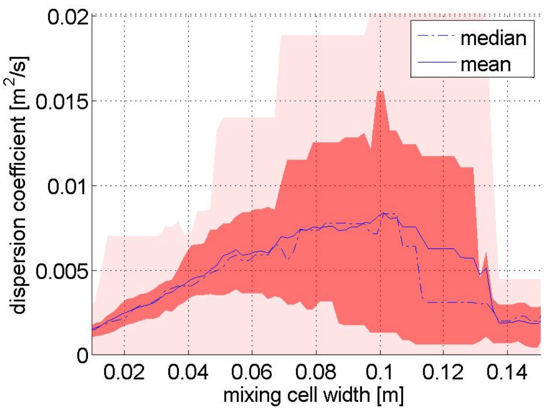

(b) y direction

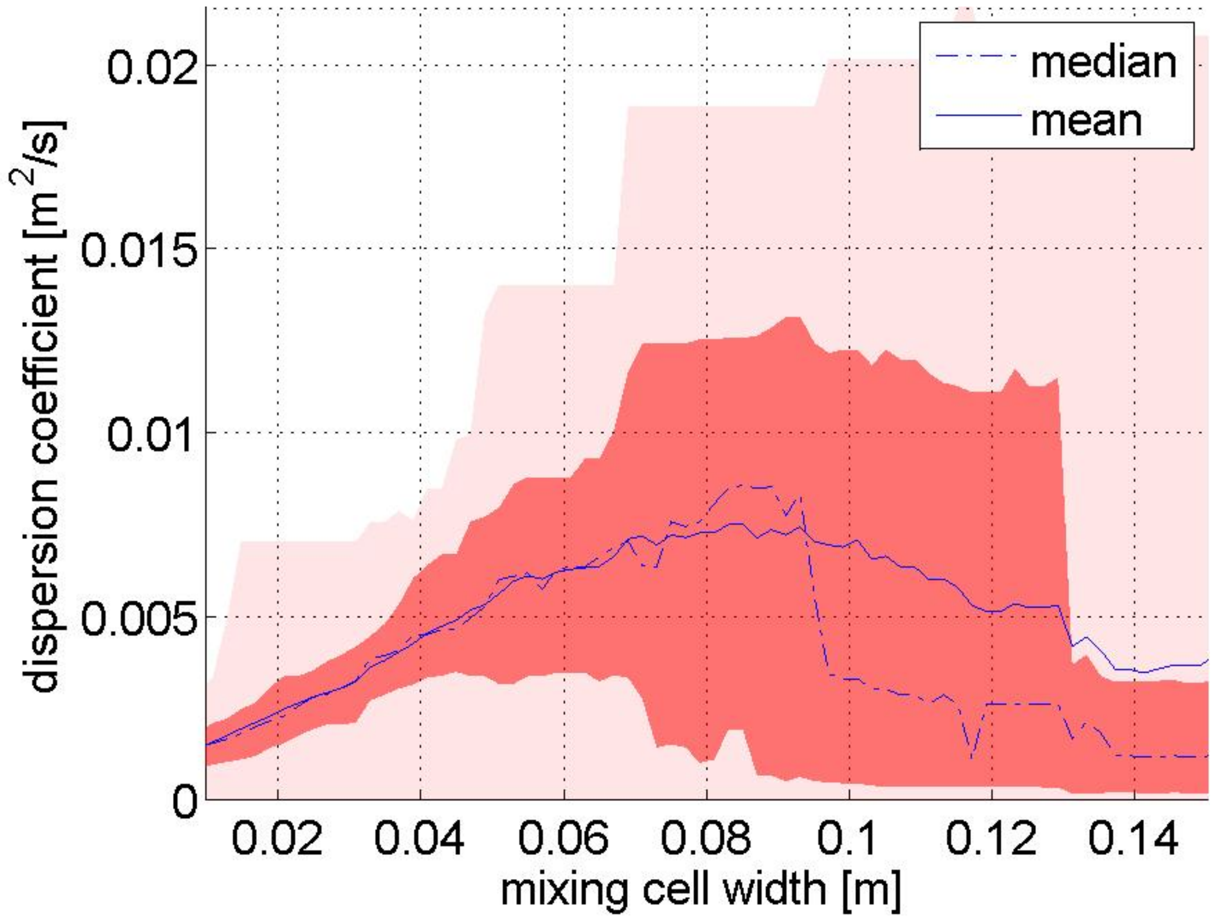

(c) x and y direction

Figure C.14: Dispersion coefficients for different mixing cell lengths at 7 cm bed height, superficial velocity of $0.375\,\mathrm{m\,s^{-1}}$, chips and tubes

Appendix D

Fist Detections in Stop Zone

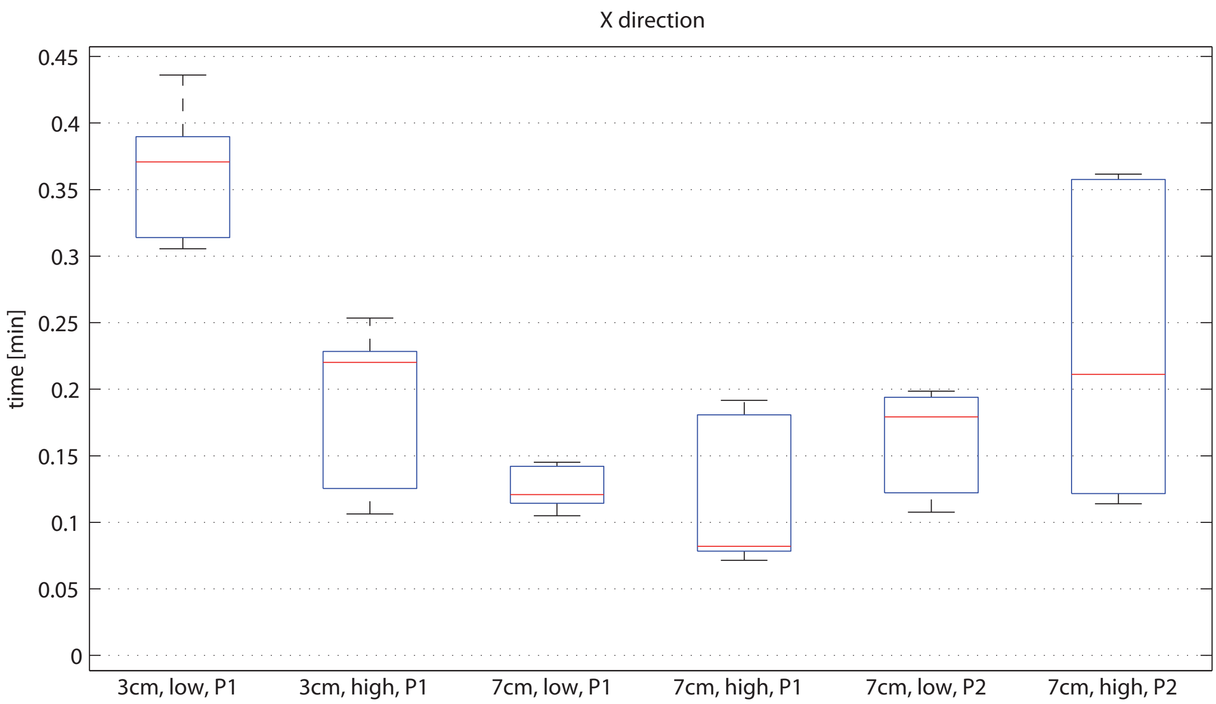

Figure D.1: Box plot off first detections in stop area (x direction) of all experiments for different conditions. P1 stands for 70 large pellets and P2 for 40 slightly smaller pellets

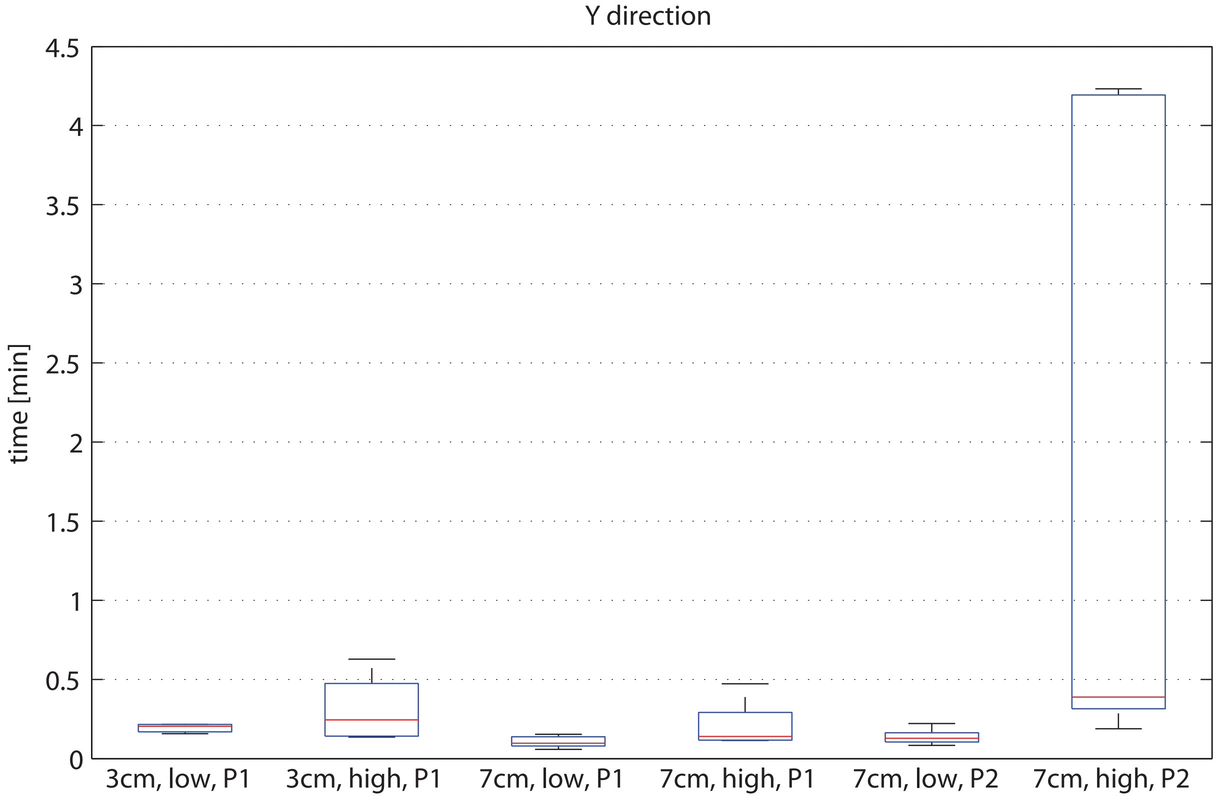

Figure D.2: Box plot off first detections in stop area (y direction) of all experiments for different conditions. P1 stands for 70 large pellets and P2 for 40 slightly smaller pellets

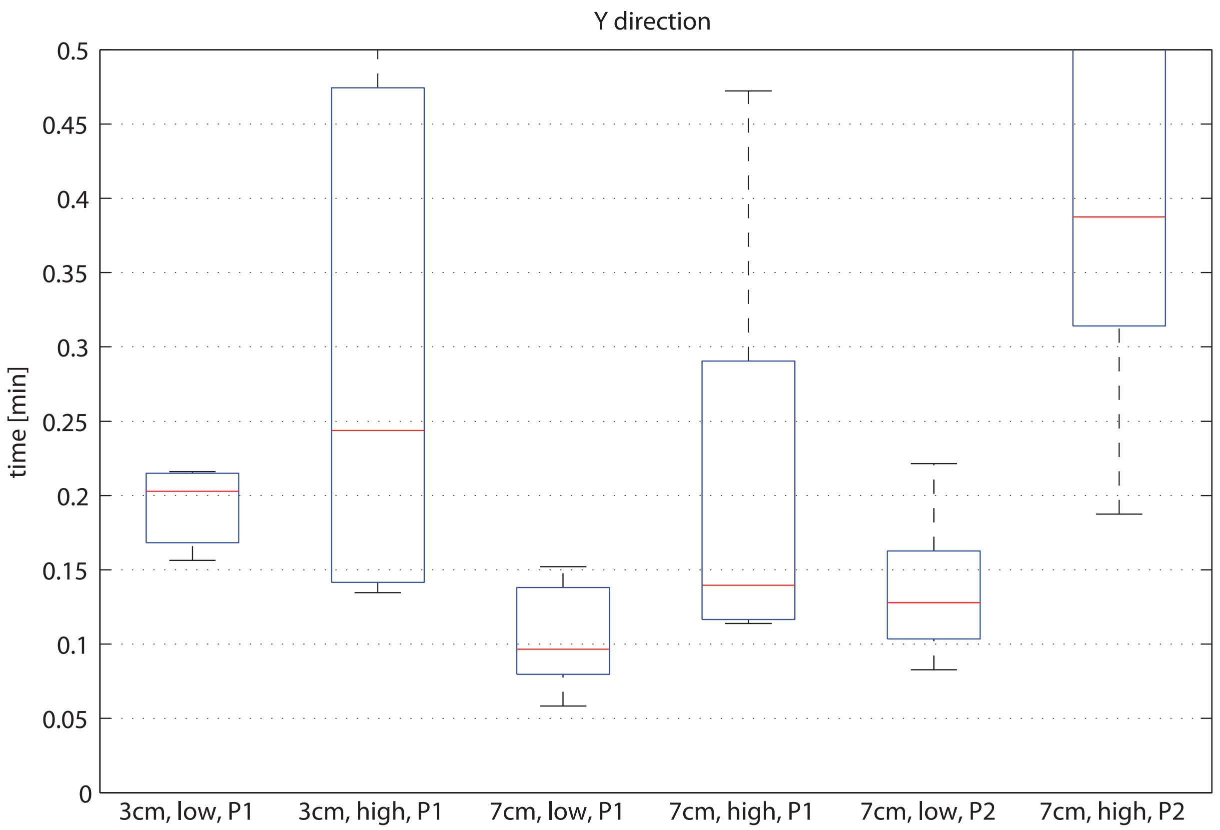

Figure D.3: Zoomed in box plot off first detections in stop area (y direction) of all experiments for different conditions. P1 stands for 70 large pellets and P2 for 40 slightly smaller pellets

Bibliography

Burger, W. and Burge, M. J. (2009). *Principles of Digital Image Processing: Fundamental Techniques*, Principles of Digital Image Processing, Springer-Verlag London.

Cattin, P. (2008). Digital image fundamentals - introduction to signal and image processing, Online.
URL: *http://miac.unibas.ch/SIP/02-Fundamentals.html* (accessed 2013.04.07)

CEN/TS 14961:2005: Feste Biobrennstoffe - Brennstoffspezifikationen und -klassen. (2005).

Cussler, E. (1997). *Diffusion: Mass Transfer in Fluid Systems*, Cambridge Series in Chemical Engineering, Cambridge University Press.

Einstein, A. (1906). Untersuchungen über die theorie der brownschen bewegung, *Annalen der Physik* **19**: 371.

Geldart, D. (1973). Types of gas fluidization, *Powder Technology* **7**(5): 285 – 292.
URL: *http://www.sciencedirect.com/science/article/pii/0032591073800373*

Glicksman, L. R., Hyre, M. R. and Farrell, P. A. (1994). Dynamic similarity in fluidization, *International Journal of Multiphase Flow* **20, Supplement 1**(0): 331 – 386. 0301-9322(94)E0022-B.
URL: *http://www.sciencedirect.com/science/article/pii/0301932294900779* (accessed 2012.11.20)

Gómez-Barea, A. and Leckner, B. (2010). Modeling of biomass gasification in fluidized bed, *Progress in Energy and Combustion Science* **36**(4): 444 – 509.
URL: *http://www.sciencedirect.com/science/article/pii/S0360128509000707*

Grace, J., Avidan, A. and Knowlton, T. (1997). *Circulating Fluidized Beds*, Blackie Academic and Professional ed.
URL: *http://books.google.at/books?id=yW-FQgAACAAJ*

Hatch, J., Association, A. and for Metals, A. S. (1984). *Aluminium: Properties and Physical Metallurgy*, Aluminum / J.E. Hatch [Hrsg.]. American Society for Metals, American Society for Metals.
URL: *http://books.google.at/books?id=dUgzGsEMhoUC*

Highley, J. and Merrick, D. (1971). Effect of the spacing between solid feed points on the perfomance of a large fluidized bed reactor., *AIChE Symposium Series* **67**: 219–227.

Ito, O., Kawabe, R., Miyamoto, T., Orita, H., Mizumoto, M. and Miyadera, H. (eds) (1999). *Direct Measurment of Particle Motion in a Large-Scale FBC Boiler Model*, 15th Fluidized Bed Combustion, Savannah, Georgia. Paper No. FBC99-0023.

Jähne, B. (2005). *Digital image processing*, EngineeringPro collection, Springer-Verlag New York Incorporated.

Johnsson, F., Vrager, A. and Leckner, B. (eds) (1999). *Solids flow pattern in the exit region of a CFB-furnace - influence of exit geometry*, 15th Fluidized Bed Combustion, Savannah, Georgia, USA.

Kaltschmitt, M., Hartmann, H. and Hofbauer, H. (2009). *Energie aus Biomasse: Grundlagen, Techniken und Verfahren*, Springer.
URL: *http://books.google.at/books?id=QpMM93jkficC*

Knoebig, T., Luecke, K. and Werther, J. (1999). Mixing and reaction in the circulating fluidized bed – a three-dimensional combustor model, *Chemical Engineering Science* **54**(13–14): 2151 – 2160.
URL: *http://www.sciencedirect.com/science/article/pii/S0009250998003595*

Kothandaraman, C. and Subramanyan, S. (2004). *Heat And Mass Transfer Data Book*, New Age International Publishers.
URL: *http://books.google.se/books?id=5FKaEznxsSMC*

Kunii, D. and Levenspiel, O. (1991). *Fluidization engineering*, Butterworth-Heinemann series in chemical engineering, Butterworth-Heinemann Limited.
URL: *http://books.google.at/books?id=ZVnb17qRz8QC*

Larsson, J. and Olsson, J. (2013). *Modelling and optimization of fuel conversion in an indirect bubbling fluidized bed gasifier*, Master's thesis, Chalmers University of Technology, Göteborg, Sweden 2013. Department of Energy and Environment, Division of Energy Technology.

Leitner, S. (2010). *Demand-Side Management - Die notwendigkeit von Planwirtschaft auf dem Energiemarkt*, Sebastian Leitner. Studienarbeit.

Moore, G. E. (1965). Cramming more components onto integrated circuits, *Electronics* **38**(8): 114–117.
URL: *http://download.intel.com/museum/Moores_Law/Articles-Press_Releases/Gordon_Moore_1965_Article.pdf* (accessed 2013.05.23)

Niklasson, F., Thunman, H., Johnsson, F. and Leckner, B. (2002). Estimation of solids mixing in a fluidized-bed combustor, *Ind. Eng. Chem. Res.* **41 (18)**: 4663–4673.
URL: *http://pubs.acs.org/doi/abs/10.1021/ie020173s*

Pallarès, D., Dìez, P. A. and Johansson, F. (2007). Experimental analysis of fuel mixing patterns in a fluidized bed, *The 12th International Conference on Fluidization - New Horizons in Fluidization Engineering* **RP4**: 929–936.
URL: *http://dc.engconfintl.org/fluidization_xii/114/* (accessed 2012.11.26)

Pallarès, D. and Johnsson, F. (2006). A novel technique for particle tracking in cold 2-dimensional fluidized beds—simulating fuel dispersion, *Chemical Engineering Science* **61**(8): 2710 – 2720.
URL: *http://www.sciencedirect.com/science/article/pii/S0009250905008845*

Pearson, K. (1905). The problem of the random walk, *Nature* **72**: 294.

REPOTEC (2013). Online. REPOTEC - Renewable Power Technologies Umwelttechnik GmbH.

URL: *http://www.repotec.at/index.php/Biomasse-Vergasungsanlage_inkl._SNG-Produktion_Göteborg.html* (accessed 2013.05.25)

Sette, E. (ed.) (2013). *Analysis of lateral fuel mixing in a fluiddynamically down-scaled bubbeling fluidized bed*, Fluidization XIV Conference, Noordwijkerhout, Netherlands.

Shi, Y.-F. and Fan, L. (1985). Lateral mixing of solids in gas-solid fluidized beds with continuous flow of solids, *Powder Technology* **41**(1): 23 – 28.
URL: *http://www.sciencedirect.com/science/article/pii/0032591085850701*

Soille, P. (1999). *Morphological Image Analysis*, Springer Berlin Heidelberg.

Soria-Verdugo, A., Garcia-Gutierrez, L., Sanchez-Delgado, S. and Ruiz-Rivas, U. (2011). Circulation of an object immersed in a bubbling fluidized bed, *Chemical Engineering Science* **66**(1): 78 – 87.
URL: *http://www.sciencedirect.com/science/article/pii/S0009250910005920*

Yang, W. (2003). *Handbook of Fluidization and Fluid-Particle Systems*, Chemical Industries Series, Marcel Dekker Incorporated.
URL: *http://books.google.at/books?id=n_UqkwcFbwkC*

Acronyms